

**PETROCHRONOLOGICAL CONSTRAINTS ON THE ORIGIN OF THE SALT LAKE
CRATER GARNET-BEARING PYROXENITE XENOLITHS, OAHU, HAWAII**

by

Zhen Zhang

A THESIS SUBMITTED IN PARTIAL FULFILLMENT OF
THE REQUIREMENTS FOR THE DEGREE OF

MASTER OF SCIENCE

in

The College Of Graduate Studies
(Environmental Sciences)

THE UNIVERSITY OF BRITISH COLUMBIA
(Okanagan)

June 2017

© Zhen Zhang, 2017

The following individuals certify that they have read, and recommend to the College of Graduate Studies for acceptance, a thesis entitled:

PETROCHRONOLOGICAL CONSTRAINTS ON THE ORIGIN OF THE SALT LAKE CRATER GARNET-BEARING PYROXENITE XENOLITHS, OAHU, HAWAII

submitted by Zhen Zhang in partial fulfillment of the requirements of the degree of Master of Science.

Dr. John Greenough, Irving K. Barber School of Arts and Sciences
Supervisor

Dr. Kyle Larson, Irving K. Barber School of Arts and Sciences
Supervisory Committee Member

Dr. Yuan Chen, Irving K. Barber School of Arts and Sciences
Supervisory Committee Member

Dr. Paul Shipley, Irving K. Barber School of Arts and Sciences
University Examiner

Dr. John Hopkinson, Irving K. Barber School of Arts and Sciences
External Examiner

Abstract

This thesis reports the results of a comprehensive major and trace element study of seven garnet-bearing pyroxenite xenoliths recovered from Oahu, Hawaii. The pyroxenites are dominated by clinopyroxene, but also contain garnet, olivine, orthopyroxene and spinel (Cpx, Gt, Ol, Opx, Sp). Four zircons extracted from two pyroxenites have been dated and the trace element signatures studied in detail. Petrological and geochemical information from optical microscopy, electron microprobe analysis (EMP; 11 major and minor element oxides) and Laser Ablation Inductively Coupled Plasma Mass Spectrometry (LA-ICP-MS; 36 trace elements) for major mineral phases indicate that the pyroxenites are cumulates formed through fractional crystallization of magma formed by partial melting of a subcontinental lithospheric mantle fragment entrained in the convecting oceanic lithosphere. Two groups of ages were acquired from zircon core and rim zones, with simultaneous, in situ, determination of trace element concentrations by a cutting-edge Laser Ablation Split Stream-ICP-MS technique. They are the first zircons yielding true ages (non-model ages) for xenoliths recovered from the oceanic lithospheric mantle. The older core (80.8 ± 2 Ma) of Zircon3 yielded clinopyroxene/zircon, garnet/zircon partitioning coefficients for most elements that match literature coefficients for

similar magma types. This suggests that clinopyroxene and garnet, the dominant minerals in the xenoliths, formed during a magmatic event \sim 81 Ma, when the zircon cores formed. Younger ages (12.9 ± 0.2 Ma to 14.5 ± 0.2 Ma) given by four zircons (Zircon2 and Zircon4, along with overgrowths on Zircon1 and Zircon3) are inferred to record a event at \sim 13 Ma, possibly due to the presence of an adjacent mantle plume. The result implies that instead of recycled oceanic crust and lithosphere, the removal of mantle lithosphere from below the continents during subduction or asthenosphere upwelling could be an important mechanism that contributes to chemical variability in the mantle.

Preface

This thesis is my own work. Dr. John Greenough designed the research program and gave research directions. He was also involved in discussion and editing. Dr. John Cottle helped acquire and process geochronology data. He also composed text describing the LASS-ICP-MS operation.

Table of Contents

Abstract	iii
Preface	v
Table of Contents	vi
List of Tables.....	ix
List of Figures	xi
List of Abbreviations	xiii
Acknowledgements	xiv
CHAPTER I INTRODUCTION	1
CHAPTER II BACKGROUND	4
2.1 Geological Setting	4
2.2 Sampling and Previous Work.....	6
2.3 Previous Research.....	9
CHAPTER III ANALYTICAL TECHNIQUES.....	12
3.1 Petrographic Analyses.....	12
3.2 Major Elements from EMPA	12
3.3 Trace Element Concentrations from LA-ICP-MS	15
3.4 Zircon Dating and Trace Element Concentration Profiling.....	20
CHAPTER IV RESULTS	22
4.1 Petrography.....	22
4.2 Elemental Mapping	27
4.3 Major Element Mineral Analyses	28
4.3.1 Clinopyroxene	29
4.3.2 Orthopyroxene	32

4.3.3 Garnet	34
4.3.4 Olivine	35
4.4 Trace Elements	36
4.4.1 Clinopyroxene	36
4.4.2 Garnets	39
4.5 Zircon Petrochronological Signatures	40
4.5.1 Morphology and texture of zircons	40
4.5.2 Zircon1 Age and Trace Element Data	41
4.5.3 Zircon2 Age and Trace Element Data	45
4.5.4 Zircon3 Age and Trace Element Data	48
4.5.5 Zircon4 Age and Trace Element Data	50
CHAPTER V DISCUSSION.....	53
5.1 Genetic Relationships	53
5.2 Origin of SLC Xenoliths.....	55
5.2.1 Frozen melt	56
5.2.2 Recycled oceanic crust	58
5.2.3 Cumulate origin	58
5.3 Source Melt and Petrogenesis of Clinopyroxene and Garnet	59
5.3.1 Melt composition	59
5.3.2 Pb enrichment and association with subcontinental lithospheric mantle	62
5.3.3 Local Pb anomaly in Cpx	63
5.4 Significance of Zircon Ages	64
5.4.1 Zircon Associated Mineral	64
5.4.2 Magmatic vs. metamorphic origin of zircon cores and rims	70
5.4.3 Interpretation of ages	75
5.5 Tectonic Implications	76

CHAPTER VI CONCLUSIONS.....	79
REFERENCES	80
APPENDICES.....	93
Appendix A Detailed Sample Processing and Extraction Procedures.....	93
Appendix B Mineral Composition Data	97

List of Tables

Table 1 Major Element Compositions of Standards	14
Table 2 Precision and Accuracy of Each Major Element.....	15
Table 3 LA-ICP-QMS Operating Parameters.....	16
Table 4 Order of Measurements	17
Table 5 Analyses of BCR-2G	19
Table 6 Petrographic Features of Seven SLC Samples.....	24
Table 7 SEM-EDX Composition of the Unknown Phase.....	27
Table 8 Summary of Ages of Four Zircons	41
Table 9 Partition Coefficients from the Literature Used to Construct the Reference Line in Figure 26.....	66
Table 10 Major Element Concentrations and Calculated Stoichiometry for Clinopyroxene	97
Table 11 Major Element Concentrations and Calculated Stoichiometry for Orthopyroxene	101
Table 12 Major Element Concentrations and Calculated Stoichiometry for Garnet.....	103
Table 13 Major Element Concentrations and Calculated Stoichiometry for Olivine.....	107
Table 14 Major and Trace Element Concentrations for Clinopyroxene from LA-ICP-MS	109
Table 15 Major and Trace Element Concentrations for Garnet from LA-ICP-MS.....	115
Table 16 Ages (Ma) of 4 Zircons with Correlated Drilling Depth	121
Table 17 Mean Age of Four Zircons	131
Table 18 LA-ICP-MS Depth Profiling Trace Element Concentrations for Zircon1 (SLCX 47).....	132
Table 19 LA-ICP-MS Depth Profiling Trace Element Concentrations for Zircon2 (SLCX 47).....	134
Table 20 LA-ICP-MS Depth Profiling Trace Element Concentrations for Zircon3 (SLCX 12).....	136

Table 21 LA-ICP-MS Depth Profiling Trace Element Concentrations for Zircon4 (SLCX	
12).....	138

List of Figures

Figure 1 Sketch map showing location of the Salt Lake Crater on the island of Oahu.....	5
Figure 2 Sample photos of the SLCX 45 hand sample.....	7
Figure 3 The four zircons involved in this project	9
Figure 4 Plane polarized photomicrographs of representative mineral assemblages and textures	25
Figure 5 Photograph of the unknown phase	26
Figure 6 Back Scattered Electron Image and elemental maps of SLCX 26 garnet.....	28
Figure 7 Compositions of SLCX clinopyroxenes and orthopyroxenes.....	30
Figure 8 Plots of Mg# versus major element oxides for clinopyroxenes	31
Figure 9 Plots of Mg# versus major element oxides for orthopyroxenes	33
Figure 10 Ternary diagram of garnet compositions.....	35
Figure 11 Primitive mantle normalized trace element abundances in SLC clinopyroxenes	38
Figure 12 Mg# vs. compatible elements (Sc, Ni) and incompatible elements (Sr, Nb) in clinopyroxenes	39
Figure 13 Primitive mantle normalized trace element abundances in SLC garnets.....	40
Figure 14 Chondrite-normalized Hf, Y and U concentrations and age profiling data for Zircon1	42
Figure 15 Chondrite-normalized REE patterns for Zircon1.....	44
Figure 16 Chondrite-normalized Hf, Y and U concentrations and age profiling data for Zircon 2	46
Figure 17 Chondrite-normalized REE pattern for Zircon2	47
Figure 18 Chondrite-normalized Hf, Y and U concentrations and age profiling data for Zircon3	48
Figure 19 Chondrite-normalized REE patterns for Zircon3.....	50
Figure 20 Chondrite-normalized Hf, Y and U concentrations and age profiling data for Zircon4	51
Figure 21 Chondrite-normalized REE pattern for Zircon4	52

Figure 22 Multi-dimensional scaling comparisons of seven samples based on the overall major, minor and trace element composition of clinopyroxene.....	54
Figure 23 Zr/Hf vs. Nd/Sm ratios of clinopyroxene in peridotite and pyroxenite from the Salt Lake Crater	57
Figure 24 Primitive mantle-normalized trace element composition of melts in equilibrium with clinopyroxene	60
Figure 25 Cpx/Gt partitioning coefficients for REE	62
Figure 26 Diagram showing zircon/clinopyroxene partition coefficients for REE in samples SLCX 47 and SLCX 12	67
Figure 27 Diagram showing zircon/garnet partition coefficients for REE in samples SLCX 47 and SLCX 12.....	69
Figure 28 Th/U vs. depth profile of two zircon cores	72
Figure 29 Th/U vs. depth profile of zircon rims.....	74
Figure 30 SLCX processing photos.....	94

List of Abbreviations

Alm	Almandine
Bld.	Below detecting limit
BSE	Back-Scattered Electron
Cpx	Clinopyroxene
EBS	Electron Back Scatter Image
EDS	Energy Dispersive Spectroscopy
EMP	Electron Microprobe
En	Enstatite
Fa	Fayalite
Fo	Forsterite
Fs	Ferrosilite
Grs	Grossular
Gt	Garnet
HREE	Heavy Rare Earth Elements
LA-ICP-MS	Laser Ablation Inductively Coupled Plasma Mass Spectroscopy
LASS	Laser Ablation Split Stream
LREE	Light Rare Earth Elements
MREE	Middle Rare Earth Elements
OI	Olivine
Opx	Orthopyroxene
PPL	Plane-Polarized Light
Prp	Pyrope
REE	Rare Earth Elements
RL	Reflected Light
SLC	Salt Lake Crater
SCLM	Subcontinental Lithospheric Mantle
Sp	Spinel
WDS	Wavelength Dispersive Spectroscopy
Wo	Wollastonite
XPL	Cross-Polarized Light

Acknowledgements

First and foremost, this project was made possible by the support and encouragement from supervisor Dr. John Greenough. His constant effort ensured the lab work was always on schedule and my questions could be quickly answered. He also sets a good example on hard-working and critical thinking. What I have learned from him will benefit me for my whole life. Sincerest thanks to him.

I would also like to thank every researcher and technician who has helped me. Thanks go to my committee members, Dr. Kyle Larson and Dr. Yuan Chen for valuable advice and feedback during the project. Dr. Daniel Layton-Matthews at Queen's University crushed the samples. Dr. Don Davis, Dr. Sandra Kamo and Yim Ying (Kim) Kwok at University of Toronto helped with zircon separation and preliminary dating. Thank David Arkinstall at UBC O for help on SEM and EMP analyses. Thanks go to Dr. Brain Fryer, Dr. Joel Gagnon, J.C. Barrette and Janet Hart at University of Windsor for help on LA-ICP-MS and data reduction. Dr. John Cottle at University of California performed the zircon petrochronology data.

I would like to thank the Department of Mineral Sciences of the Smithsonian Institution for providing reference materials USNM 111356, USNM 111356 and USNM 111312. I thank Dr. David Clague for assistance in identifying the sampling locality, and EESC 2004 students for helping collect the xenoliths.

This project was funded by NSERC and UBC O graduate fellowships.

Last but not least, I would like to thank my parents for their mental and financial support on my abroad research and life. Without them, I would not have the chance to come to Canada and

investigate the fantastic place in the past four years. I would like to thank my friend and roommate Wayne for showing me Canadian culture and beauty. Finally, I thank my girlfriend Jing for always being with me.

CHAPTER I INTRODUCTION

The famous garnet bearing pyroxenite xenoliths from the Salt Lake Crater (SLC), Oahu, Hawaii, have been widely studied for nearly four decades (Bizimis *et al.*, 2013; 2005; Clague, 1987; Frey, 1980; Keshav and Sen, 2003; Keshav *et al.*, 2007; Lassiter *et al.*, 2000; Peslier *et al.*, 2015; Sen *et al.*, 1993). People are interested in these xenoliths because they represent samples of the mantle below Oahu, but more importantly, they are the deepest-origin rocks yet formed in the ocean basins. These samples carry critical information about the chemical and physical composition of the mantle, or the mantle-crust transition boundary, and have been treated as probes of chemical variability in the mantle. Two groups of nano-diamonds were reported from the SLC pyroxenites (Frezzotti and Peccerillo, 2007; Wirth and Rocholl, 2003). The discovery of diamonds indicates that the samples may be a result of subduction of oceanic lithosphere billions of years ago, or recent removal of ancient subcontinental lithospheric mantle (SLM) from below the continents during Phanerozoic subduction or rifting.

Several geologists have examined the petrology and chemical composition of the SLC xenoliths in detail in the past decades. The samples are classified as garnet clinopyroxenites with clinopyroxene dominating the mineral assemblage, along with the presence of garnet, orthopyroxene, olivine and spinel (Keshav and Sen, 2003). Major and trace element systematics and the presence of cumulate textures in some samples suggest that the SLC pyroxenites are cumulates formed as a result of high pressure fractional crystallization (Bizimis *et al.*, 2005). The depth where the samples formed is controversial (Bizimis and Peslier, 2015; Keshav and Sen, 2004; Keshav *et al.*, 2005), but they are generally considered to come from the lower oceanic lithospheric mantle. Geobarometry on a few samples yielded asthenospheric depths (Keshav and Sen, 2003). Based on Lu-Hf and Nd-Sm isotopic systematics, Bizimis suggested that these xenoliths have a near-zero age and formed right before being brought to the surface (Bizimis *et al.*, 2005). However, this estimate is not necessarily robust because secondary alteration or metamorphism can reset the isotope pairs.

In the fall of 2015, seven zircons were extracted from two garnet pyroxenite xenoliths. With recent cutting-edge techniques such as LA-ICP-MS (Laser Ablation Inductively Coupled Plasma

Mass Spectrometry) and the newly developed LASS-ICP-MS (Laser Ablation Split-Stream Inductively Coupled Plasma Mass Spectrometry) method, we are able to acquire zircon U-Pb ages along with in situ trace element concentrations, which carry information on the conditions where the samples formed. This research investigates the relationships between the ages, the rock-forming phases and associated geological events. The results bring new insights to our understanding of the geodynamic processes occurring within the oceanic lithosphere.

CHAPTER II BACKGROUND

2.1 Geological Setting

The Hawaiian Island Chain in the North Pacific Ocean is composed of numerous volcanic islands that trend toward the South East. The Hawaiian island chain is thought to be the surface expression of an upwelling mantle plume, which heats up the older lithosphere (~ 100 Ma) and leads to extensive intra-plate volcanism (Hart *et al.*, 1992; Ren *et al.*, 2005; Ribe, 1988). The chain was initiated ~ 80 Ma, and north-westward movement of the Pacific oceanic plate has left a trail of islands and seamounts. Oahu, which is the third largest island of the Hawaiian Island chain, occupies a total area of 1545 km^2 . The Oahu island has an age of ~ 5 Ma, and was built due to the eruption of the Waianae and Koolau volcanoes. The Koolau caldera was formed due to tholeiitic lava eruptions between 1.8 and 2.6 Ma, and this shield building stage was followed by an erosional stage lasting 1.8 Myr (Clague, 1987; Frey, 1980; Lanphere and Dalrymple, 1980; Lassiter *et al.*, 2000; Sen *et al.*, 1993). The crust was thinned during the erosional stage, which ultimately triggered decompression melting during a rejuvenated stage that began at 0.6 Ma, producing the Honolulu Volcanics (HV) at several vents scattered across the caldera.

(Lassiter *et al.*, 2000; Rocholl *et al.*, 1996; Sen and Jones, 1990). One of the vents, the Salt Lake Crater, located on the flank of the caldera, is the place where the SLCX samples were recovered (Figure 1).

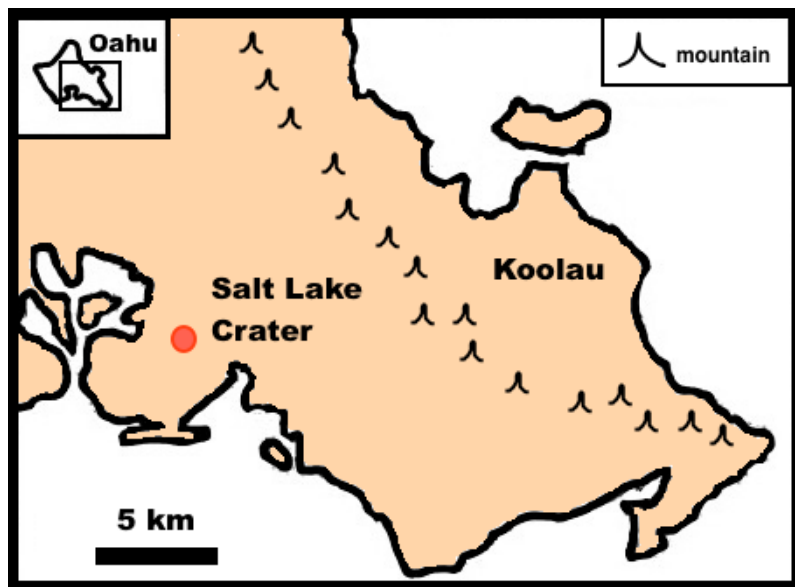


**Figure 1 Sketch map showing location of the Salt Lake Crater on the island of Oahu.
Modified from Google Earth.**

Xenoliths of dunite, spinel lherzolite and pyroxenite are common at the vents. Dunites are recovered at or close to the Koolau caldera vents, whereas spinel lherzolites are spread out around the caldera (Bizimis *et al.*, 2004; Clague and Frey, 1982; Keshav *et al.*, 2007; Sen and Jones, 1990; Sen *et al.*, 1993). Garnet-bearing pyroxenites, unlike dunites and lherzolites, only occur at the Salt Lake Crater, where spinel lherzolite and garnet-bearing pyroxenite are the dominant xenolith types (Bizimis *et al.*, 2005; Frey, 1980; Keshav *et al.*, 2007). In most cases the

pyroxenite is hosted in nephelinitic tuff (Clague and Frey, 1982), and lherzolite usually occurs together with pyroxenite (Keshav and Sen, 2003).

2.2 Sampling and Previous Work

The seven samples (SLCX 11, SLCX 12, SLCX 21, SLCX 25, SLCX 26, SLCX 45, SLCX 47) (Figure 2) included in this project were selected from a suite of 48 xenoliths (SLCX 1-48) collected by Dr. John Greenough and UBC O students during a 2004 trip to the Salt Lake Crater. The recovery location lies behind the Hoaloha Park, on the slope of a small hill ($21^{\circ}21.174' N$, $157^{\circ}54.727' W$, 28 m). Samples include lherzolite, pyroxenite, and host basalt. In anticipation of doing Laser Ablation Inductively Coupled Plasma Mass Spectrometry (LA-ICP-MS), thick sections (200 μm) were cut to permit laser drilling on small grains if necessary.



Figure 2 Sample photos of the SLCX 45 hand sample.

In 2013, a major element and trace element focused honours project (Rusk, 2013) studied garnet and pyroxene compositions in five xenoliths from the SLCX suite. The major element results outlined two populations of subtly distinct garnet pyroxenite xenoliths. The low Cr (< 1 %) and high Ca (~ 5 %) concentrations from garnet resemble those found in diamond bearing kimberlitic pipes. REE diagrams from LA-ICP-MS trace element data also show similarities to diamond associated garnets. These observations, together with the previous nano-diamond

discovery (Wirth and Rocholl, 2003), indicated that the SLCX samples are potentially ancient, and may even have subcontinental lithospheric mantle origin.

Neither petrography, Energy Dispersive Spectroscopy mapping, nor Back-Scatter Scanning Electron Microscopy imaging revealed zircons for in-situ dating; whole-sample separation was required. In August 2015, seven golf-ball to fist-sized samples were disaggregated using the Queen's University selFrag and mineral separation was conducted at the University of Toronto the following month. Seven datable zircons were discovered in two of the seven samples, with four from SLCX 12 and three from SLCX 47. See Appendix A for details in processing procedures. Preliminary dating by LA-ICP-MS returned ages between 12 Ma (from rim), and 70 Ma (from core). Three of the seven zircons were dissolved for isotopic research, and the remaining four (Figure 3), which are involved in this project, were sent to the University of California for further dating and trace element analysis.

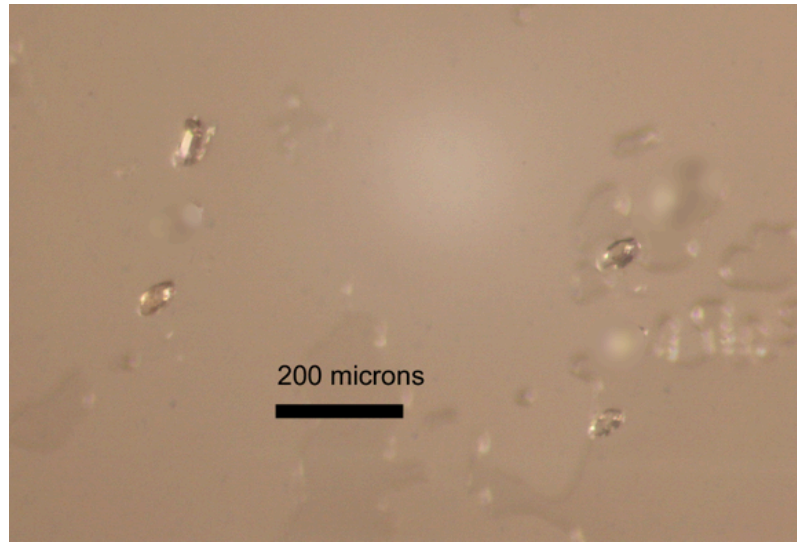


Figure 3 The four zircons involved in this project. Photo taken by Dr. Sandra Kamo, University of Toronto.

2.3 Previous Research

The SLC garnet-bearing pyroxenite xenoliths have attracted significant research interest during the past four decades. The presence of garnets in the mineral assemblage suggests a deep lithosphere to upper mantle asthenosphere origin (Bizimis *et al.*, 2005; Frey, 1980; Frezzotti *et al.*, 1992; Keshav *et al.*, 2007; Lassiter *et al.*, 2000). In 2003, nanocrystalline diamonds were found in silicate melt inclusions (Wirth and Rocholl, 2003), suggesting that at least some of the pyroxenite samples were derived from great mantle depths (> 150 km), though metastable diamonds can apparently form at lithospheric depths. This great depth proposal was strengthened

by another pyroxenite nano-diamond discovery in 2007 (Frezzotti and Peccerillo, 2007), but in this case the diamonds were recovered from carbonate melt inclusions.

Based on more recent studies, the garnet-bearing pyroxenites are generally thought to be high pressure cumulates formed by fractional crystallization of melts that chemically resemble HV lavas (Bizimis *et al.*, 2005; Frey, 1980; Keshav *et al.*, 2007; Sen and Jones, 1990). This conclusion is supported by a layered 'cumulate' texture, high Fe/Mg ratios, low abundances of incompatible elements and Hf-Nd-Sr-Pb systematics. Although it is agreed that the xenoliths represent samples of the mantle beneath Oahu, the depth where crystallization happened is controversial (Keshav and Sen, 2003; Keshav *et al.*, 2007; Lassiter *et al.*, 2000; Sen *et al.*, 2005), and estimates vary from the lower lithospheric mantle to asthenosphere.

So far, no U-Pb zircon geochronology data on the SLC xenoliths have been published in the literature because zircons have never been found. Based on the radiogenic Os composition and the positive correlation between $^{187}\text{Os}/^{188}\text{Os}$ and $^{187}\text{Re}/^{188}\text{Os}$ ratios, it was inferred that the pyroxenite xenoliths formed at 80-100 Ma, with the formation of the oceanic lithosphere beneath Oahu (Lassiter *et al.*, 2000). However, recent work suggests that the high abundance of

unradiogenic Os was produced by sulphide assimilation (Sen *et al.*, 2010). Bizimis et al. (2005) suggested that, based on Lu-Hf and Sm-Nd isotopic equilibrium between garnet and clinopyroxene and the reconstructed bulk rock composition, the garnet-bearing pyroxenite xenoliths should have a near zero-age, thus they cannot have formed at \sim 100 Ma at the Pacific mid ocean ridge. However, in a study on spinel lherzolite (occurring together with the pyroxenite) conducted by the same research group, it was suggested that the lherzolites represent ancient (> 2 Ga) recycled lithosphere entrained in the mantle plume based on a Hf-Os isotopic study (Bizimis *et al.*, 2007). Considering that the pyroxenites can occur as veins in lherzolite, the great variation in model ages between the two rock types lead to doubt about the validity of these model ages. The ages assumed that there was no alteration after formation of the rock, which might be invalid if HV melts have metasomatized these xenoliths during the transportation process (Ducea *et al.*, 2002). Therefore, the zircon U-Pb ages given by this study and associated zircon, garnet and clinopyroxene geochemistry have the potential to provide new insights into the formation of these xenoliths.

CHAPTER III ANALYTICAL TECHNIQUES

3.1 Petrographic Analyses

Petrographic analysis was conducted using a Nikon LV100 petrographic microscope, with photos taken using a Nikon D300 digital camera attached to the microscope. Prior to the electron microprobe (EMP) work, a Tescan Mira3 XMU Field Emission Scanning Electron Microscope with an Oxford Aztec X-Max energy-dispersive spectrometer (EDS) system was used to study the thin sections, identify minerals and select grains for EMP analyses. An Oxford Instruments Nordlys electron backscattered detector (EBSD) supplied back-scatter images.

3.2 Major Elements from EMPA

Major element concentrations of clinopyroxene, orthopyroxene, garnet and olivine were acquired using wavelength dispersive spectroscopy on a Cameca SX5 Field Emission Electron Microanalyser (EMP) at the University of British Columbia, Okanagan, Fipke Laboratory for Trace Element Research (FiLTER), in Kelowna, British Columbia, Canada. The EMP analyses were made at 15 keV accelerating voltage, with a 20 nA beam current, and a 10 μm beam size.

Each oxide was calibrated by a standard with known and relatively abundant major element concentrations. Ti, Na and K were calibrated on hornblende, Ca was calibrated on apatite, Si was calibrated on omphacite, Mn used spessartine garnet, Cr was calibrated on chromite, Fe and Mg were calibrated on olivine, Ni used millerite and Al was calibrated on almandine garnet.

The EMP work was completed in three days. In most cases three analyses were attained on each mineral in each of the seven slides, and an average composition calculated. Duplicates and repeat measurements were made on different days. Smithsonian olivine, anorthite and hornblende with known composition (Table 3.1) served as external standards to determine precision and accuracy, and check performance of the instrument. Eight measurements were performed on each mineral, four at the start and four at the end of the analysis periods. Precision and accuracy are reported in Table 3.2 as percent relative standard deviation (%RSD) and mean percent error (MPE) with calculation equations in the Table 2.2 footnote. Accuracy and precision for major oxides (> 5 wt%) of each day's measurement are better than $\pm 5\%$ and 2 %, respectively (Table 3.2). As a check on data quality, all clinopyroxene, garnet, orthopyroxene and olivine analyses from the xenoliths had major element oxide totals between 98.5 wt% and

101.5 wt%. As a further check, stoichiometry was calculated on the basis of 6 O for Cpx and Opx, 12 O for garnet and 4 O for olivine, and all analyses have total cations within \pm 2 % of the ideal number.

Table 1 Major Element Compositions of Standards

	Hornblende (wt%)	Anorthite (wt%)	Olivine (wt%)
SiO ₂	41.46	44.00	40.81
Al ₂ O ₃	15.47	36.03	
Fe ₂ O ₃	5.60		
FeO	6.43	0.62	9.55
MgO	14.24	0.02	49.42
CaO	11.55	19.09	0.05
Na ₂ O	1.91	0.53	
K ₂ O	0.21	0.03	
TiO ₂	1.41	0.03	
P ₂ O ₅	0.01		0.00
MnO	0.15		0.14
Cr ₂ O ₃			
NiO			0.37
H ₂ O	1.21		
Total	99.64	100.33	100.29

*Reference minerals were provided by the Department of Mineral Sciences of the Smithsonian Institution.

Table 2 Precision and Accuracy of Each Major Element

Oxide	Day1			Day2			Day3			Standard Recommend (wt%)
	Mean (wt%)	MPE %	%RSD	Mean (wt%)	MPE %	%RSD	Mean (wt%)	MPE %	%RSD	
SiO ₂	43.92	-0.19	0.42	43.80	-0.46	0.30	43.71	-0.66	0.61	44.00
TiO ₂	1.45	2.48	1.92	1.42	0.80	2.11	1.42	0.98	1.06	1.41
Al ₂ O ₃	35.61	-1.16	0.48	35.63	-1.11	0.36	35.02	-2.81	0.47	36.03
Cr ₂ O ₃	0.01		73.24	0.01			37.03	0.02		79.68
FeO	9.84	3.05	0.70	9.90	3.69	1.32	9.83	2.97	0.88	9.55
MnO	0.12	-18.33	35.92	0.15	-3.33	11.66	0.13	-10.83	11.26	0.15
NiO	0.35	-5.41	9.04	0.36	-3.72	15.15	0.38	1.69	6.80	0.37
MgO	49.17	-0.50	0.55	49.28	-0.29	0.39	49.23	-0.38	0.32	49.42
CaO	19.67	3.05	0.58	19.59	2.61	0.43	19.48	2.06	0.39	19.09
Na ₂ O	2.27	18.91	1.70	2.27	18.72	1.02	2.27	19.04	0.94	1.91
K ₂ O	0.22	5.95	7.50	0.22	3.57	5.36	0.22	3.57	7.27	0.21

*Total Fe is given as FeO. MPE% = mean percent error = $\frac{100\%}{n} * \sum_{t=1}^n \frac{\text{measured}(t) - \text{recommend}}{\text{recommend}}$, where n = total number of measurements = 8, t = number of measurements, measured values are given in Appendix B. %RSD = relative standard deviation = $\frac{\text{the sample standard deviation}}{\text{sample mean}} * 100\%$.

3.3 Trace Element Concentrations from LA-ICP-MS

The trace element composition of clinopyroxene, orthopyroxene, garnet and olivine was determined using a laser ablation inductively coupled plasma quadrupole mass spectrometry (LA-ICP-QMS) system at the University of Windsor, Great Lakes Institute for Environmental Research (GLIER), Windsor, Ontario, Canada. The system comprises a Photon machines Excite 193 ultra short pulse Argon Fluoride Excimer laser ablation system coupled to an Agilent 7900

fast-scanning quadrupole inductively coupled plasma mass spectrometres (ICP-QMS). A mixed gas flow with argon and helium was used to deliver the aerosol generated in the ablation chamber to the ICP-QMS. The operating parameters are listed in Table 3.3.

Table 3 LA-ICP-QMS Operating Parameters

LA-ICP-QMS parameters	Unit	Value
RF power	W	1250
Carrier gas flow rate (Ar)	L/min	0.8
Cell gas flow rate (He)	L/min	0.36
Sampling arm gas flow rate (He)	L/min	0.84
Laser fluence (energy)	J/cm ²	3.46 (50 %)
Laser rep rate	Hz	20
Spot size	µm	25
Scan pattern		line & spot
Scan rate	µm/s	5

Due to the small size of three target minerals in SLCX 12, measurements on the seven samples were completed in three runs. The measurement sequence (sample and standards) is listed in Table 3.4. Forty one elements, including major elements and trace elements, were quantified. The signal file generated from the LA-ICP-MS was reduced with IOLITE software to yield actual element concentrations. NIST SRM 610 served as an external standard using the concentrations in (Jochum et al., 2011). Si concentrations from EMP analyses of all minerals acted as the internal standard for the 36 reported trace elements.

Table 4 Order of Measurements

Run	Thin Section/Standard	Laser Mode	Mineral
1	NIST 610	Linear	
1	NIST 610	Linear	
1	BCR-2G	Linear	
1	BCR-2G	Linear	
1	SLCX 26	Linear	2 Cpx, 1 Opx, 1 Gt
1	SLCX 47	Linear	4 Cpx, 3 Gt, 2 Ol
1	SLCX 25	Linear	3 Cpx, 3 Opx, 2 Gt, 1 Ol
1	SLCX 12	Linear	2 Cpx, 2 Opx, 2 Gt
1	NIST 610	Linear	
1	NIST 610	Linear	
1	BCR-2G	Linear	
1	BCR-2G	Linear	
2	NIST 610	Spot	
2	NIST 610	Spot	
2	BCR-2G	Spot	
2	BCR-2G	Spot	
2	SLCX 12	Spot	1 Cpx, 1 Opx, 1 Gt
2	NIST 610	Spot	
2	NIST 610	Spot	
2	BCR-2G	Spot	
2	BCR-2G	Spot	
3	NIST 610	Linear	
3	NIST 610	Linear	
3	BCR-2G	Linear	
3	BCR-2G	Linear	
3	SLCX 45	Linear	2 Cpx, 1 Ol
3	SLCX 21	Linear	1 Cpx, 1 Gt
3	SLCX 11	Linear	2 Cpx, 1 Opx, 2 Gt, 2 Ol
3	NIST 610	Linear	
3	NIST 610	Linear	
3	BCR-2G	Linear	
3	BCR-2G	Linear	

*One clinopyroxene, one orthopyroxene and one garnet from the SLCX 12 were ablated under a spot laser mode due to the small size.

Duplicate analyses of USGS glass standard BCR-2G (Table 2.5) were made in order to estimate precision and accuracy. The precision is reported as %RSD and the accuracy is reported as MPE%. Concentration data, except As, were calibrated using values from Jochum *et al.* (2005). Concentrations in BCR-2G, which was treated as unknown, agree well with the recommended values. Precision for Sc, Ti, V, Mn, Co, Zn, Rb, Sr, Y, Zr, Nb, Ba, La, Ce, Pr, Nd, Eu, Tb, Ho, Hf, Ta, and U is better than 5 %; 5 %-10 % for Cu, Cs, Sm, Gd, Dy, Er, Yb, Pb, and Th; 10 %-20 % for others. Cr has a large variation in precision (> 20 %). Accuracy for the majority of detected elements is better than \pm 2.5 %, except for Cr, which has low abundances in BCR-2G. Although NIST SRM 610 (Jochum *et al.*, 2011) is used as an external standard, estimates of precision and accuracy using it produce similar numbers for all elements (except for Cr) compared to BCR-2G.

Table 5 Analyses of BCR-2G

	Section1			Section2			Section3			Recommend
	Mean	MPE	%RSD	Mean	MPE	%RSD	Mean	MPE	%RSD	
Sc	32.9	-0.14	2.99	33.2	0.76	5.42	33.2	0.52	3.04	33
Ti	1.41E+4	-0.20	2.40	1.41E+4	0.11	2.87	1.41E+4	-0.04	2.79	14100
V	425	0.11	2.49	426	0.35	3.26	425	0.12	2.86	425
Cr	18.6	11.76	23.10	16.7	0.59	24.02	19.1	15.74	29.77	17
Mn	1.55E+3	-0.16	2.34	1.55E+3	-0.19	2.50	1.55E+3	0.02	2.42	1550
Co	38.1	0.26	0.57	38.1	0.26	3.14	38.0	-0.07	1.73	38
Ni	13.2	1.54	10.16	13.0	0.00	6.75	13.2	2.12	10.00	13
Cu	21.4	2.02	7.92	21.6	3.10	8.23	21.6	3.12	8.00	21
Zn	126	1.16	4.09	125	0.16	5.23	125	-0.22	1.28	125
As	469			188			543			
Rb	47.0	0.11	1.37	46.9	-0.21	2.73	47.1	0.16	2.41	47
Sr	342	-0.02	2.77	337	-1.31	4.00	341	-0.17	2.86	342
Y	35.0	-0.02	3.39	34.4	-1.36	7.78	34.9	-0.29	3.94	35
Zr	183	-0.34	2.82	185	0.50	4.26	184	-0.05	3.20	184
Nb	12.5	-0.36	3.10	12.5	-0.08	2.19	12.7	1.50	4.16	12.5
Sb	0.357	2.43	10.52	0.238	-32.14	200.00	0.374	8.07	17.14	0.35
Cs	1.18	2.26	6.37	1.16	0.00	1.86	1.16	0.32	2.82	1.16
Ba	684	0.22	2.76	687	0.62	3.74	684	0.22	3.48	683
La	24.6	-0.39	3.38	24.8	0.30	2.69	24.7	0.08	3.41	24.7
Ce	52.8	-0.94	4.01	53.5	0.52	4.18	53.2	-0.09	2.91	53.3
Pr	6.73	0.49	4.42	6.74	0.75	7.32	6.71	0.26	3.81	6.7
Nd	28.8	-0.30	4.76	28.9	0.09	5.02	28.9	0.09	4.18	28.9
Sm	6.58	-0.04	5.42	6.58	0.53	12.97	6.59	-0.04	0.23	6.59
Eu	1.98	0.51	2.51	2.00	2.41	14.98	1.98	0.63	4.52	1.97
Gd	6.66	-0.48	7.45	6.76	0.97	8.66	6.71	0.04	4.35	6.71
Tb	1.02	0.15	3.67	1.01	0.00	11.74	1.02	0.29	2.92	1.02
Dy	6.48	0.85	6.89	6.49	1.67	15.42	6.44	0.00	0.63	6.44
Ho	1.27	0.00	4.86	1.29	2.17	13.48	1.29	1.36	4.01	1.27
Er	3.71	0.47	5.71	3.71	0.74	10.46	3.71	0.27	1.80	3.70
Yb	3.39	0.00	5.40	3.39	0.07	5.00	3.38	-0.29	4.13	3.39
Lu	0.508	1.54	11.35	0.515	5.86	29.84	0.51	2.24	9.08	0.50
Hf	4.84	-0.05	1.91	4.83	0.00	8.00	4.89	1.29	8.87	4.84
Ta	0.782	0.35	4.56	0.785	1.28	13.28	0.781	0.16	1.99	0.78
Pb	11.0	0.16	5.08	11.0	0.41	4.89	11.0	0.25	1.48	11
Th	5.87	-0.34	5.95	5.88	-0.08	8.02	5.91	0.17	2.38	5.9
U	1.70	0.74	3.34	1.69	0.15	1.01	1.70	0.89	5.35	1.69

* MPE% = mean percent error = $\frac{100 \%}{n} * \sum_{t=1}^n \frac{\text{measured (t)} - \text{recommend}}{\text{recommend}}$, where n = total number of measurements = 4, t = number of measurement, measured values are given in

Appendix. %RSD = relative standard deviation = $\frac{\text{the sample standard deviation}}{\text{sample mean}} * 100 \%$.

Recommend BCR-2G values are from Jochum *et al.*, (2005).

3.4 Zircon Dating and Trace Element Concentration Profiling

Zircon U-Th/Pb isotopic and trace element data were acquired simultaneously at the University of California, Santa Barbara using a Photon Machines 193 nm ArF Excimer laser ablation system connected via split stream to a multi-collector Nu Plasma (U-Th-Pb data) and an Agilent 7700S Quadrupole (trace element data) inductively-coupled plasma mass spectrometer. Analytical procedures are outlined in (Cottle *et al.*, 2013; Kylander-Clark *et al.*, 2013) with modifications described in (McKinney *et al.*, 2015). Data were collected over a single analytical session with the laser operated at a spot size of 24 μm , 2 Hz frequency, a laser energy of 100 % of 3 mJ (equating to a fluence of $\sim 1.5 \text{ J/cm}^2$) and 160 shots per analysis that produced pit depths of $\sim 12 \text{ um}$. U-Th/Pb age and trace element concentration data reduction, including corrections for baseline, instrumental drift, mass bias, down-hole fractionation and uncorrected age calculations were carried out using Igor Pro and the plugin Iolite v. 2.5 (see Paton *et al.* (2010) for details on data reduction methodology).

A primary reference zircon '91500' (1065 Ma Pb/U ID-TIMS age, (Wiedenbeck *et al.*, 1995))

was used to monitor and correct for instrument drift, mass bias, and down-hole inter-element

fractionation for zircon unknowns. A secondary reference zircon, 'GJ1' (601.86 ± 0.37 Ma,

Horstwood *et al.*, (2016) ID-TIMS age) was analyzed concurrently and treated as an unknown to

assess accuracy and precision. During the analytical period, repeat analyses of GJ1 gave a

weighted mean $^{206}\text{Pb}/^{238}\text{U}$ age of 602 ± 2 Ma (MSWD = 1.1, n = 9). Trace element

concentrations were normalized to GJ-1 reference zircon using the values of (Liu *et al.*, 2010).

Typical uncertainties (2σ) are 5 % for elemental concentrations > 1 ppm. All uncertainties for the

age data are quoted at 2σ and include contributions from the reproducibility of the reference

materials for $^{207}\text{Pb}/^{206}\text{Pb}$, $^{206}\text{Pb}/^{238}\text{U}$ and $^{207}\text{Pb}/^{235}\text{U}$.

CHAPTER IV RESULTS

4.1 Petrography

Seven samples from the Salt Lake Crater Xenolith suite were examined in detail. Among all samples, clinopyroxene (Cpx) was the dominant phase, which gave these ultramafic rocks the name pyroxenite. Orthopyroxene (Opx) was observed in five samples, and is often present as the second dominant phase. Garnet (Gt) was widely present in all samples but could only be identified in SLCX 45 using back scatter images and EDS/EMP analyses. Olivine (Ol), though present in four samples, was not an abundant constituent (< 5% in most of slides). Spinel (Sp) and other accessory minerals only had minor modal percentages.

Due to the large crystal size of clinopyroxenes (up to 25 mm), it was difficult to accurately estimate the modal proportion for each phase because the estimated value from thin section may not reflect the actual phase distribution in coarse grained rock samples. A summary of the mineral mode and assemblages in samples is listed in Table 4.1. In the following sample/mineral descriptions, abbreviations are defined as follows: PPL = plane polarized light, XPL = cross-polarized light, RL = reflected light and EBS = electron back scatter image. Text below provides

detailed mineralogy and textures in the seven samples examined, with emphasis on the two samples (SLCX 12 and SLCX 47) that yielded zircons. Groups are divided based on petrographic features. Representative images of all samples appear in Figure 4.

Overall, the samples share similar granular texture (Figure 4 a, f), with extensive fluid inclusions in clinopyroxene and olivine (Figure 4 b). Most of mineral grains, especially large ones, are highly fractured. Clinopyroxene and olivine are usually present as primary phases. In contrast, orthopyroxene and garnet have bimodal sizes: euhedral to subhedral larger grains and anhedral smaller grains (Figure 4 d, e). The later are more likely to have formed later because they occur as blebs in primary phases or fill interstitial spaces between clinopyroxenes. Locally Clinopyroxenes show triple-junction grain boundaries (Figure 4 c). Spinel tends to occur in the core of euhedral garnet grains, though it is also present within clinopyroxene grains. Sulphide phases are locally present in all seven samples.

Table 6 Petrographic Features of Seven SLC Samples

Sample	Minerals	Size & Shape	Texture
SLCX 11	75 % Cpx + 1 % Opx + 14 % Gt + 10 % Ol	Cpx \leq 3 mm, subhedral to anhedral	Ol included in Gt
		Opx \leq 0.5 mm, anhedral	Opx included in Ol
		Gt \leq 2 mm, subhedral	Cpx included in Ol
		Ol \leq 2 mm, subhedral	
SLCX 12 (yields zircon)	60 % Cpx + 30 % Opx + 10 % Gt	Cpx \leq 5 mm, subhedral	Opx have bimodal sizes
		Opx \leq 3 mm, subhedral	Opx blebs in Cpx
		Gt \leq 2 mm, anhedral	
SLCX 21	67 % Cpx + 5 % Opx + 25 % Gt + 3 % Spl	Cpx \leq 25 mm, euhedral to subhedral	Opx blebs in Cpx
		Opx \leq 0.5 mm, anhedral	extensive presence of fluid inclusions
		Gt \leq 5 mm, subhedral	Sp occurring as core of Gt
		Spl \leq 2 mm, anhedral	
SLCX 25	50 % Cpx + 30 % Opx + 10 % Gt + 10 % Ol	Cpx \leq 3 mm, subhedral	Ol&Gt form corona around Opx
		Opx \leq 1.5 mm, euhedral	triple junction
		Gt \leq 0.5 mm, anhedral	
		Ol \leq 0.5 mm, anhedral	
SLCX 26	60 % Cpx + 10 % Opx + 25 % Gt + 5 % Spl	Cpx \leq 10 mm, subhedral	Sp occurring as core of Gt
		Opx \leq 6 mm, euhedral to subhedral	
		Gt \leq 5 mm, euhedral	
		Spl \leq 1.5 mm, anhedral	
SLCX 45	65 % Cpx + 30 % Gt + 5 % Ol	Cpx \leq 4 mm, subhedral	Cpx have bimodal sizes
		Gt \leq 0.3 mm, subhedral	
		Ol \leq 0.5 mm, anhedral	
SLCX 47 (yields zircon)	60 % Cpx + 25 % Gt + 15 % Ol	Cpx \leq 3 mm, subhedral	Cpx&Gt locally included in Ol
		Gt \leq 6 mm, euhedral to subhedral	
		Ol \leq 5.5 mm, euhedral to subhedral	

* Modal percentages are approximate; they were determined by visual estimation. However, since the rock is coarse grained and phases can occur in clusters, the estimated modal percentages from thin sections may not represent the true modal percentages in samples.

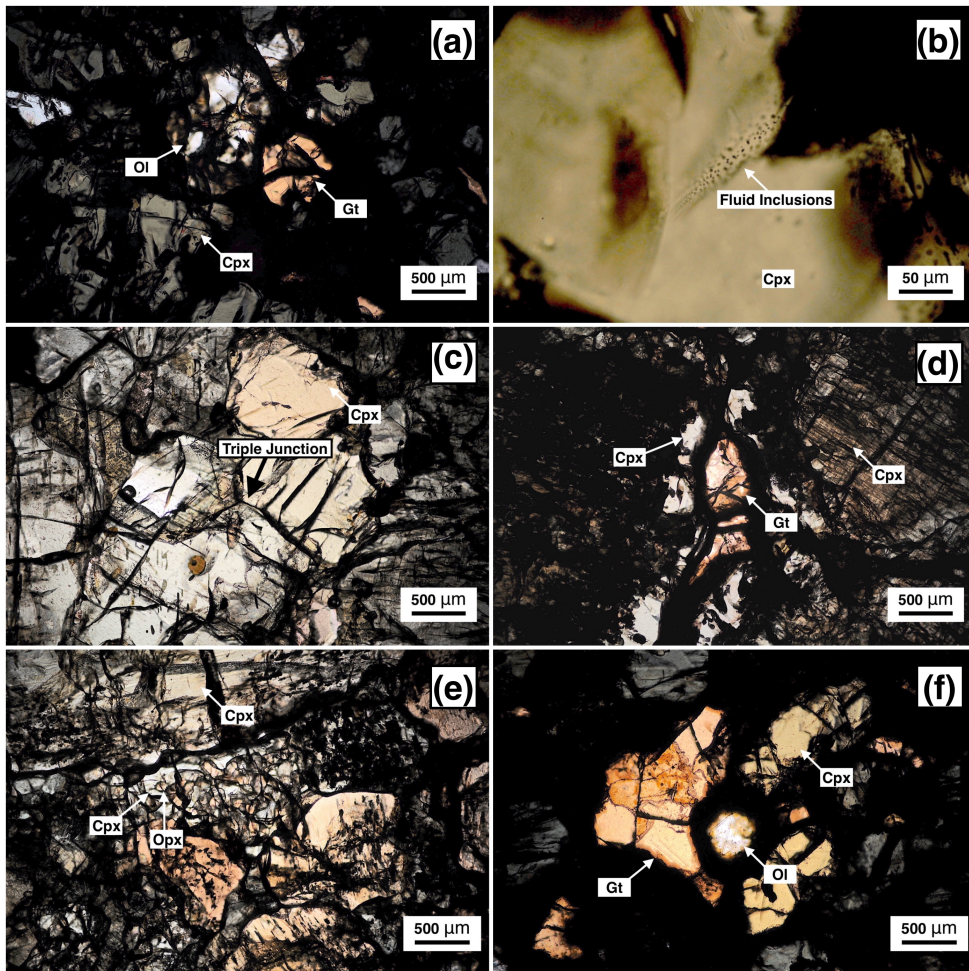


Figure 4 Plane polarized photomicrographs of representative mineral assemblages and textures. (a) Granular texture (b) fluid inclusions in Cpx (c) a triple junction (d) an anhedral garnet filling interstitial space (e) orthopyroxene exsolution blebs in a clinopyroxene (f) an olivine enclosed by garnet and clinopyroxene

A volatile-rich, nearly opaque, high relief phase is common in SLCX 47. Locally, it occurs in olivine cores, but more commonly, it forms granular crystals in contact with clinopyroxene or

garnet (Figure 5 a). Under reflected light, the phase seems composed of two components, one is in dark colour and the other in light colour.

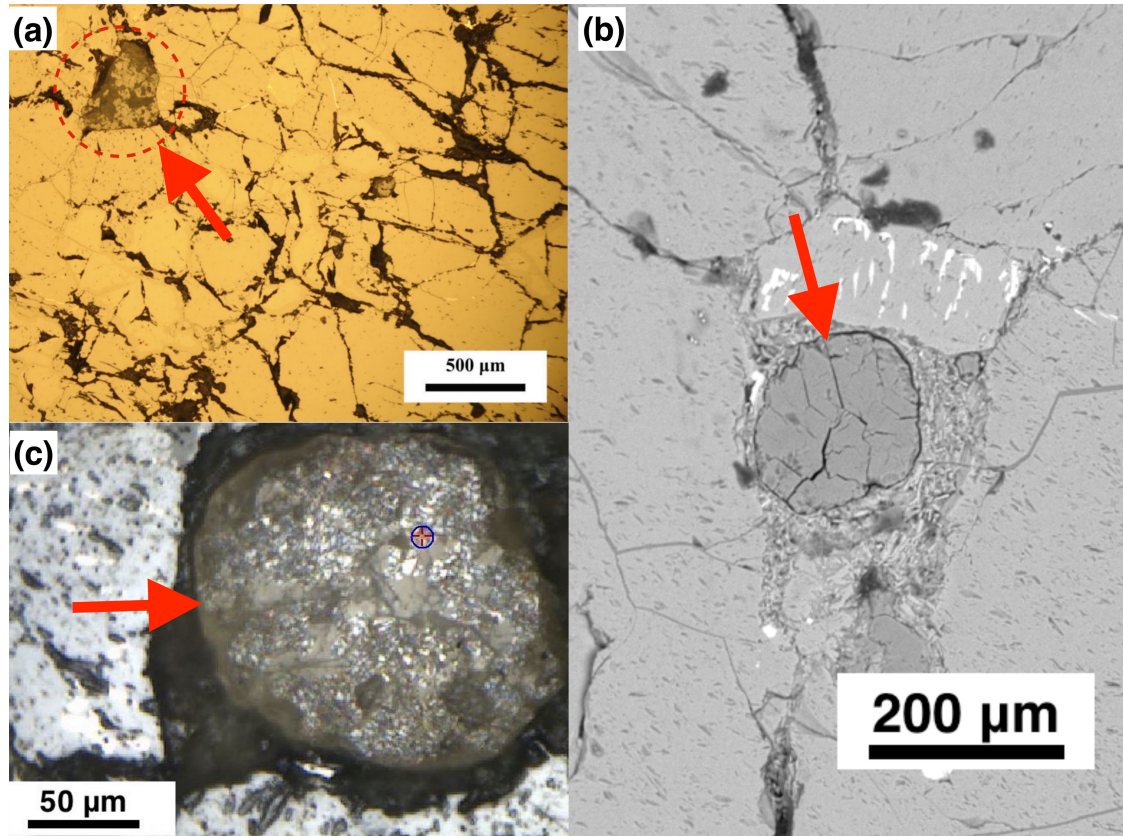


Figure 5 Photograph of the unknown phase. (a) under reflected light (b) back scattered electron image (c) under the electron microscope.

Table 7 SEM-EDX Composition of the Unknown Phase

Element	wt%	SD
O	45.79	0.08
Na	1.75	0.22
Al	13.93	0.06
Si	25.55	0.09
Cl	0.34	0.14
K	6.00	0.06
Ca	5.74	0.14
Fe	0.30	0.08
Ba	0.60	0.1
Total	100	

*Element concentrations are reported in weight percent (wt%). SD stands for standard deviation for three analyses. Results were normalized to 100 % and are semi quantitative.

4.2 Elemental Mapping

In samples SLCX 26 and SLCX 21, large garnets generally have a spinel core (Figure 6).

Back-scatter images and wave-length dispersive maps show that the garnet is homogeneous in terms of Fe, Mg, Ca, Si and Mn. Mg concentrations are the same in garnet and spinel but the latter shows lower Ca, Si, Mn and higher Fe. At the edge of the garnet, high Mg# anhedral olivines form a corona, and are enclosed in clinopyroxenes.

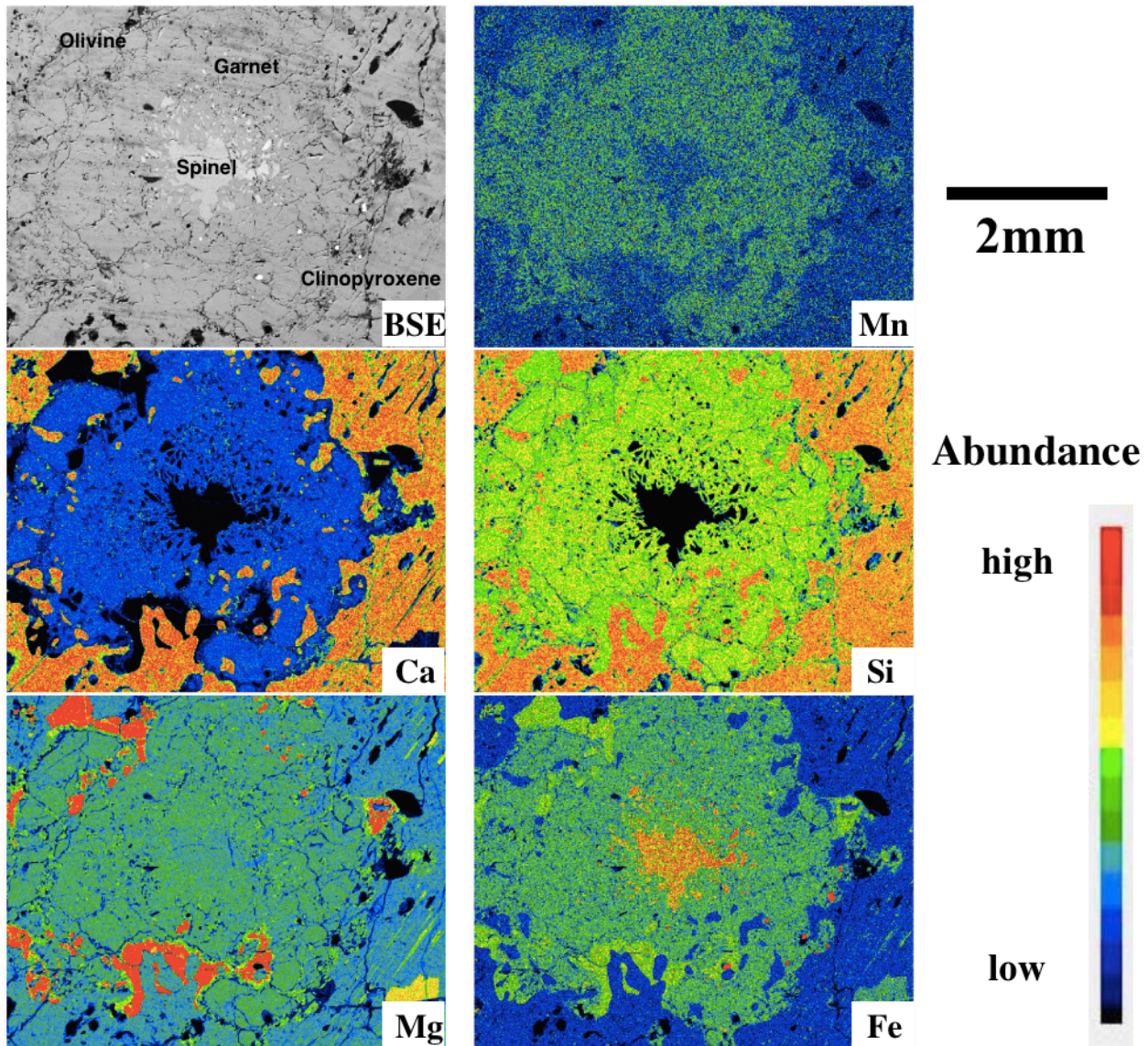


Figure 6 Back Scattered Electron Image and elemental maps of SLCX 26 garnet. The map reveals a spinel-garnet-olivine-clinopyroxene complex.

4.3 Major Element Mineral Analyses

Fifty one grains of clinopyroxene, orthopyroxene, garnet and olivine were selected for analysis from seven samples with three analyses on each grain for major element concentrations.

The data (Tables B.1-B.4) are average compositions for each individual grain where there was restricted chemical variation.

4.3.1 Clinopyroxene

Clinopyroxene (Cpx) is the dominant phase in all seven samples. Compositions are restricted to the diopside and augite fields (Figure 7). Although clinopyroxene sizes show a bimodal distribution, the small, anhedral grains exhibit little chemical variation from large, subhedral ones. The low Cr_2O_3 (< 0.5 wt%), high Al_2O_3 (6.0 wt%-8.3 wt%) and high FeO (5.3 wt%-8.3 wt%) characteristics are consistent with those reported in the literature for other SLC garnet pyroxenite xenoliths (Bizimis *et al.*, 2005; Keshav *et al.*, 2007).

The Mg# of most clinopyroxenes is between 78 and 83, but those in SLCX 21 have values between 72 and 73 (Figure 8). Mg# shows a systematic relationship to FeO, but correlation with other oxides are more scattered. Analyses form four clusters (SLCX 21, SLCX 45, SLCX 12 and SLCX 11 + 25 + 26 + 47), but all samples appear subtly distinct. Sample SLCX 21 clinopyroxenes are most distinct with low Si and high Ti, Al, Fe, Na contents.

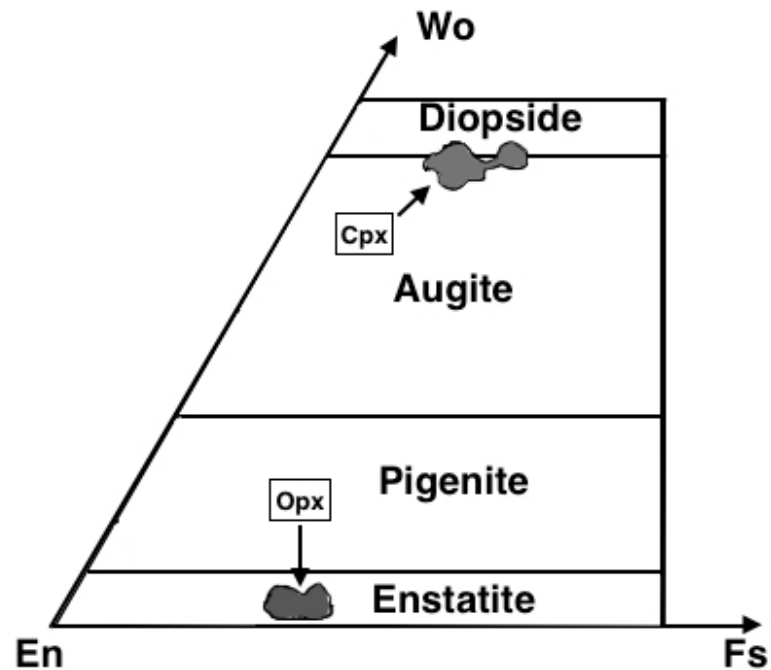


Figure 7 Compositions of SLCX clinopyroxenes and orthopyroxenes. Samples are plotted on a wollastonite (Wo), enstatite (En) and ferrosilite (Fs) classification diagram.

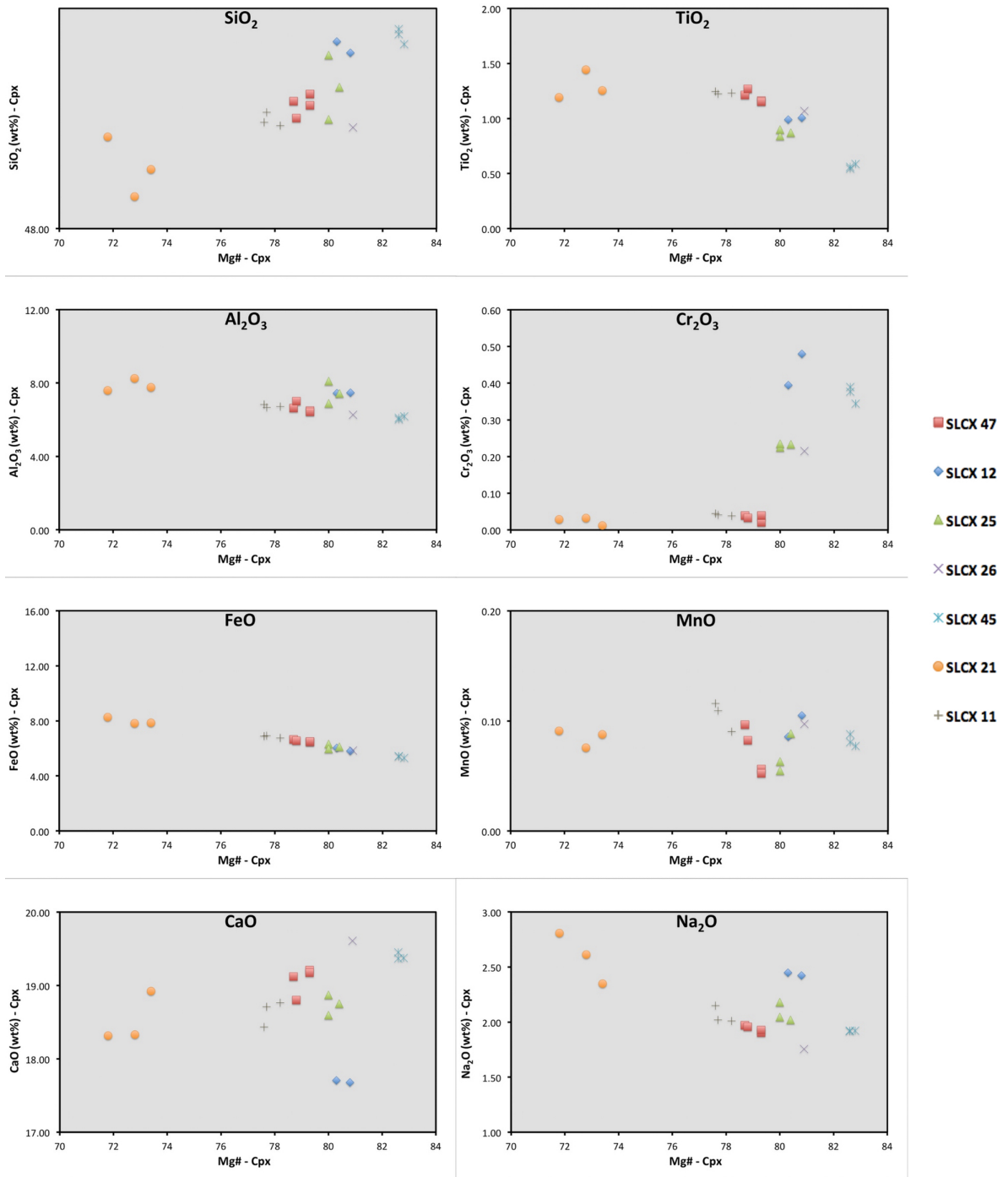


Figure 8 Plots of Mg# versus major element oxides for clinopyroxenes.

4.3.2 Orthopyroxene

Orthopyroxene (Opx) found in four samples is Enstatitic (Figure 7) and has high Al_2O_3 (4.0 wt%-5.6 wt%), consistent with analyses reported in the literature (Bizimis *et al.*, 2005; Keshav *et al.*, 2007; Sen, 1988). Mg# varies from 79 to 82, with low values associated with $\text{FeO} \leq 13.1$ wt%. Based on Mg# (Figure 9), the analyses form two clusters, but the clusters are not sample dependent. For example, the low Mg# cluster contains one SLCX 11 and two SLCX 25 analyses. Analyzed orthopyroxenes from the same sample are not chemically homogenous, and this heterogeneity has also been reported in the literature (Keshav *et al.*, 2007; Sen, 1988). Considering the major element composition data together with petrography, it turns out that orthopyroxenes with low Mg# are usually enclosed by olivines, but high Mg# Opx is an exsolution phase in clinopyroxene, or forms small, granular, anhedral crystals.

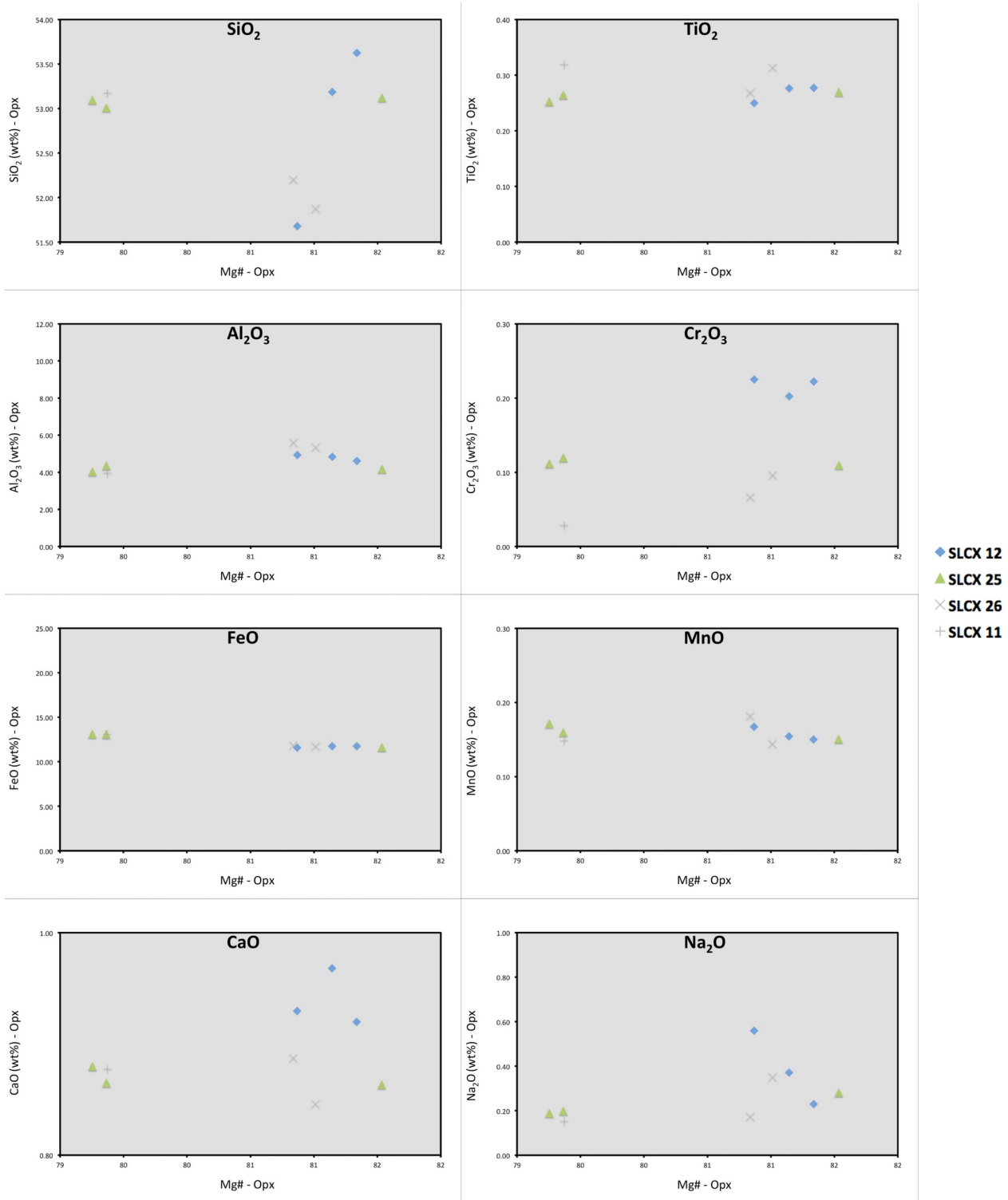


Figure 9 Plots of Mg# versus major element oxides for orthopyroxenes.

4.3.3 Garnet

Both large subhedral, and small anhedral garnets in the samples are chemically unzoned. The Mg# varies from 60.3 to 69.5, which overlies SLC garnet pyroxenite reported in the literature (Bizimis *et al.*, 2005; Keshav *et al.*, 2007; Sen, 1988). Although all garnets are pyropes (Figure 10), analyses form two clusters: one is the SLCX 21 garnets and the other comprises garnets from the rest of the samples.

Garnets with spinel cores in SLCX 21 have higher FeO and lower MgO contents. They resemble garnets exsolved from clinopyroxene reported by Keshav and Sen, (2003). The authors argued that garnet exsolution was triggered by the addition of kimberlitic melts to the primary olivine-bearing pyroxenite. The extensive presence of fluid inclusions in SLCX 21 supports that hypothesis. Although garnets from both SLCX 21 and SLCX 26 developed spinel cores, garnets from SLCX 26 have similar compositions to garnets from spinel-absent samples.

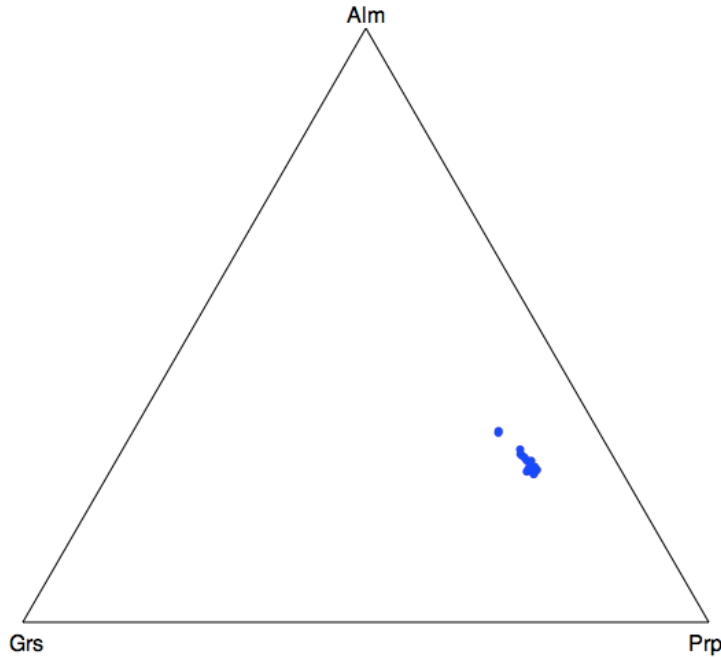


Figure 10 Ternary diagram of garnet compositions. End-members are pyrope (Prp), almandine (Alm) and grossular (Grs).

4.3.4 Olivine

Olivines from any single xenolith have equivalent fosterite (Fo) contents, but between samples they vary from Fo₇₇ to Fo₈₂, values similar to those reported in the literature (Keshav *et al.*, 2007; Sen and Jones, 1990). The anhedral small olivines from SLCX 45 are distinct and have the highest Fo content (Fo₈₂). The concentrations of Cr₂O₃ are below 0.02 wt% and NiO varies from 0.27 to 0.37 wt%.

4.4 Trace Elements

Trace element concentrations were measured on clinopyroxenes, orthopyroxenes, garnets and olivines, but only clinopyroxenes and garnets provide useable REE data, because orthopyroxenes and olivines have concentrations typically below detection limits. Thus, this section only presents clinopyroxene and garnet trace element data. Data appear in Table B.5 and B.6.

4.4.1 Clinopyroxene

Figure 11 shows clinopyroxene compositions on a primitive mantle (McDonough & Sun, 1995) normalized diagram. The data reported here are largely identical to those for Salt Lake Crater pyroxenite xenolith clinopyroxenes reported by Bizimis *et al.* (2005), suggesting that they are from the same sample group. An exception is that Ba in SLCX 12-Cpx1 and SLCX 25-Cpx3 is much higher, and Lu in SLCX 47-Cpx3 appears much lower than in the primitive mantle. Three samples have clinopyroxene with high Pb abundances, and two of them (SLCX 12 and SLCX 47) yielded zircons. High Ba could be due to sampling Ba-enriched fluid inclusions during laser ablation. High Pb in SLCX 11, 12 and 47 clinopyroxene may be due to dissolution

of ancient zircons, release of radioactive Pb, and growth of new clinopyroxene (see details in Discussion).

The Light Rare Earth Element (LREE) and Middle Rare Earth Element (MREE) abundances in clinopyroxene can be almost an order of magnitude higher than in primitive mantle (Figure 11). The Heavy Rare Earth Elements (HREE) are depleted, and Bizimis et al. (2005) suggested that this is due to the presence of coexisting garnets, which are highly HREE compatible. The High Field Strength Elements (HFSE; e.g. Nb, Zr) and Large Ion Lithophile Elements (LILE; e.g. Ba) are generally depleted compared to the adjacent REE. This HFSE depletion feature has also been reported in pyroxenite xenoliths recovered from Hannuoba, North Chia Craton (Xu, 2002). Note that in Xu's paper, the REE trend is nearly identical to our result. HFSE depletion in pyroxenite clinopyroxene may be a chemical fingerprint for subcontinental lithospheric mantle.

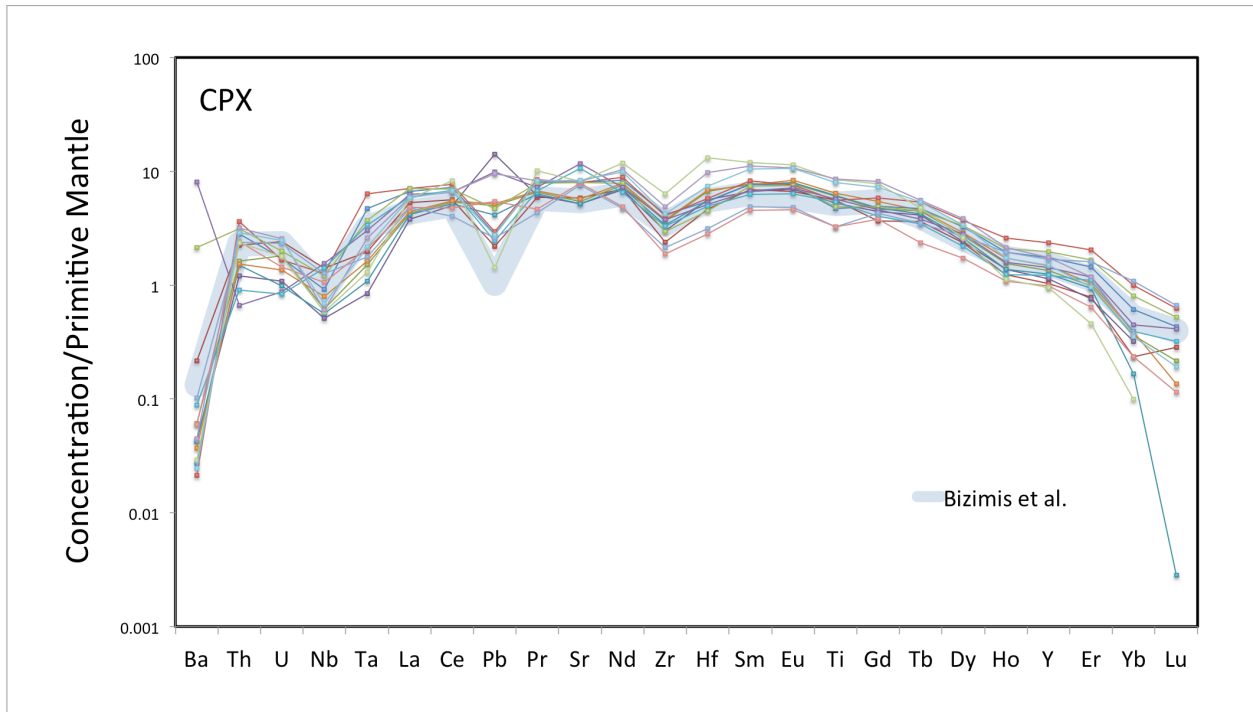


Figure 11 Primitive mantle normalized trace element abundances in SLC clinopyroxenes.
The grey field data are for similar SLC rocks studied by Bizimis et al. (2005). Primitive mantle normalizing values are from McDonough & Sun (1995).

Figure 12 reveals Mg# vs. compatible/incompatible elements plots. It appears that for clinopyroxenes, the Mg# does not have a linear correlation with either compatible elements (Sc, Ni) or incompatible elements (Sr, Nb). This observation is consistent with the argument given by Bizimis *et al.* (2005), in which they suggested the change in clinopyroxene composition is not associated with increasing degrees of melting.

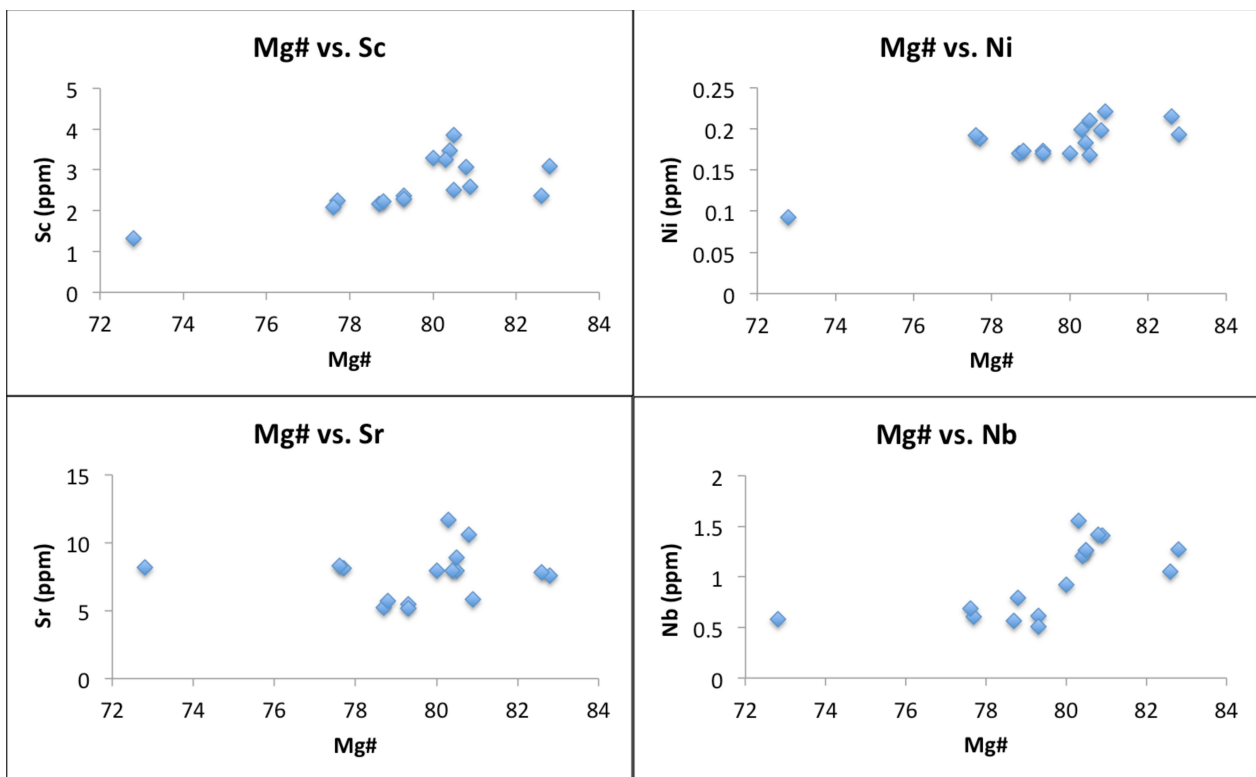


Figure 12 Mg# vs. compatible elements (Sc, Ni) and incompatible elements (Sr, Nb) in clinopyroxenes. The element concentrations were normalized by primitive mantle values from McDonough & Sun (1995).

4.4.2 Garnets

All garnets except SLCX 26-Gt1 and SLCX 47-Gt3 display negative Hf anomalies on a primitive mantle normalized diagram (Figure 13). Pb abundances in our samples are ~10x higher than the average values reported by Bizimis et al. (2005), though two of his samples (601 and 714) gave similar high Pb abundances.

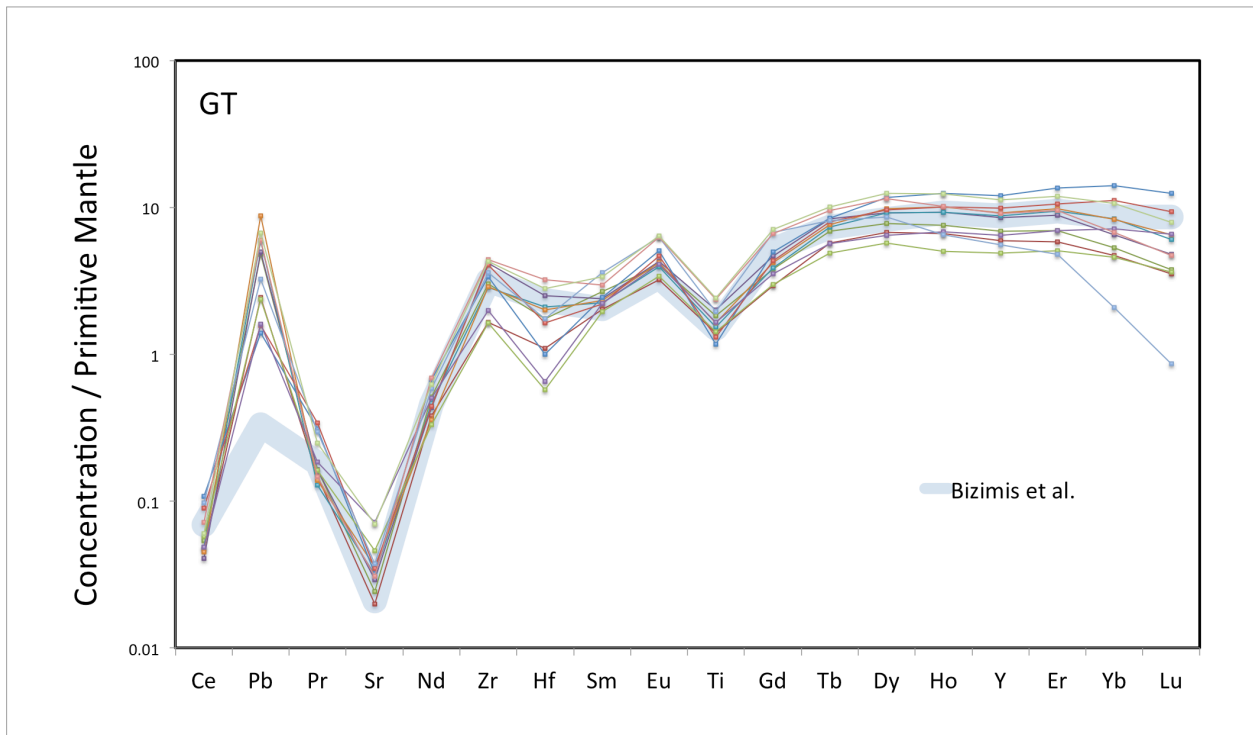


Figure 13 Primitive mantle normalized trace element abundances in SLC garnets. The grey field data are average trace element concentrations for similar SLC rocks studied by Bizimis et al. (2005). Primitive mantle normalizing values are from McDonough & Sun (1995).

4.5 Zircon Petrochronological Signatures

4.5.1 Morphology and texture of zircons

The four dated zircons (Zircon1, Zircon2 from SLCX 47; Zircon3, Zircon4 from SLCX 12) are euhedral, tabular to prismatic and show tetragonal dipyramidal forms (Figure 3), indicating a magmatic or high-grade metamorphic origin (Hoskin & Schaltegger, 2003). The LA-ICP-MS

depth profiling data (Table B.7-B.12) especially for Zircon1 and Zircon3 indicate the presence of zoned cores, with relatively homogeneous overgrowth rims.

4.5.2 Zircon1 Age and Trace Element Data

Zircon1 is characterized by continuously increasing ages from the rim (~ 13 Ma) to the core (~ 82 Ma) (Figure 14). The average rim gives an age of 13.4 ± 0.2 Ma (2SE), based on data obtained from depths between 0 and 10 μm (Table 4.3). The oldest age, 82.2 Ma, was measured at a depth of 12.05 μm . An average of 76.9 Ma was obtained from analyses between ~ 11.85 μm and 12.15 μm depth. Because the ages given by the core did not form 'plateau' (unlike Zircon3), the 76.9 Ma age represents a minimum date for the core.

Table 8 Summary of Ages of Four Zircons

	Age (Ma)	Depth (μm)
Zircon1 (SLCX 47)	13.4 ± 0.2 (rim)	0-10
	76.9 (core)	11.85-12.15
Zircon2 (SLCX 47)	14.5 ± 0.2	0-11.5
Zircon3 (SLCX 12)	12.9 ± 0.2 (rim)	0-6.25
	80.8 ± 2 (core)	10-11.25
Zircon4 (SLCX 12)	14.2 ± 0.3	0-12.25

*Plots involving zircon trace element concentrations data from depth ranges that coincide with ages in the table.

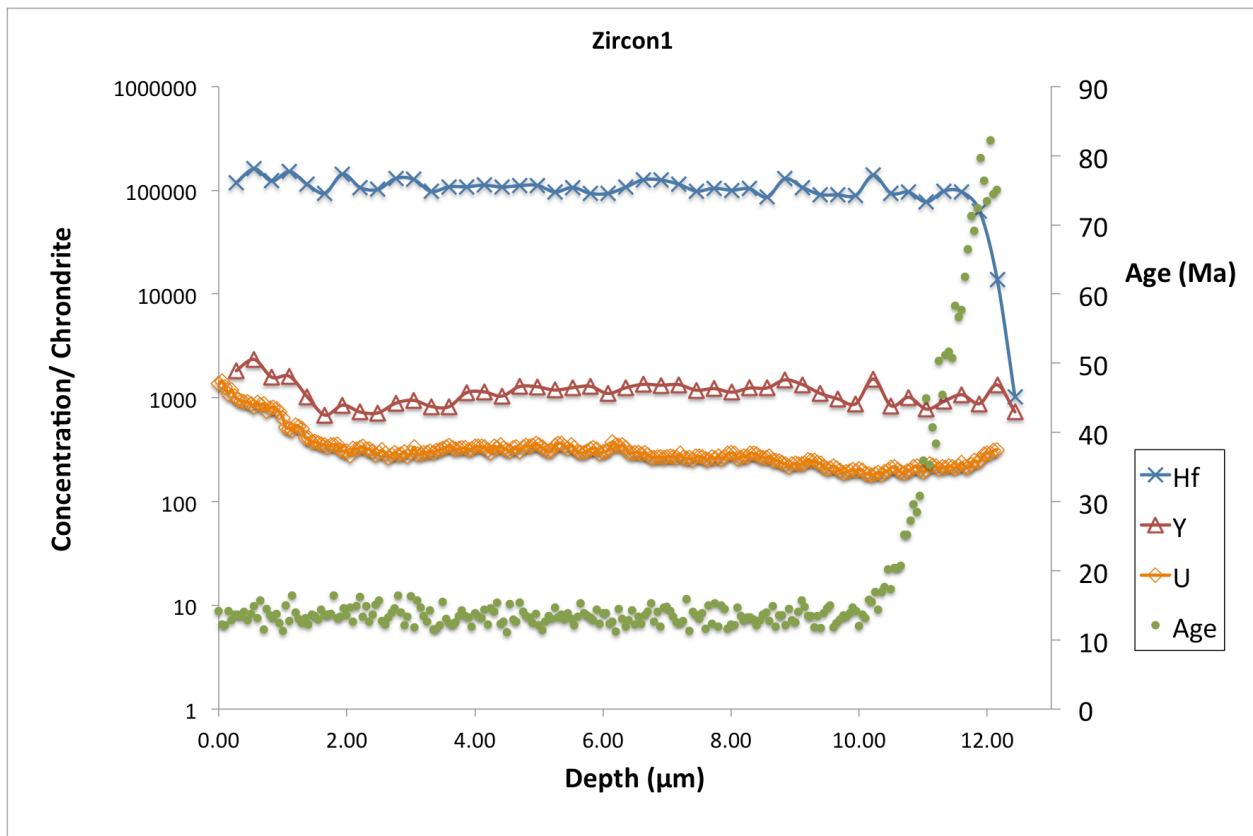


Figure 14 Chondrite-normalized Hf, Y and U concentrations and age profiling data for Zircon1. Chondrite normalizing values are from McDonough & Sun (1995).

Hf is enriched in the zircon, with an average concentration of 9457 ppm (Figure 14). The highest value, 16582 ppm, occurs in the rim, and the lowest, 106 ppm, occurs in the core (Figure 14). Although the Hf abundance shows great variability between the rim and core, the rim (0-10 μm) shows a relatively homogeneous Hf concentration. The overall enriched pattern resembles zircons extracted from mafic rocks, but the 106 ppm given by the core is lower than zircons derived from any known tectonic setting (Belousova *et al.*, 2002). Similar to Hf, Y is enriched in magmatic zircons (Belousova *et al.*, 2002; Grimes *et al.*, 2015; Hoskin and Ireland, 2000), with

abundances up to 8500 ppm (Guo *et al.*, 1996). The Y abundance of Zircon1 ranges from 1070 ppm (core) to 3676 ppm (rim), which is typical of magmatic zircons, but distinct from mantle-derived zircons found in kimberlites (Belousova *et al.*, 1998; Hoskin and Ireland, 2000), which usually have Y below 100 ppm.

Figure 15 shows average chondrite-normalized REE patterns for the rim and the core of Zircon1, with data collected from 0.28 μm to 9.95 μm representing the rim, and 11.88 μm to 12.16 μm representing the core. Ages indicated on the diagram are average U-Pb dates given by the above depths.

The overall chondrite-normalized REE patterns (Figure 15) show HREE (Tb to Lu) enrichment, with La and Pr below the detection limit. Cerium, which can be both trivalent and tetravalent, tends to be more compatible in zircons than La and Pr (Hoskin & Ireland, 2000). Abundances in Zircon1 vary from 0.7 ppm (rim) to 18.3 ppm (core), which is within the range of zircons from various tectonic settings (Belousova *et al.*, 2002). The MREE (Nd to Gd) show increasing chondrite-normalized abundances with decreasing ionic radii, except there is a negative Eu anomaly. The HREE are more abundant than the LREE and MREE with

concentrations between 10^3 and $10^4 \times$ chondrite. Although Lu has a radius more comparable to Zr,

the most abundant element is Yb, ranging from 1235 ppm in the rim to 14 ppm in the core.

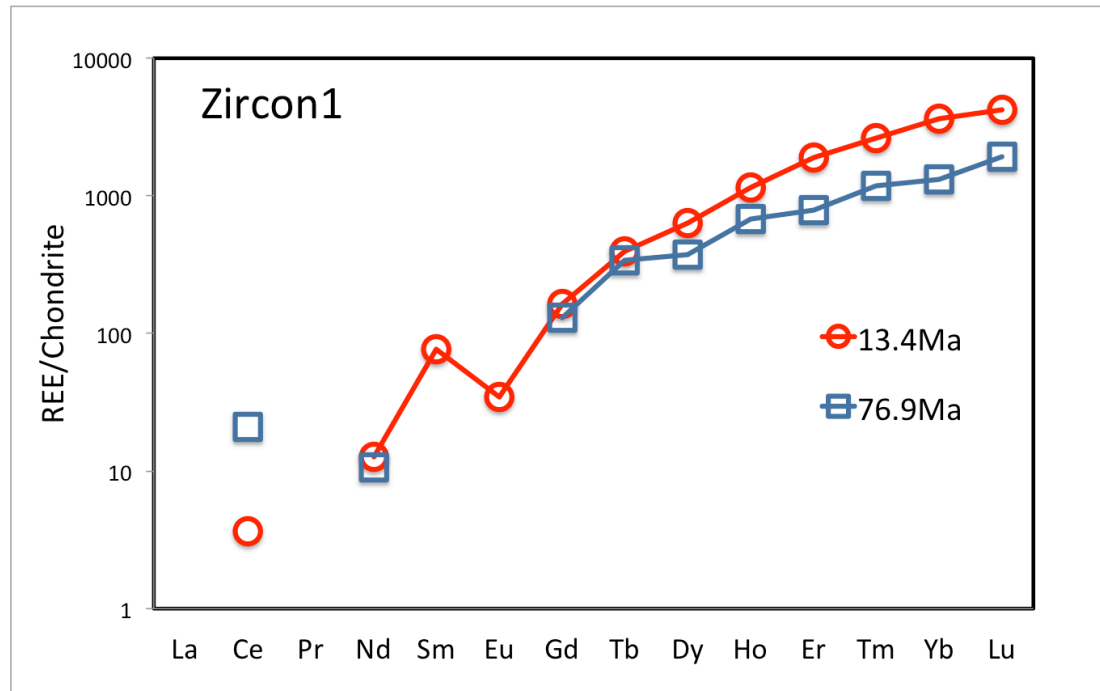


Figure 15 Chondrite-normalized REE patterns for Zircon1. Chondrite normalizing values are from McDonough & Sun (1995).

Overall, both trends have steep positive LREE to HREE slopes (Figure 15), but the rim is more enriched in HREE and depleted in LREE. The core has a normalized Ce value higher than Nd, indicating a potentially large positive Ce anomaly in the core, and a possible smaller anomaly for the rim. A large positive Ce anomaly is a feature of zircons with a magmatic origin, and it is believed to reflect oxidizing conditions (Grimes *et al.*, 2015; Hoskin and Schaltegger, 2003; Liu *et al.*, 2010). Zircons lacking Ce anomalies have only been found in meteorites, lunar

rocks and kimberlites (Belousova *et al.*, 1998; Ireland and Wlotzka, 1992), which are expected to have crystallized under reducing conditions.

4.5.3 Zircon2 Age and Trace Element Data

Dates from Zircon2 form one cluster (Figure 16), with an average age of 14.5 ± 0.2 Ma (2SE) measured between 0 and 11.5 μm , which is comparable to the rim zone of Zircon1. An anomalous age (50.4 Ma) at a depth of 10.1 μm was ignored in calculating the average age. An old core was not discovered.

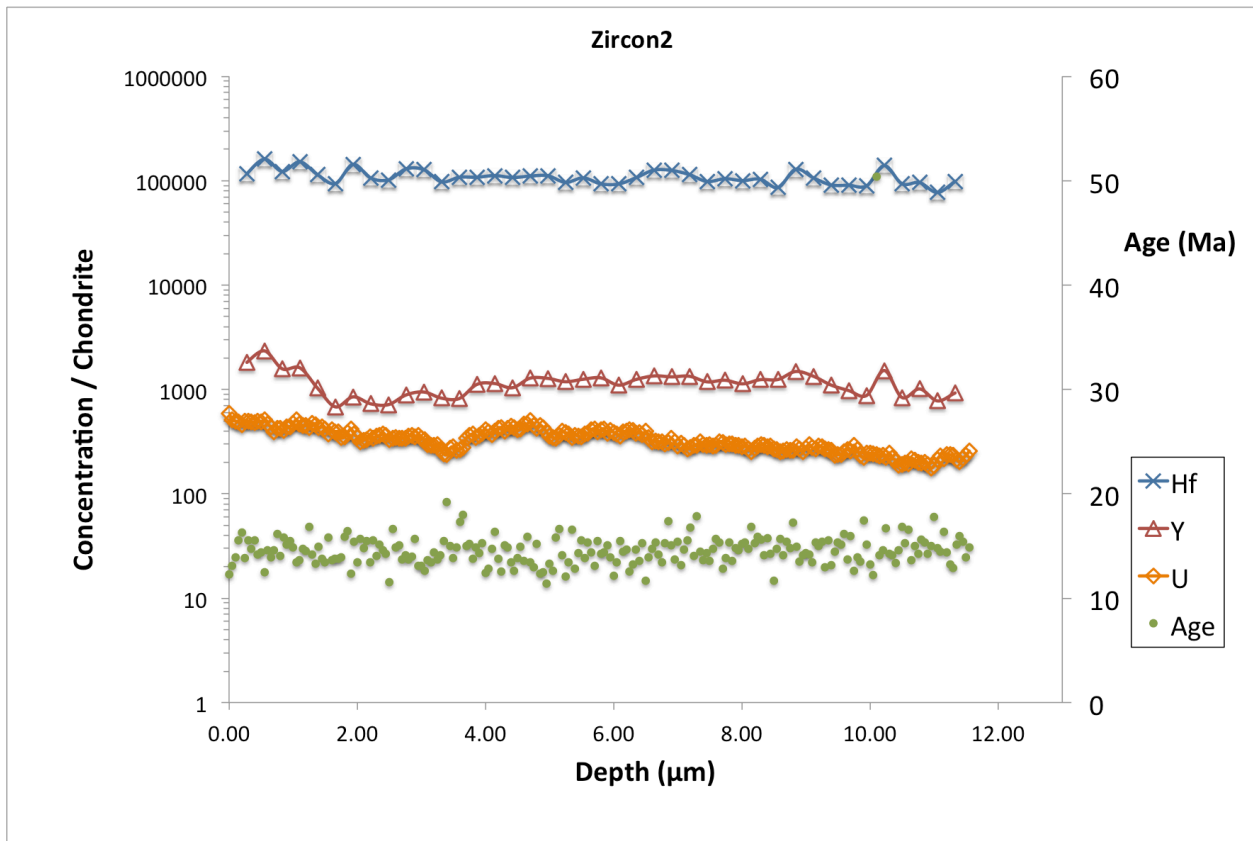


Figure 16 Chondrite-normalized Hf, Y and U concentrations and age profiling data for Zircon 2. Chondrite normalizing values are from McDonough & Sun (1995).

The average Hf content is 10564 ppm, with the highest value of 17163 ppm in the rim and the lowest value of 8049 ppm occurring at the depth of 8.29 μm (Figure 16). These values resemble the Hf enriched rim of Zircon1. The Y contents range from 1289 ppm to 3679 ppm, which is comparable to Zircon1. The Σ REE ranges from 852 ppm to 2457 ppm, with an average of 1466 ppm, which is comparable to the rim zone for Zircon1.

The average chondrite-normalized REE diagram (data collected from 0.28 μm to 11.6 μm) shows a steep, positive, chondrite-normalized REE pattern with a distinct negative Eu anomaly.

The pattern resembles the rim of Zircon1 but lacks a positive Ce anomaly. The LREE are extremely depleted (Figure 17), and both La and Pr fall below the detection limit. The abundance of Ce is comparable to the rim of Zircon1. The MREE, similar to Zircon1, show increasing abundances from Nd to Gd, and a negative Eu anomaly. The HREE are enriched, and the most abundant element is Yb, ranging from 322 ppm to 1053 ppm.

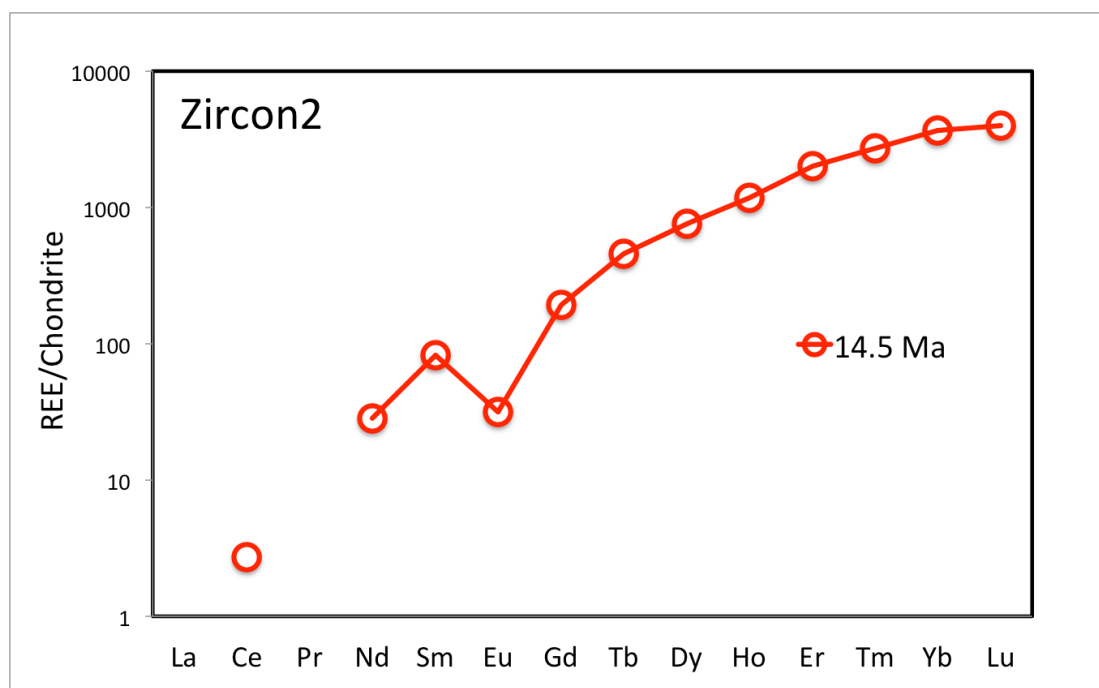


Figure 17 Chondrite-normalized REE pattern for Zircon2. Chondrite normalizing values are from McDonough & Sun (1995).

4.5.4 Zircon3 Age and Trace Element Data

Zircon3 has ages increasing toward the core (Figure 18). The rim (0 to 6.25 μm) gives an average age of 12.9 ± 0.2 Ma (2SE). The core (10 μm to 11.25 μm), unlike Zircon1, shows an 'age plateau' with an average age of 80.8 ± 2 Ma (2SE).

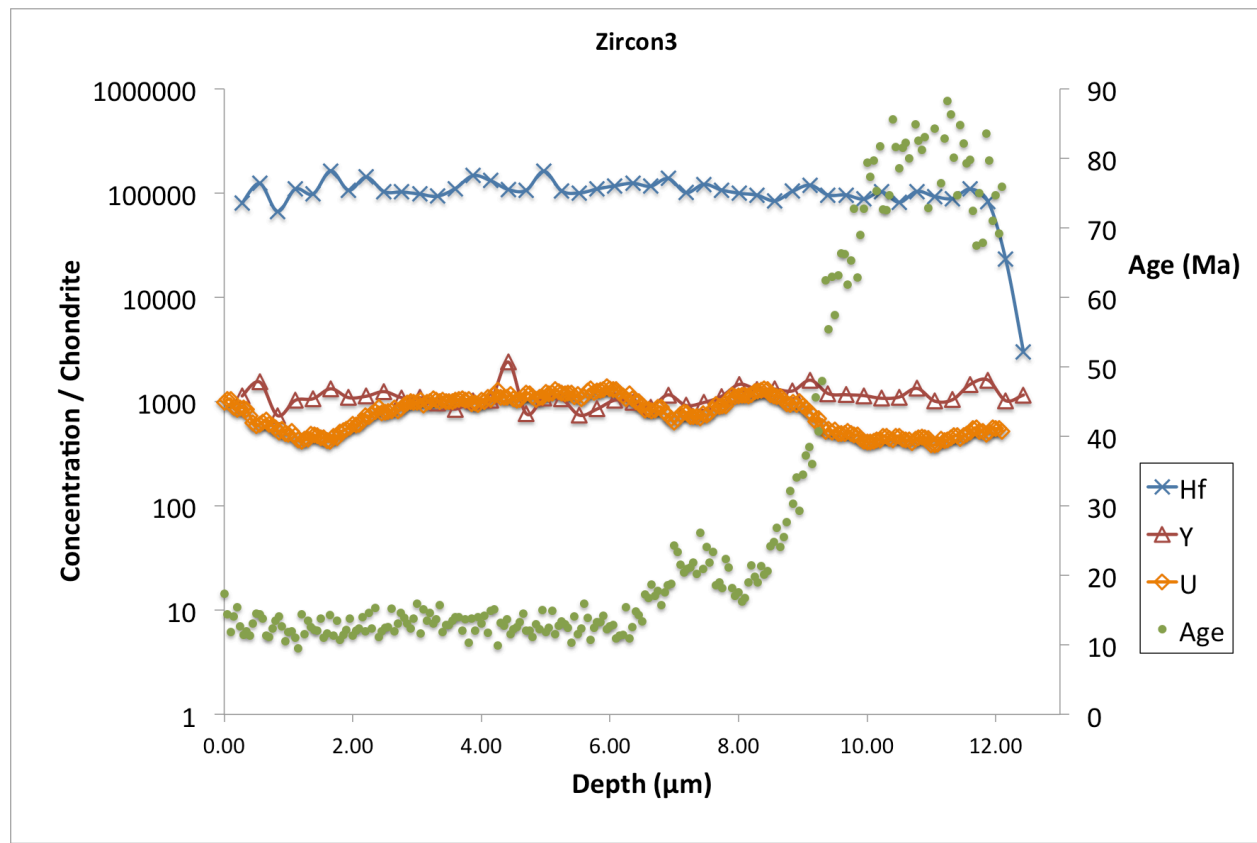


Figure 18 Chondrite-normalized Hf, Y and U concentrations and age profiling data for Zircon3. Chondrite normalizing values are from McDonough & Sun (1995).

Hafnium abundances are similar to Zircon1, with large variability between the young rim and the old core. Concentrations range from 16899 ppm (rim) to 311 ppm (core), with an average of 10702 ppm. Similarities to Zircon1 indicate that although the two zircons occur in

different samples, they could form from similar melts. The Y abundances in Zircon3 range from 1166 ppm to 3762 ppm, with an average of 1806 ppm. These values are comparable to Zircon1, but are much higher than in kimberlitic zircons. The Σ REE ranges from only 127 ppm in the core to 2182 ppm in the rim, with an average concentration of 1561 ppm, and a peak concentration (1934 ppm-2182 ppm) between 6.91 μm and 8.29 μm . This pattern of relative enrichment/depletion with depth is not identical to that in Zircon1.

Overall, the chondrite-normalized REE pattern and REE concentrations for Zircon3 resemble Zircon1 (Figure 19). Similar to Zircon1 and 2, La and Pr are below the detection limit. Cerium increases with depth, reaching a peak of 105 ppm at 10.77 μm , a concentration much higher than in the Zircon1's core. In the rim, the MREE show a U-shaped chondrite-normalized pattern. The rim trend of Zircon3 is distinguished from Zircon1 by the absence of a negative Eu anomaly,

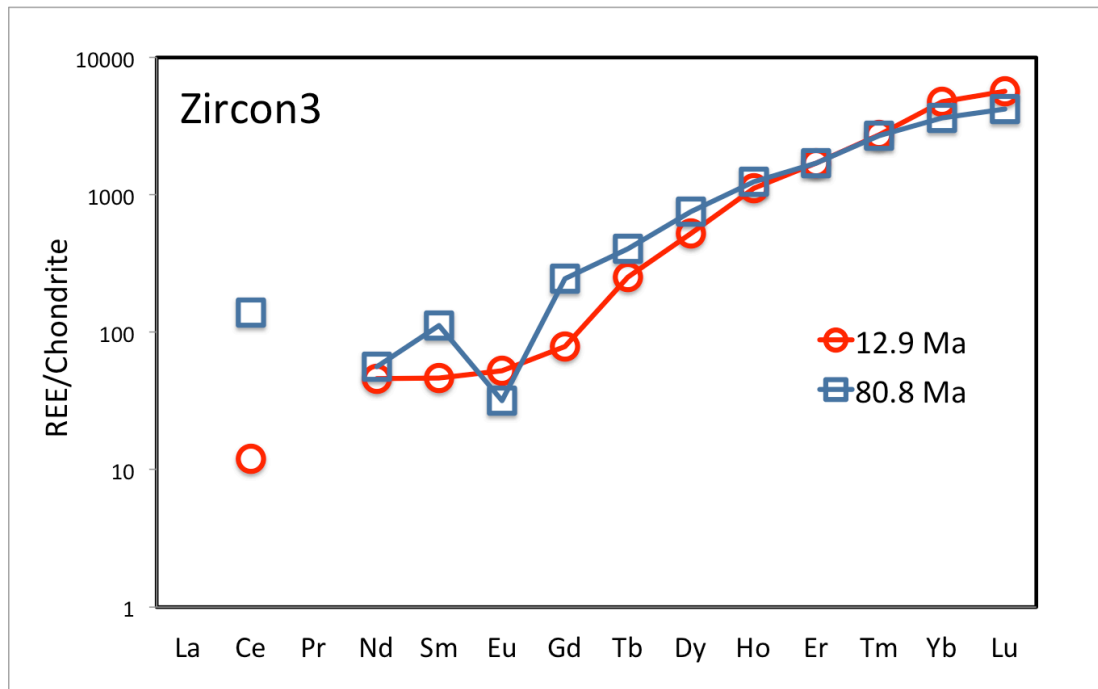


Figure 19 Chondrite-normalized REE patterns for Zircon3. Chondrite normalizing values are from McDonough & Sun (1995).

4.5.5 Zircon4 Age and Trace Element Data

The age given by Zircon4 is 14.2 ± 0.3 (2SE) Ma, which is an average age from U/Pb dates obtained between $0 \mu\text{m}$ and $12.25 \mu\text{m}$ (Figure 20). This age is comparable to the age of Zircon2, and is older than the rim of Zircon1 and 3, but between $11.9 \mu\text{m}$ and $12.25 \mu\text{m}$ ages are older (~ 20 Ma). Furthermore, ~ 20 Ma ages appear several times through the rim. This may be because the laser had partly sampled a portion of the zircon that is older.

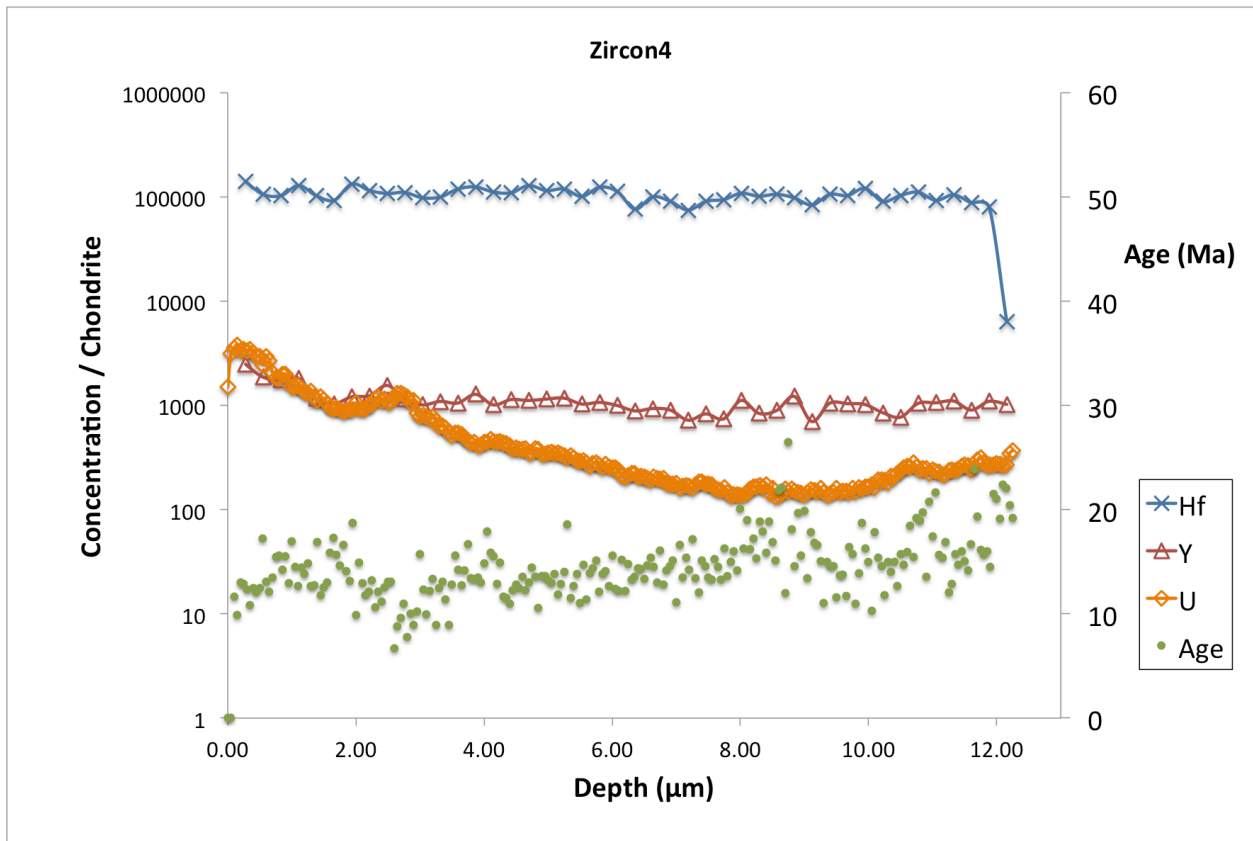


Figure 20 Chondrite-normalized Hf, Y and U concentrations and age profiling data for Zircon4. Chondrite normalizing values are from McDonough & Sun (1995).

The Hf abundance varies from 660 ppm in the inner core (12.16 μm) to 14429 ppm for the rim, with an average of 10074 ppm. Overall, Hf increases from the core to the rim. The Hf abundance shown by this zircon is identical to Zircon2, and comparable to the rim of Zircon3.

The Y abundances of Zircon4 range from 1099 ppm to 3875 ppm, with an average of 1753 ppm. This value is identical to the other three zircons. The abundance increases from the core towards the rim, and Zircon1, 2 and 4 show a jump in Y at the outer (1-2 μm) edge. The ΣREE averages

1408 ppm, varying from 123 ppm (core) to 2841 ppm (rim). Variation is more extensive than in Zircon2. Overall, the Σ REE pattern increases in the rim, similar to that seen in Zircon1.

The chondrite-normalized REE plot (Figure 21) is based on average data obtained between 0 and 12.16 μm at depth. Both La and Pr are below the detection limit. The plot shows a steep positive slope. The lack of a positive Ce anomaly and the presence of a negative Eu anomaly resemble Zircon2 and the rim of Zircon1. Note that the Nd content in Zircon4 is higher than in Zircon2.

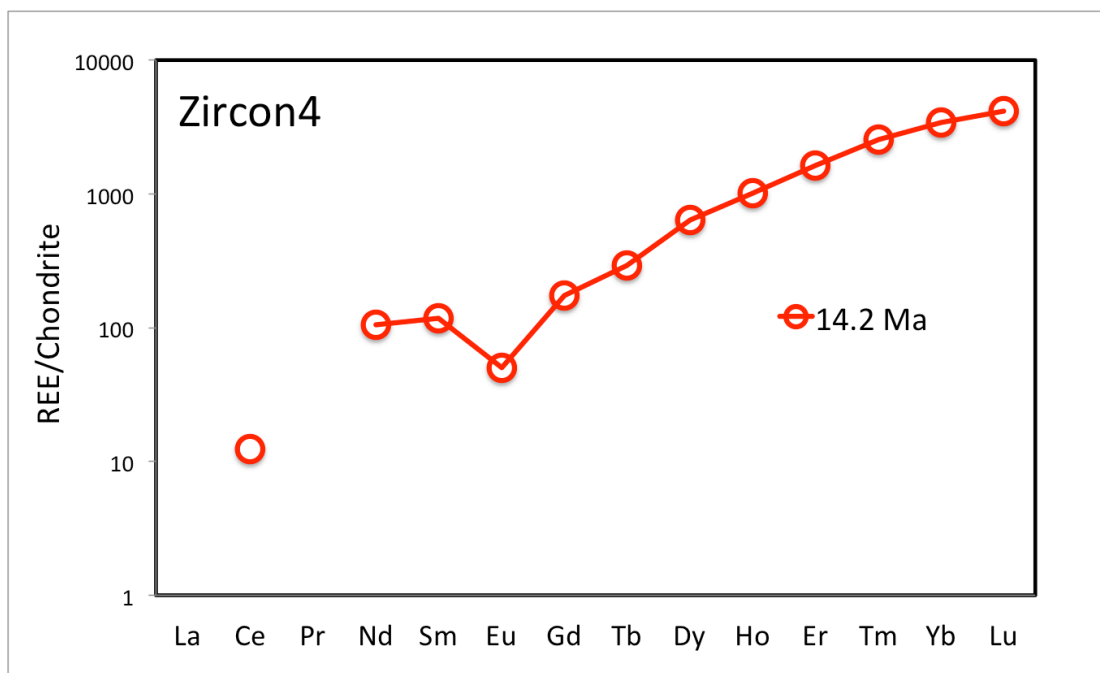


Figure 21 Chondrite-normalized REE pattern for Zircon4. Chondrite normalizing values are from McDonough & Sun (1995).

CHAPTER V DISCUSSION

5.1 Genetic Relationships

It is important to investigate whether the seven samples studied here are genetically related (form from a single magma series). Although clinopyroxene and garnet occur in all samples, olivine was not observed in SLCX 12, 21 and 26, and samples SLCX 45 and SLCX 47 lack orthopyroxene. Considering the great variation of grain sizes and mineral assemblages (Table 4.1), it is unlikely that these samples were derived from the exact same location beneath Oahu. The presence of olivine in four samples indicates they may be more primitive than the other three. Possibly the seven samples can be linked by crystal fractionation process.

To assess genetic relationships, one of the most useful tools is variation diagram. Major element variation diagrams for clinopyroxene and orthopyroxene (Figure 8 & 9) reveal that, except for FeO, there is no linear correlation between Mg# and other major element oxides, and most of the plots show considerable scatter. Although patterns for the low-concentration elements (Mn, Cr) could be affected by detection limits, the scattered CaO and Al₂O₃ plots indicate that the seven samples are not all genetically related.

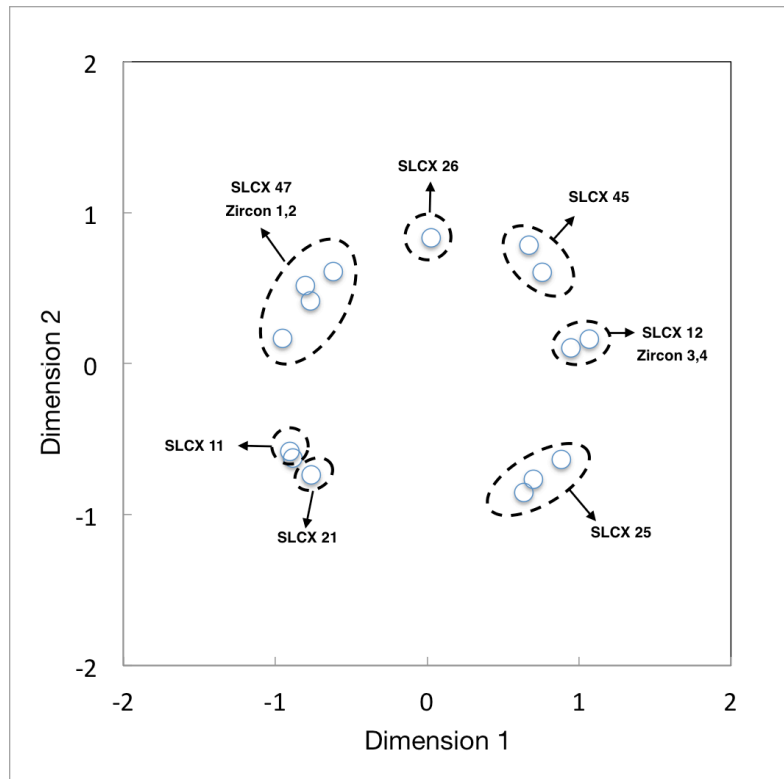


Figure 22 Multi-dimensional scaling comparisons of seven samples based on the overall major, minor and trace element composition of clinopyroxene.

Multi-dimensional scaling (Greenough *et al.*, 2007) is a powerful tool used to uncover relationships within a group of samples. Major, minor and trace element data were used to compare the samples (Figure 22). It appears that there are no clear relationships among the seven samples, though SLCX 21 plots close to SLCX 11, indicating there are no genetic relationships between samples. Each sample has its own distinct geochemical characteristics (Figure 22).

The primitive mantle-normalized trace element patterns for clinopyroxene (Figure 11) reveal that all samples are enriched in LREE, but depleted in HREE. Additionally, similar negative

anomalies in HFSE (Zr, Nb) and LILE (Ba, Pb) occur in most samples. Such chemical characteristics indicate that the melts parental to the pyroxenites formed in the same petrological and tectonic environment. Neither compatible elements (Ni, Sc) nor incompatible elements (Sr, Nb) are linearly associated with Mg# (Figure 12), indicating that the pyroxenites were not crystallized from a single fractionating melt.

5.2 Origin of SLC Xenoliths

Pyroxenites, which comprise around 5 % of the upper mantle, have been widely discussed in the recent literature (Choi and Kim, 2012; Hirschmann and Stolper, 1996; Hirschmann *et al.*, 2003; Kogiso *et al.*, 2003). Pyroxenites are usually attributed to one of three origins: 1) interaction between mantle peridotite and melt/fluid (Liu *et al.*, 2001; Xu, 2002), 2) segments of recycled oceanic crust (Allègre *et al.*, 1983; Pearson *et al.*, 1993), and 3) cumulates precipitated from melts. Origins of the SLC pyroxenites will be assessed based upon chemical signatures exhibited by analyzed phases.

5.2.1 Frozen melt

Since the pyroxenite can occur together with peridotite (Bizimis *et al.*, 2004; Sen *et al.*, 1993), the first question to be answered is whether they represent frozen melt derived from partial melting of the peridotite. Incompatible elements (e.g. REE) should be enriched in the melt during partial melting, and if the melt crystallized to form pyroxenite, these trace elements should be concentrated in crystallized phases. In ultramafic rocks, clinopyroxene is the major reservoir for the REE due the comparable ionic radius between Ca^{2+} and REE^{3+} , and incorporation is enhanced for the HREE (Olin and Wolff, 2010). If the pyroxenites represent frozen peridotite-derived melt, they should hold more $\sum\text{REE}$ than the peridotite. The peridotite clinopyroxenes have $\sum\text{REE}$ ranging from 21 ppm to 95 ppm, with an average of 42 ppm (Bizimis *et al.*, 2004), whereas our clinopyroxenes have $\sum\text{REE}$ ranging from 25 ppm to 48 ppm, with an average of 35 ppm. It appears that the SLCX pyroxenites are more depleted in incompatible elements than the host peridotite. This observation is in contrast with a frozen melt origin for the pyroxenites. Thus the pyroxenites are unlikely to be partial melts derived from associated peridotite.

During partial melting, ratios of elements with similar incompatibility tends to be minimally affected by the degree of melting (Greenough *et al.*, 2007). If the pyroxenites crystallized from a peridotite-derived melt, similarly-incompatible element ratios (E.g. Nd/Sm, Zr/Hf) should be similar for peridotite and pyroxenite. However, it appears that the peridotite ratios are higher and scattered (Figure 23). This, together with the difference in total REE abundances, suggests that the pyroxenites do not represent solidified melt derived from melting of the fertile peridotites, and there is no direct genetic relationship between the two groups of xenoliths.

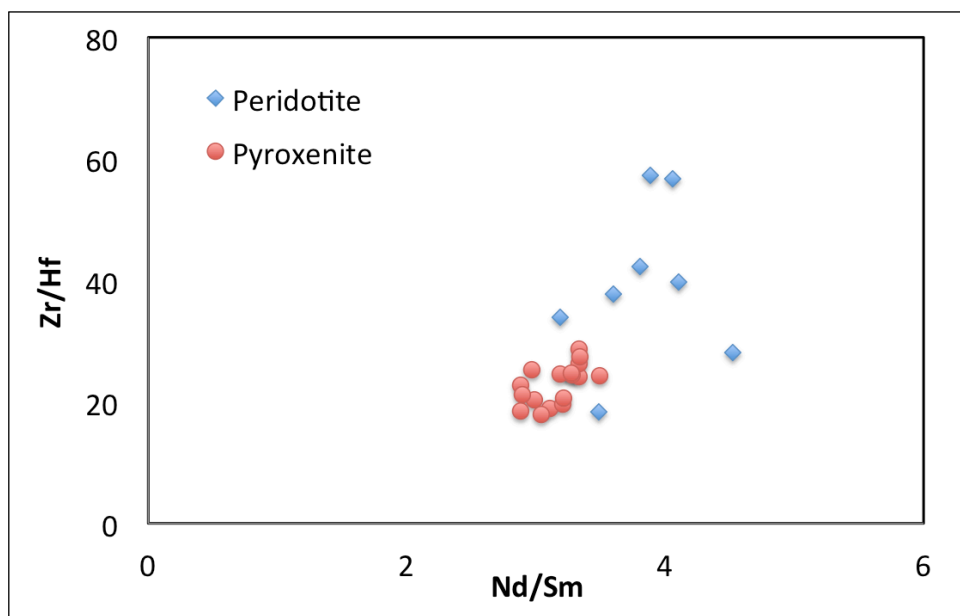


Figure 23 Zr/Hf vs. Nd/Sm ratios of clinopyroxene in peridotite and pyroxenite from the Salt Lake Crater. Peridotite trace element data were derived from (Bizimis *et al.*, 2004).

5.2.2 Recycled oceanic crust

The common occurrence of the chlorine-bearing unknown mineral (Figure 5) indicates that the pyroxenite may be related to recycled oceanic crust which absorbed sea water. However, the absence of Al_2O_3 depletion (< 1 wt%) in orthopyroxene (Figure 9) and the lack of a positive Eu anomaly in clinopyroxene (Figure 11), are in contrast with a conventional recycled oceanic crust model (Allègre & Turcotte, 1986; Kornprobst *et al.*, 1990; Morishita *et al.*, 2003). This indicates the samples are not recycled/recrystallized fragments of oceanic crust. It is difficult to assess the equilibrium between the chlorine-bearing phase and the other minerals (clinopyroxene, garnet, olivine) because without identifying the mineral, partitioning coefficients cannot be compared to literature data. Detailed research on the origin of this phase is beyond the scope of this study.

5.2.3 Cumulate origin

Previous studies concluded that the pyroxenite xenoliths recovered from the Salt Lake Crater are cumulates crystallized at lower lithosphere or even deeper depths as a result of fractional crystallization (Bizimis *et al.*, 2005; Keshav and Sen, 2003; Keshav *et al.*, 2007). Our trace element data show that these pyroxenites are depleted in incompatible elements, which is a

feature commonly attributed to cumulate phases from fractional crystallization (Pearson *et al.*, 1993). Thus, our garnet-bearing pyroxenite xenoliths are considered cumulates formed due to fractional crystallization.

5.3 Source Melt and Petrogenesis of Clinopyroxene and Garnet

5.3.1 Melt composition

It is widely accepted that the parental melt that crystallized the SLC pyroxenite xenoliths was never erupted at the surface (Bizimis *et al.*, 2005; Keshav and Sen, 2003; Lassiter *et al.*, 2000), though the origin of this melt remains unclear. Sen & Jones (1990) suggested that the parental melt of the xenoliths was similar to Koolau tholeiitic magma. However, recent combined Nd-Sr-Hf isotope data and melt composition modelling indicate that there is no apparent genetic relationship between the Koolau tholeiitic magma and the xenoliths, but the melt was compositionally similar to Honolulu Volcanic series magma (Bizimis *et al.*, 2005).

The trace element composition of melts parental to clinopyroxene have been reconstructed by using the equation $C_{melt} = C_{phase}/D_{phase/melt}$, where C_{melt} represents the concentration of a trace element in the melt, C_{phase} represents the element's concentration in a rock forming phase

(clinopyroxene), and $D_{\text{phase/melt}}$ represents the phase/melt partitioning coefficients for each element. Cpx-Gt D values have been experimentally determined for basalt under high temperature-pressure conditions (Hauri *et al.*, 1994).

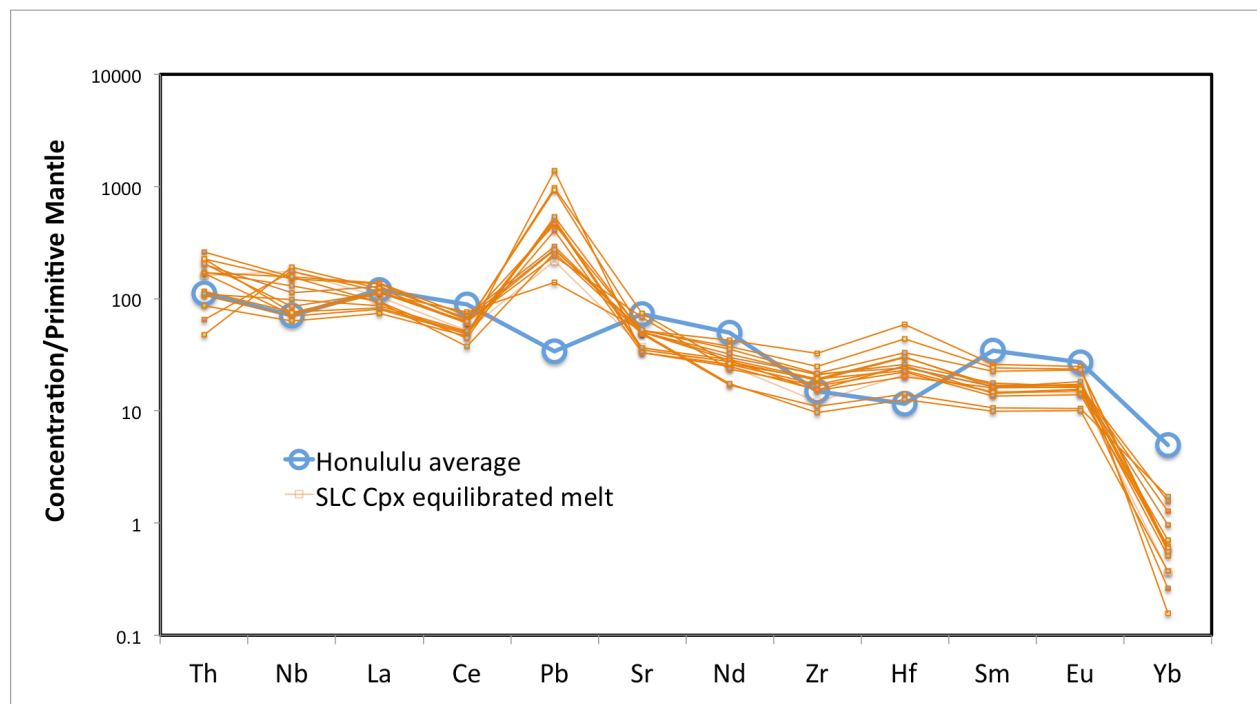


Figure 24 Primitive mantle-normalized trace element composition of melts in equilibrium with clinopyroxene. Partitioning coefficients were from (Hauri *et al.*, 1994). Composition of the primitive mantle is from (McDonough and Sun, 1995). HV data are an average of Honolulu Series volcanic rocks derived by Clague & Frey (1982).

Overall, the parental melts of the clinopyroxene are comparable to the Honolulu Series (Clague & Frey, 1982) with a negative slope from Th to Yb, and absence of an Eu anomaly (Figure 24). However, parental clinopyroxene melts distinguish themselves from the HV lava by showing a strong positive Pb anomaly, subtle positive Hf anomaly and depletion in Yb. The

strong lead anomaly is a signature that can be correlated to Archean age subcontinental lithospheric mantle, and this will be discussed in detail in the next section (Hoffmann 2008).

The equilibrium between clinopyroxene and garnet has been evaluated by comparing calculated Cpx/Gt partitioning coefficients for REE (Figure 25) with values from (Harte & Kirkley, 1997). The calculated partitioning coefficients show considerable similarities to values from the literature, with a negative slope from Ce to Yb, indicating clinopyroxenes are in equilibrium with garnets. This indicates that the inference drawn from the Cpx-equilibrated melt composition could also be applied to garnets.

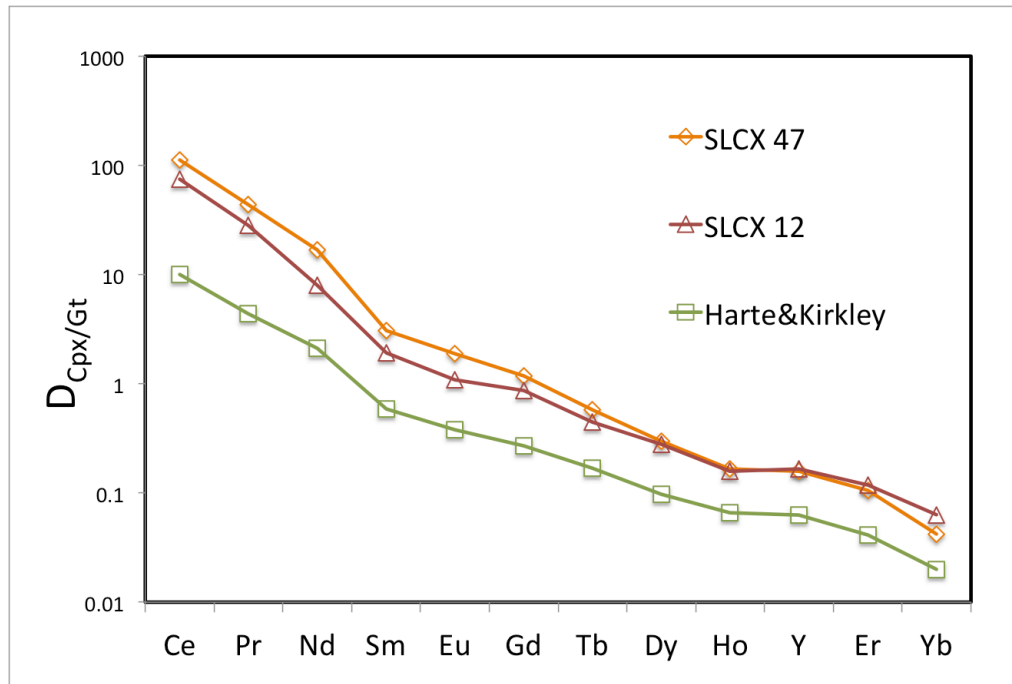


Figure 25 Cpx/Gt partitioning coefficients for REE. Data presented are average partitioning coefficients in SLCX 47 and SLCX 12. Values from (Harte & Kirkley, 1997) are used for comparison.

5.3.2 Pb enrichment and association with subcontinental lithospheric mantle

Lead is a key element for understanding the evolution of the mantle and continental crust (Hoffmann 2008) and may provide useful information on the tectonic environment of formation of the SLCX pyroxenite xenoliths. The calculated melt composition is characterized by anomalous enrichment in Pb, which is a signature commonly observed in xenoliths derived from the Archean subcontinental lithospheric mantle (SCLM) (Arndt *et al.*, 2009; Aulbach *et al.*, 2007; Aulbach, 2012). Greenough & Kyser (2003) suggested that the recycling of oceanic crust/lithosphere during ancient continent formation could result in significant Pb accumulation in the SCLM, which could be subsequently sampled by xenoliths or continental flood basalts. Therefore the parent melt of SLCX could have a SCLM origin. If a fragment of ancient SCLM was detached and then entrained in the oceanic lithospheric mantle, melting of this reservoir could produce magma with Pb enrichment as observed in our samples. Therefore, it is inferred that the Pb enrichment reflects derivation from a SCLM-related source.

5.3.3 Local Pb anomaly in Cpx

Like Bizimis et al. (2005) found, clinopyroxenes reported here generally show negative, Pb, primitive-mantle-normalized trace element patterns (Fig. 4.8). However, in both this study and in Bizimis et al. (2005) a few analyses show positive anomalies, and this study demonstrates that Cpxs can show both positive and negative Pb anomalies in a single sample (SLCX 11, SLCX 12, SLCX 47). This mm-scale variation in Pb is challenging to explain. One possibility is that the Cpxs were formed by different processes (igneous, metamorphic, metasomatic) but this does not explain why they are so similar, except for Pb. Lead variation may be due to randomly-distributed, micron-scale, Pb-hosting sulphide grains in Cpx, randomly sampled by the laser. This explanation appears unlikely because Pb spikes were not observed during processing of the LA-ICP-QMS signals.

Lead concentrations were determined using ^{208}Pb . Nucleosynthetic processes that produced the solar nebula supplied ^{208}Pb to Earth (Hoffmann 2008), but the decay of ^{232}Th , with a long half-life of 1.405×10^{10} years, has added ^{208}Pb too. Zircons tend to incorporate ^{232}Th into their structure and therefore ancient zircons bear abundant ^{208}Pb (Hoskin & Schaltegger, 2003). If an

ancient zircon dissolved, it would produce high local Pb concentrations. An explanation for the positive Pb anomalies in a few Cpxs could be that during crystallization, they incorporated Th-derived Pb locally from dissolved zircons. This explanation also supports the hypothesis that the parent melts that formed SLC xenoliths could be derived from an ancient source.

5.4 Significance of Zircon Ages

5.4.1 Zircon Associated Mineral

In order to assess the significance of the zircon ages, it is important to know which minerals formed in equilibrium with zircon cores and outer rims. The zircons were extracted by whole rock processing, and textural relations with other minerals were lost. Similarly, zircons were not observed in thin sections. Zircon/mineral partitioning coefficient can help provide information on the relationship between zircon and other phases.

Since Clinopyroxene is the dominant and 'primary' phase in all SLC pyroxenites (Bizimis *et al.*, 2005; Keshav *et al.*, 2007), there is a good chance that it formed together with the zircons.

The partition coefficient D, defined as a ratio $D = C_{\text{phase1}}/C_{\text{phase2}}$, can be used to evaluate equilibrium. C_{phase1} is the concentration of an element in phase 1, and C_{phase2} is the concentration

of in phase 2. If calculated zircon/clinopyroxene D values are the same or similar to experimentally determined values in the literature, it can be assumed that clinopyroxenes formed in equilibrium with the zircons.

$D_{\text{zircon/Cpx}}$ values were calculated from experimentally determined $D_{\text{zircon/melt}}$ (Lesnov, 2013) and $D_{\text{Cpx/melt}}$ (Sun & Liang) values using the following equation: $D_{\text{zircon/Cpx}} = D_{\text{zircon/melt}}/D_{\text{Cpx/melt}}$. The $D_{\text{zircon/melt}}$ and $D_{\text{Cpx/melt}}$ values are listed in Table 5.1. Temperature, mineral composition and melt composition are the dominant factors affecting partition coefficients (Green *et al.*, 1989; Guay, 2007; Lesnov, 2013; Rubatto and Hermann, 2007; Sun and Liang, 2011; Taylor *et al.*, 2015; Yao *et al.*, 2012). Our samples were crystallized at temperatures of ~ 1300 °C (Bizimis *et al.*, 2005; Keshav *et al.*, 2007), similar to the conditions under which partitioning coefficient in the literature were determined. Melts in both experiments (Lesnov, 2013; Sun and Liang, 2011) are basaltic melts with similar compositions. The Al_2O_3 concentration in clinopyroxene, which is the major factor influencing REE partitioning between clinopyroxene and zircon (Sun & Liang, 2011), shows similar values (~ 7 wt%) in our samples and in the literature.

Table 9 Partition Coefficients from the Literature Used to Construct the Reference Line in Figure 26

REE	D _{zircon/melt} (Lesnov, 2013)	D _{Cpx/melt} (Sun & Liang, 2011)	D _{zircon/Cpx}
Ce	0.022	0.108	0.20
Nd	0.176	0.277	1.03
Sm	1.06	0.462	2.29
Eu	2.3	0.458	5.02
Gd	5.01	0.446	11.23
Tb	10.9	0.497	21.94
Dy	23.7	0.538	44.04
Ho	48.6	0.566	85.91
Er	94	0.581	161.90
Yb	293	0.582	503.52
Lu	472	0.573	823.30

* D_{zircon/melt} are from Table 12 in (Lesnov, 2013). D_{Cpx/melt} are from Table 3 in (Sun and Liang, 2011).

Compared with literature D_{zircon/Cpx} values for REE (Figure 26), which represents ideal REE partition coefficients between zircon and clinopyroxene under similar conditions, SLCX D_{zircon/Cpx} values are similar. For both zircon-bearing samples, D_{zircon/cpx} values for the zircon core and rim domains are very similar: both show a steep positive slope. This trend is consistent with the fact that, compared to the LREE, the HREE are favoured by zircon due to smaller ionic radii. Core D_{zircon/Cpx} values for Ce are higher than in the rim, reflecting higher Ce in the core. For all other elements, D values are identical for the cores and rims. This implies that the rim domain is genetically related to the core domain.

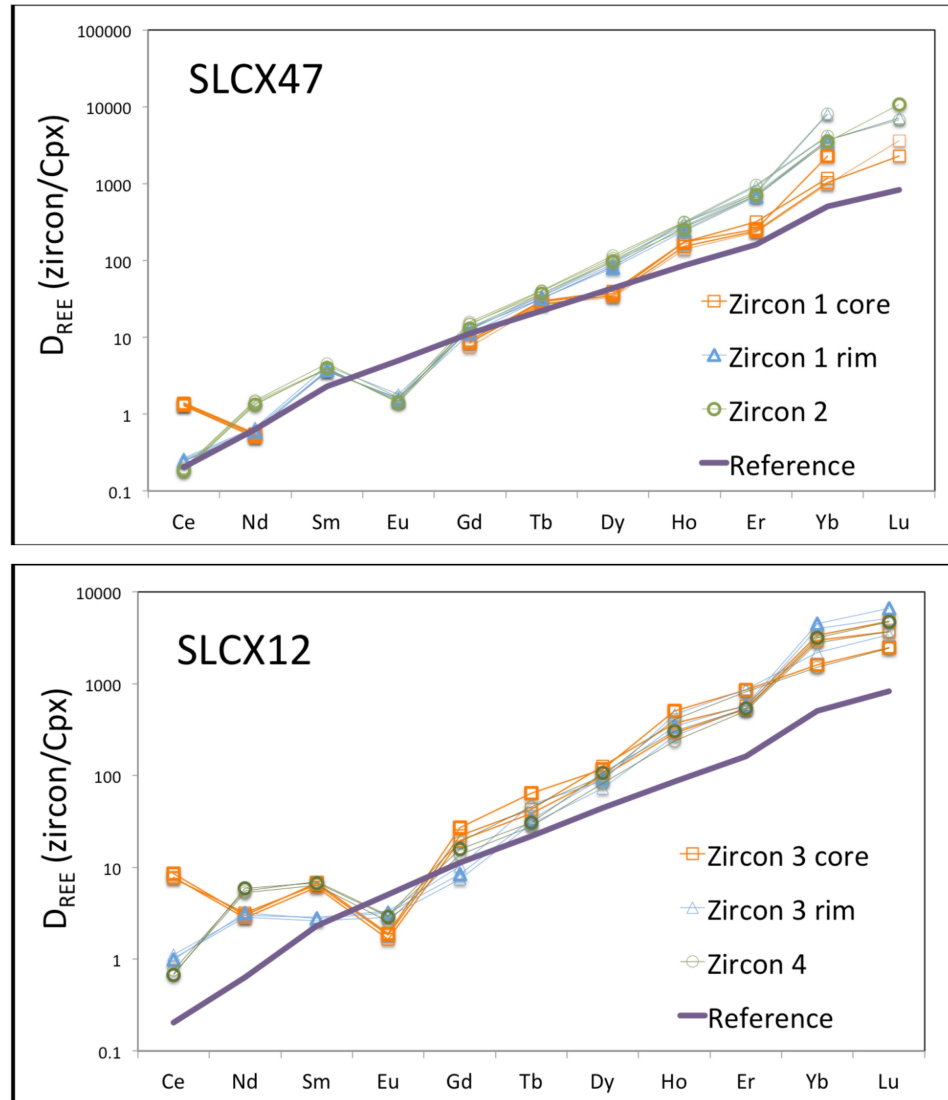


Figure 26 Diagram showing zircon/clinopyroxene partition coefficients for REE in samples SLCX 47 and SLCX 12. Data from (Lesnov, 2013) and (Sun and Liang, 2011) were used to construct the zircon/clinopyroxene D-value reference line.

The similarity between the core and rim, despite forming ~ 65 million years apart, is consistent with the rim forming from dissolution of core zircons, and then reprecipitated, with composition similar to the dissolved zircon. The primary difference between rim and core is

reflected by the $D_{\text{zircon/Cpx}}$ values for Ce, which are higher in the cores but lower in the rims and unzoned zircons. Unlike other REEs that form 3+ cations, Ce has two oxidation states (3+ and 4+) and under oxidizing conditions Ce^{4+} can predominantly substitute for Zr^{4+} in the zircon structure (Trail *et al.*, 2012). Higher Ce in zircon cores is consistent with formation under more-oxidizing conditions, then transferred to less-oxidizing or reducing conditions during formation of the rims. The clinopyroxene and garnet compositions do not provide any trace element evidence for formation at variable $f\text{O}_2$, but the rim $D_{\text{zircon/Cpx}}$ values for Ce are closer to the literature-derived reference line (Figure 26). Thus, the clinopyroxenes more likely crystallized/recrystallized during a thermal/geochemical event that formed the zircon rims.

Zircon/Garnet partitioning coefficients for REE were also calculated for comparison with values determined from natural metamorphic rocks (Figure 27). Zircon/garnet partitioning coefficients used in Figure 27 were from Table 3 in Rubatto (2002). The granulites formed at ~800 °C, and the protolith is felsic in composition, thus both the temperature of formation and lithology are distinctly different from those for the SLC xenoliths. Therefore, the following inferences, based on $D_{\text{zircon/Gt}}$, may not be as reliable as those made based on the Cpxs.

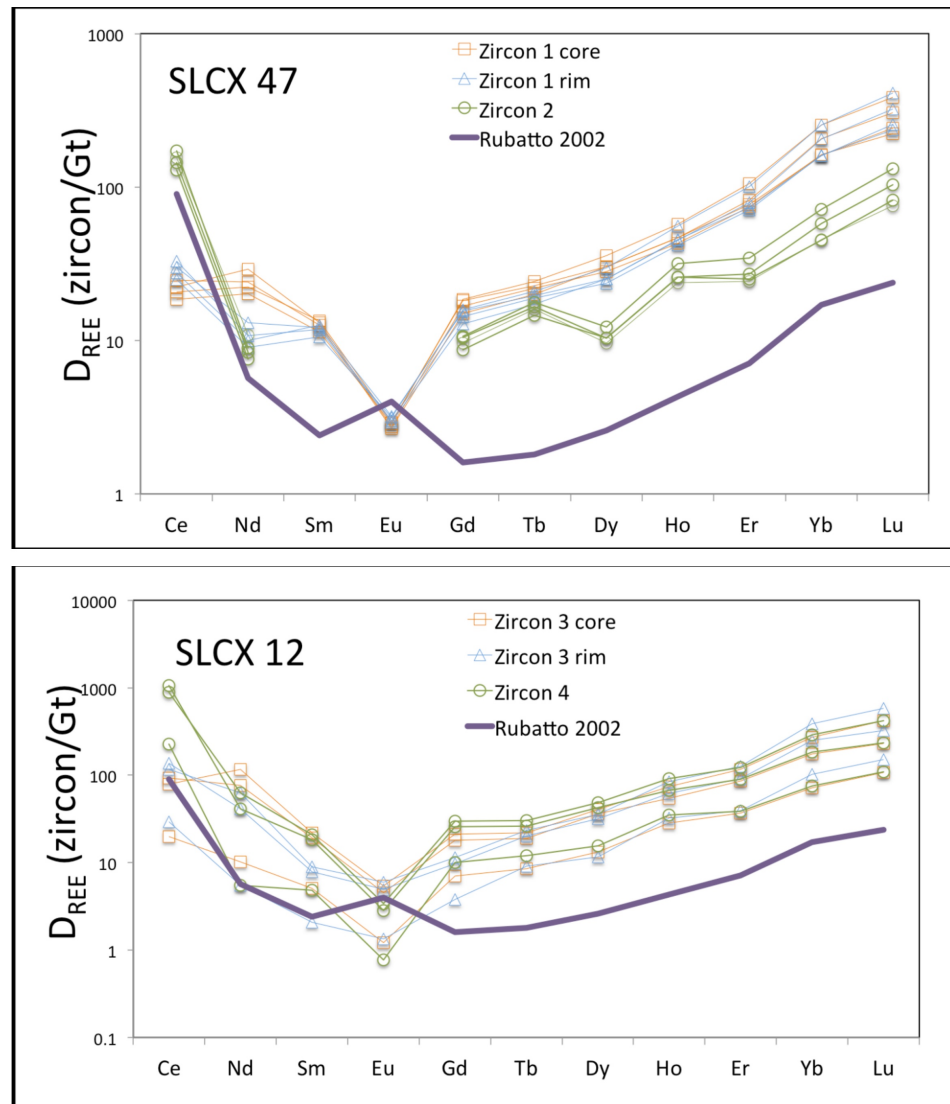


Figure 27 Diagram showing zircon/garnet partition coefficients for REE in samples SLCX 47 and SLCX 12. Data from (Rubatto 2002) were used for comparison purposes.

Both the SLCX zircon/garnet REE partitioning coefficients and experimentally determined values show a U-shaped pattern with higher values for the light REE and heavy REE. Although the calculated partitioning coefficients do not exactly match the literature values, they show

similar trends, and rims/unzoned zircons match predicted values better than cores do. The calculated partitioning coefficients differ from Rubatto's values by the presence of lower Ce values (Zircon 1 and 3) and a negative Eu anomaly, which implies comparatively more reducing crystallization conditions for SLCX zircons (Trail *et al.*, 2012).

Overall, the $D_{\text{zircon/Cpx}}$ and $D_{\text{zircon/Gt}}$ show considerable similarity to natural or experimentally determined values. Considering the Cpxs are in equilibrium with garnets, it is likely that garnet, zircon and clinopyroxene were in chemical equilibrium when formed. Partitioning coefficients for the redox-sensitive element, Ce, show significant difference between old cores and young rims, suggesting the redox conditions changed to more reducing conditions at the time the ~ 13 Ma zircons formed.

5.4.2 Magmatic vs. metamorphic origin of zircon cores and rims

The geochronology data clearly define two zircon groups with distinct ages: 1) two old zircon cores (Zircon1 and 3) with ~ 80 Ma ages and 2) two unzoned zircons (Zircon2 and 4) and rims (Zircon1 and 3) with younger ages ranging from 12.9 to 14.2 Ma. From the above evidence, it seems that both the cores and rims of the zircons have partitioning coefficients consistent with

formation in equilibrium with clinopyroxenes and garnet in samples SLCX 12 and SLCX 47.

However, it is not clear whether the zircons formed by magmatic crystallization or metamorphic recrystallization or both. The REE plot (Figure 15, 17, 19 and 21) together with Th/U ratios of zircons (Figure 28 and 29) may provide insight into the origin of these zircons.

Both zircon cores show elevated Ce abundances, and a steep positive HREE trend, and the Zircon3 core shows a negative Eu anomaly (Figure 15 and Figure 19), features that distinguish igneous zircons from metamorphic and hydrothermal zircons (Hoskin and Ireland, 2000; Hoskin and Schaltegger, 2003). Th/U ratios for the two old cores (Figure 28) reveal that they have identical, high Th/U ratios (~ 0.8), which is also a feature commonly seen in igneous zircons (Hoskin and Schaltegger, 2003; Poletti *et al.*, 2016). The available evidence suggests that the cores of Zircon1 (76.9 Ma) and Zircon3 (80.8 Ma) formed due to magmatic crystallization.

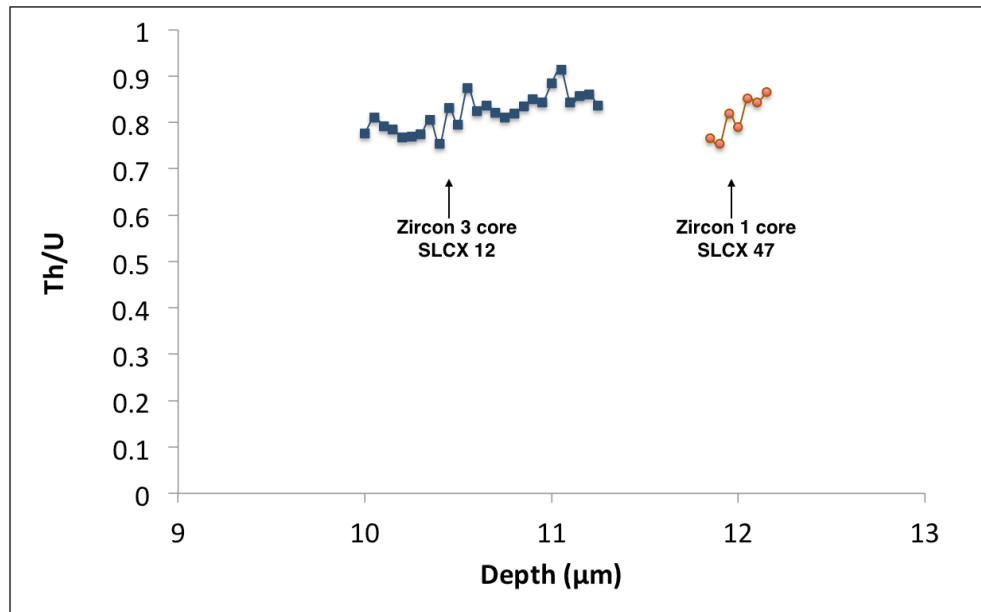


Figure 28 Th/U vs. depth profile of two zircon cores.

The two rim domains and two unzoned zircons have similar REE patterns, but are characterized by lacking a positive Ce anomaly (Figure 15, 17, 19 & 21). Igneous zircons that lack a positive Ce anomaly have been found in kimberlite and lunar basalt samples (Belousova *et al.*, 1998; 2002; Hoskin and Schaltegger, 2003). However, kimberlitic zircons have trace element abundances that are usually two orders of magnitude lower than in our samples (Grimes *et al.*, 2015). Hydrothermal alteration, on the other hand, is able to produce zircons that are depleted in Ce. However, the REE patterns exhibited by the cores and rims are identical, implying that the composition of melts that were in equilibrium with the zircons should be similar. This makes the possibility of a hydrothermal origin of the rim unlikely. Metamorphic solid-state recrystallization,

on the other hand, could result in depletion in Ce. Similar trends have been documented by other researchers looking at zircons with magmatic cores and metamorphic rims (Belousova *et al.*, 2002; Cates and Mojzsis, 2009; Hoskin and Schaltegger, 2003; Kirkland *et al.*, 2015).

Furthermore, lack of a positive Ce anomaly is considered a characteristic of metamorphic rims (Hoskin & Black, 2000). All this evidence points to a metamorphic origin for the rims and unzoned zircons.

The Th/U ratios for three out of four zircons drop from the core to the rim (Figure 29), and this trend is consistent with a metamorphic rim origin (Hoskin and Schaltegger, 2003). The decreasing Th/U ratios can be attributed to either the formation of Th-compatible phases such as monazite, allanite etc. during metamorphism (Möller *et al.*, 2003), or increasing U⁴⁺ content in zircon with consumption of external U⁶⁺ when the redox condition becomes more reducing (Hoskin and Schaltegger, 2003). Additionally, Hoskin & Black (2000) suggested that during recrystallization, compared to U⁴⁺, Th⁴⁺ would be preferentially purged from the zircon lattice due to its larger ionic radius, resulting in lower Th/U ratios. Thus, the decreasing Th/U ratios observed in Zircon1, 2 and 3 rims are consistent with a metamorphic recrystallization origin.

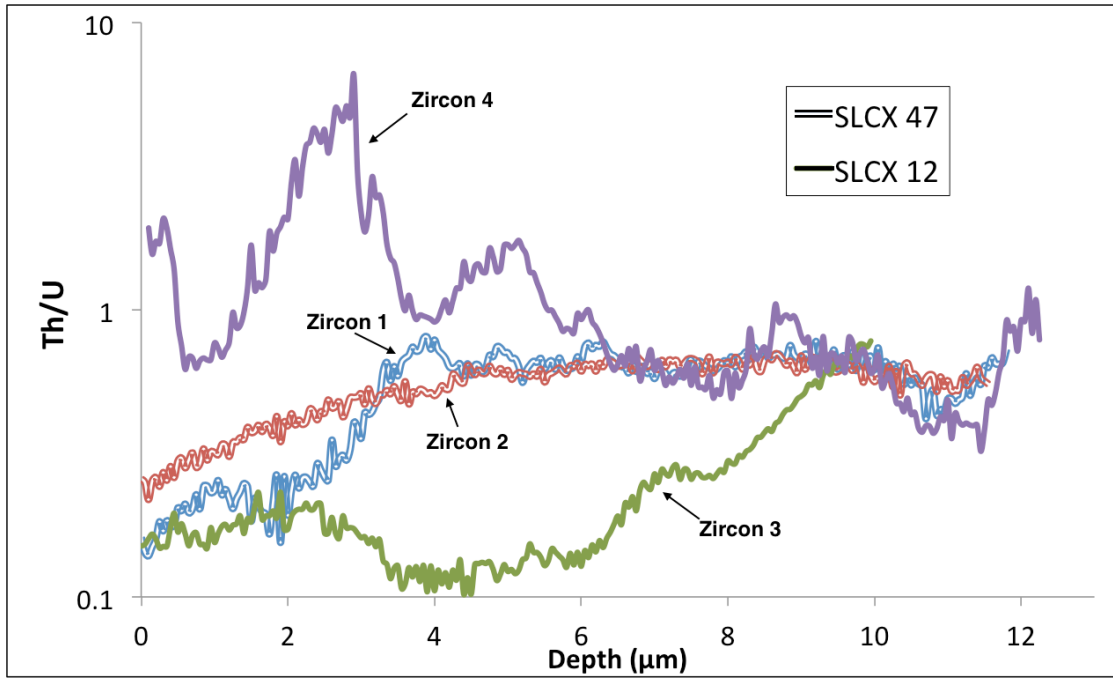


Figure 29 Th/U vs. depth profile of zircon rims.

The reason for the abrupt Th/U depletion shown by Zircon3's rim from 2.2 μm to 9.2 μm is unknown. The periodic pattern exhibited by Zircon4 is either due to the interaction between crystals and melt during rim growth, or reflect the occurrence of fractures and cracks within the zircon. Zircons from SLCX 12 show more variation in Th/U ratios compared to SLCX 47, which may indicate that they experienced more intense metamorphism or metasomatism, which created local disequilibrium during rim growth. .

In summary, both REE plot and Th/U ratios reveal that the low-age (12.9-14.5 Ma) zircon rims are overgrowths formed due to metamorphism. The ~ 80 Ma old cores are products of

magmatic crystallization. Decreasing Th/U ratios exhibited by the rims indicates a shift from relatively oxidizing conditions to more reducing conditions during metamorphism.

5.4.3 Interpretation of ages

Zircons from the pyroxenites record two major events. The steep positive REE patterns from La to Lu, elevated Ce abundance, negative Eu anomaly, along with high Th/U ratios all point to an igneous origin for the cores for Zircon1 and Zircon3. Since the cores are in equilibrium with the clinopyroxenes and garnets, the 80.8 ± 2 Ma is best interpreted as the igneous crystallization age of SLCX 12. The 76.9 Ma date, on the other hand, represents the minimum igneous crystallization age of SLCX 47.

Zircon2 and 4 and the rims of Zircon1 and 3 record a second period of zircon growth between 12.9 Ma and 14.5 Ma. The young zircon rims show many of the chemical characteristics of the old zircon cores (positive slope of REE plot, negative Eu anomaly) and even the compositions are similar, consistent with 'equilibrium' with the clinopyroxene and garnet. This suggests that they did not form as a result of new melt infiltrating the rocks.

However, they have characteristics such as low Ce and lower Th/U ratios, consistent with

formation during a metamorphic event. Thus the younger 12.9-14.5 Ma dates are best interpreted as a metamorphic period.

5.5 Tectonic Implications

To my knowledge, before this study, the age of the oceanic lithospheric and asthenospheric mantle has never been quantitatively dated because mantle samples (xenoliths) are difficult to date with most of radiogenic isotopic dating systems (e.g. Rb-Sr, Nd-Sm). Uranium-Thorium-rich minerals permitting U/Th-Pb dating have never been observed in oceanic mantle xenoliths. There have been model Pb-Pb dates suggesting mantle rocks are ancient, but this study is unique in providing actual dates for mantle-derived rocks.

The 80.8 ± 2 Ma yielded by a zircon from SLCX 47 places timing constraints on the formation of the lithospheric mantle beneath Hawaii. This age is roughly coincident with when the ocean floor below Oahu formed at the Pacific mid ocean ridge (Lassiter *et al.*, 2000; Norton, 2007). Therefore, there is the possibility that the formation of the pyroxenites (at least clinopyroxene and garnet) is related to crust formation at the mid ocean ridge. However, based on Hf-Nd-Sr isotope systematics, previous studies found that these xenoliths have near zero ages

and their isotopic compositions are unlikely linked to mid-ocean ridge basalt (Bizimis *et al.*, 2005). However, if the temperature of the systems has consistently been higher than the closure temperatures, it is possible to produce the zero ages reported. Secondary overprinting is related to heating, metasomatism and magmatism by the Hawaiian plume occurring 12-14 Ma ago. Since then the continued cooling of the ocean floor captured the rocks and incorporated them into the lithosphere for sampling by the Honolulu magma that brought them to the surface 0.6 Ma ago.

Although the ~ 80 Ma ages are coincident with MORB melting to form ocean floor, the composition of SLCX is not MORB-like. Rather they resemble pyroxenite xenoliths from the North China Craton subcontinental lithosphere (Xu *et al.*, 2002). If there is a detached, subcontinental lithosphere fragment entrained in the oceanic lithosphere mantle below Hawaii, the opening of the mid ocean ridge ~ 80 Ma ago may have lead to partial melting of this old, Pb-rich reservoir (Griffin *et al.*, 2009) to form magma that underwent fractional crystallization in several magma chambers but with a similar tectonic setting. Subsequent thermal metamorphism, potentially caused by the Hawaiian mantle plume, could lead to the formation of zircon

overgrowth rims \sim 13 Ma ago. If this is true, it appears that the chemical heterogeneity existing within Earth's mantle is not only contributed by recycling of subducted oceanic crust and lithosphere, but also involving delaminated subcontinental lithosphere as a critical component.

CHAPTER VI CONCLUSIONS

Seven Salt Lake Crater garnet-bearing pyroxenite xenoliths are textually and compositionally distinct from each other, but share common geochemical signatures such as positive Pb anomaly in some clinopyroxenes and all garnets, depletion in HFSE and flat LREE and MREE trends. They are inferred as magmatic cumulates crystallized from melts that were potentially derived from partial melting of an old depleted delaminated subcontinental lithosphere fragment entrained in the mantle.

Ages produced by U-Pb dating are distinct from the estimated near-zero modelling ages reported by previous researchers. The ~ 80 Ma age yielded by the core zone of two zircons represents the magmatic crystallization age of the xenoliths, whereas the ~ 13 Ma rim zones record a metamorphic event which led to the solid state recrystallization of the samples.

The results suggest that instead of recycled oceanic crust and lithosphere, the removal of mantle lithosphere from below the continents during subduction or asthenosphere upwelling could also be an important mechanism that contributes to chemical variability in the mantle.

REFERENCES

- Allègre, C. J. & Turcotte, D. L. (1986). Implications of a two-component marble-cake mantle. *Nature*, 323, 123–127.
- Allègre, C. J., Hart, S. R. & Minster, J. F. (1983). Chemical structure and evolution of the mantle and continents determined by inversion of Nd and Sr isotopic data, II. Numerical experiments and discussion. *Earth and Planetary Science Letters*, 66, 191–213.
- Arndt, N. T., Coltice, N., Helmstaedt, H. & Gregoire, M. (2009). Origin of Archean subcontinental lithospheric mantle: Some petrological constraints. *Lithos*, 109, 61–71.
- Aulbach, S. (2012). Craton nucleation and formation of thick lithospheric roots. *Lithos*, 149, 16–30.
- Aulbach, S., Pearson, N. J., O'Reilly, S. Y. & Doyle, B. J. (2007). Origins of Xenolithic Eclogites and Pyroxenites from the Central Slave Craton, Canada. *Journal of Petrology*, 48, 1843–1873.
- Belousova, E. A., Griffin, W. L. & Pearson, N. J. (1998). Trace element composition and cathodoluminescence properties of southern African kimberlitic zircons. *Mineralogical Magazine*, 62, 355–366.

Belousova, E., Griffin, W., O'Reilly, S. Y. & Fisher, N. (2002). Igneous zircon: trace element composition as an indicator of source rock type. *Contributions to Mineralogy and Petrology*, 143, 602–622.

Bizimis, M., Sen, G. & Salters, V. J. M. (2004). Hf–Nd isotope decoupling in the oceanic lithosphere: constraints from spinel peridotites from Oahu, Hawaii*. *Earth and Planetary Science Letters*, 217, 43–58.

Bizimis, M., Sen, G., Salters, V. J. M. & Keshav, S. (2005). Hf-Nd-Sr isotope systematics of garnet pyroxenites from Salt Lake Crater, Oahu, Hawaii: Evidence for a depleted component in Hawaiian volcanism. *Geochimica et Cosmochimica Acta*, 69, 2629–2646.

Cates, N. L. & Mojzsis, S. J. (2009). Metamorphic zircon, trace elements and Neoarchean metamorphism in the ca. 3.75 Ga Nuvvuagittuq supracrustal belt, Québec (Canada). *Chemical Geology*, 261, 99–114.

Choi, S. H. & Kim, N. K. (2012). Petrogenesis of anhydrous clinopyroxenite xenoliths and clinopyroxene megacrysts in alkali basalts from the Ganseong area of South Korea. *Island Arc*, 21, 101–117.

Clague, D. A. (1987). Hawaiian xenolith populations, magma supply rates, and development of magma chambers. *Bulletin of Volcanology*, 49, 577–587.

CLAGUE, D. A. & Frey, F. A. (1982). Petrology and trace element geochemistry of the Honolulu Volcanics, Oahu: implications for the oceanic mantle below Hawaii. *Journal of Petrology*, 23, 447–504.

Cottle, J. M., Burrows, A. J., Kylander-Clark, A., Freedman, P. A. & Cohen, R. S. (2013). Enhanced sensitivity in laser ablation multi-collector inductively coupled plasma mass spectrometry. *Journal of Analytical Atomic Spectrometry*. The Royal Society of Chemistry, 28, 1700–1706.

Ducea, M., Sen, G., Eiler, J. & Fimbres, J. (2002). Melt depletion and subsequent metasomatism in the shallow mantle beneath Koolau volcano, Oahu (Hawaii). *Geochem. Geophys. Geosyst.*, 3.

Frey, F. A. (1980). The origin of pyroxenites and garnet pyroxenites from Salt Lake Crater, Oahu, Hawaii: trace element evidence. *Am J Sci*, 427–449.

Frezzotti, M. L., Burke, E., Devivo, B., Villa, I. M. & Stefanini, B. (1992). Mantle Fluids in Pyroxenite Nodules From Salt Lake Crater (Oahu, Hawaii). *European Journal of Mineralogy*, 4, 1137–1153.

Frezzotti, M.-L. & Peccerillo, A. (2007). Diamond-bearing COHS fluids in the mantle beneath Hawaii. *Earth and Planetary Science Letters*, 262, 273–283.

- Green, T. H., Sie, S. H., Ryan, C. G. & Cousens, D. R. (1989). Proton microprobe-determined partitioning of Nb, Ta, Zr, Sr and Y between garnet, clinopyroxene and basaltic magma at high pressure and temperature. *Chemical Geology*, 74, 201–216.
- Greenough, J. D., Dostal, J. & Mallory-Greenough, L. M. (2007). Incompatible element ratios in French Polynesia basalts: describing mantle component fingerprints. *Australian Journal of Earth Sciences*, 54, 947–958.
- Greenough, J. D., & Kyser, T. K. (2003). Contrasting Archean and Proterozoic lithospheric mantle: isotopic evidence from the Shonkin Sag sill (Montana). *Contributions to Mineralogy and Petrology*, 145(2), 169-181.
- Griffin, W. L., O'Reilly, S. Y., Afonso, J. C. & Begg, G. C. (2009). The Composition and Evolution of Lithospheric Mantle: a Re-evaluation and its Tectonic Implications. *Journal of Petrology*, 50, 1185–1204.
- Grimes, C. B., Wooden, J. L., Cheadle, M. J. & John, B. E. (2015). “Fingerprinting” tectono-magmatic provenance using trace elements in igneous zircon. *Contributions to Mineralogy and Petrology*, 170, 46.
- Guay, M. H. (2007). Rare Earth Element Behavior in Zircon–Melt Systems. *Elements*, 3, 37–42.

- Guo, J., O'Reilly, S. Y. & Griffin, W. L. (1996). Zircon inclusions in corundum megacrysts: I. Trace element geochemistry and clues to the origin of corundum megacrysts in alkali basalts. *Geochimica et Cosmochimica Acta*, 60, 2347–2363.
- Hart, S. R., Hauri, E. H., Oschmann, L. A. & Whitehead, J. A. (1992). Mantle Plumes and Entrainment: Isotopic Evidence. *Science*, 256, 517–520.
- Harte, B., & Kirkley, M. B. (1997). Partitioning of trace elements between clinopyroxene and garnet: data from mantle eclogites. *Chemical Geology*, 136, 1-24.
- Hauri, E. H., Wagner, T. P. & Grove, T. L. (1994). Experimental and natural partitioning of Th, U, Pb and other trace elements between garnet, clinopyroxene and basaltic melts. *Chemical Geology*, 117, 149–166.
- Hirschmann, M. M. & Stolper, E. M. (1996). A possible role for garnet pyroxenite in the origin of the “garnet signature” in MORB. *Contributions to Mineralogy and Petrology*, 124, 185–208.
- Hirschmann, M. M., Kogiso, T., Baker, M. B. & Stolper, E. M. (2003). Alkaline magmas generated by partial melting of garnet pyroxenite. *Geology*, 31, 481–484.
- Hofmann, A. W. (2008). Chemical geodynamics: The enduring lead paradox. *Nature Geoscience*, 1, 812-813.

- Horstwood, M. S. A. *et al.* (2016). Community-Derived Standards for LA-ICP-MS U-(Th-)Pb Geochronology – Uncertainty Propagation, Age Interpretation and Data Reporting. *Geostandards and Geoanalytical Research*, 40, 311–332.
- Hoskin, P. W. O. & Ireland, T. R. (2000). Rare earth element chemistry of zircon and its use as a provenance indicator. *Geology*, 28, 627-630.
- Hoskin, P. W. O. & Schaltegger, U. (2003). The Composition of Zircon and Igneous and Metamorphic Petrogenesis. *Reviews in Mineralogy and Geochemistry*, 53, 27–62.
- Hoskin, P. W. O. & Black, L.P. (2000). Metamorphic zircon formation by solid-state recrystallization of protolith igneous zircon. *Journal of Metamorphic Geology*, 18, 423–439.
- Ireland, T. R. & Wlotzka, F. (1992). The oldest zircons in the solar system. *Earth and Planetary Science Letters*, 109, 1–10.
- Jochum, K. P. *et al.* (2011). Determination of Reference Values for NIST SRM 610-617 Glasses Following ISO Guidelines. *Geostandards and Geoanalytical Research*, 35, 397–429.
- Jochum, K. P., Willbold, M., Raczek, I., Stoll, B. & Herwig, K. (2005). Chemical Characterisation of the USGS Reference Glasses GSA-1G, GSC-1G, GSD-1G, GSE-1G, BCR-2G, BHVO-2G and BIR-1G Using EPMA, ID-TIMS, ID-ICP-MS and LA-ICP-MS. *Geostandards and Geoanalytical Research*, 29, 285–302.

- Keshav, S. & Sen, G. (2003). A rare composite xenolith from Salt Lake Crater, Oahu: high-pressure fractionation and implications for kimberlitic melts in the Hawaiian mantle. *Contributions to Mineralogy and Petrology*, 144, 548–558.
- Keshav, S. & Sen, G. (2004). The depth of magma fractionation in the oceanic mantle: Insights from garnet- bearing xenoliths from Oahu, Hawaii. *Geophysical Research Letters*, 31, 1-4.
- Keshav, S., Corgne, A., Gudfinnsson, G. H., Bizimis, M., McDonough, W. F. & Fei, Y. (2005). Kimberlite petrogenesis: Insights from clinopyroxene-melt partitioning experiments at 6 GPa in the CaO-MgO-Al₂O₃-SiO₂-CO₂ system. *Geochimica et Cosmochimica Acta*, 69, 2829–2845.
- Keshav, S., Sen, G. & Presnall, D. C. (2007). Garnet-bearing Xenoliths from Salt Lake Crater, Oahu, Hawaii: High-Pressure Fractional Crystallization in the Oceanic Mantle. *Journal of Petrology*, 48, 1681–1724.
- Kirkland, C. L., Smithies, R. H., Taylor, R. J. M., Evans, N. & McDonald, B. (2015). Zircon Th/U ratios in magmatic environs. *Lithos*, 212, 397–414.
- Kogiso, T., Hirschmann, M. M. & Frost, D. J. (2003). High-pressure partial melting of garnet pyroxenite: possible mafic lithologies in the source of ocean island basalts. *Earth and Planetary Science Letters*, 216, 603–617.

- Kornprobst, J., Piboule, M., Roden, M. & Tabit, A. (1990). Corundum-bearing Garnet Clinopyroxenites at Beni Bousera (Morocco): Original Plagioclase-rich Gabbros Recrystallized at Depth within the Mantle? *Journal of Petrology*, 31, 717–745.
- Kylander-Clark, A. R. C., Hacker, B. R. & Cottle, J. M. (2013). Laser-ablation split-stream ICP petrochronology. *Chemical Geology*, 345, 99–112.
- Lanphere, M. A. & Dalrymple, G. B. (1980). Age and strontium isotopic composition of the Honolulu Volcanic Series, Oahu, Hawaii. *American Journal of Science*, 280-A, 736–751.
- Lassiter, J. C., Hauri, E. H., Reiners, P. W. & Garcia, M. O. (2000). Generation of Hawaiian post-erosional lavas by melting of a mixed lherzolite/pyroxenite source. *Earth and Planetary Science Letters*, 178, 269–284.
- Lesnov, F. (2013). Consistent patterns of rare earth element distribution in accessory minerals from rocks of mafic-ultramafic complexes. *Open Geosciences*, 5, 121–173.
- Liu, Y. S., Gao, S., Jin, S. Y., Hu, S. H., Sun, M., Zhao, Z. B. & Feng, J. L. (2001). Geochemistry of lower crustal xenoliths from Neogene Hannuoba Basalt, North China Craton: Implications for petrogenesis and lower crustal composition. *Geochimica et Cosmochimica Acta*, 65, 2589–2604.

Liu, Y., Hu, Z., Zong, K., Gao, C., Gao, S., Xu, J. & Chen, H. (2010). Reappraisal and refinement of zircon U-Pb isotope and trace element analyses by LA-ICP-MS. *Chinese Science*, 55, 1535–1546.

McDonough, W. F. & Sun, S. S. (1995). The composition of the Earth. *Chemical Geology*, 120, 223–253.

McKinney, S. T., Cottle, J. M. & Lederer, G. W. (2015). Evaluating rare earth element mineralization mechanisms in Proterozoic gneiss, Music Valley, California. *The Geological Society of America Bulletin*, 127, 1135-1152.

Morishita, T., Arai, S. & Green, D. H. (2003). Evolution of Low-Al Orthopyroxene in the Horoman Peridotite, Japan: an Unusual Indicator of Metasomatizing Fluids. *Journal of Petrology*, 44, 1237–1246.

Möller, A., O'Brien, P. J. & Kennedy, A. (2003). Linking growth episodes of zircon and metamorphic textures to zircon chemistry: an example from the ultrahigh-temperature granulites of Rogaland (SW Norway). *Geological Society, London, Special Publications*, 220, 65–81.

Norton, I. O. (2007). Speculations on Cretaceous tectonic history of the northwest Pacific and a tectonic origin for the Hawaii hotspot. *Geological Society of America Special Papers*. Geological Society of America, 430, 451–470.

- Olin, P. H. & Wolff, J. A. (2010). Rare earth and high field strength element partitioning between iron-rich clinopyroxenes and felsic liquids. *Contributions to Mineralogy and Petrology*, 160, 761–775.
- Paton, C., Woodhead, J. D., Hellstrom, J. C., Hergt, J. M., Greig, A. & Maas, R. (2010). Improved laser ablation U-Pb zircon geochronology through robust downhole fractionation correction. *Geochem. Geophys. Geosyst.*, 11, 1–36.
- Pearson, D. G., Davies, G. R. & Nixon, P. H. (1993). Geochemical Constraints on the Petrogenesis of Diamond Fades Pyroxenites from the Beni Bousera Peridotite Massif, North Morocco. *Journal of Petrology*, 34, 125–172.
- Poletti, J. E., Cottle, J. M., Hagen-Peter, G. A. & Lackey, J. S. (2016). Petrochronological Constraints on the Origin of the Mountain Pass Ultrapotassic and Carbonatite Intrusive Suite, California. *Journal of Petrology*, 57, 1555–1598.
- Ren, Z.-Y., Ingle, S., Takahashi, E., Hirano, N. & Hirata, T. (2005). The chemical structure of the Hawaiian mantle plume. *Nature*, 436, 837–840.
- Ribe, N. M. (1988). Dynamical geochemistry of the Hawaiian plume. *Earth and Planetary Science Letters*, 88, 37–46.
- Rocholl, A., Heusser, E., Kirsten, T., Oehm, J. & Richter, H. (1996). A noble gas profile across a Hawaiian mantle xenolith: Coexisting accidental and cognate noble gases derived from the

lithospheric and asthenospheric mantle beneath Oahu. *Geochimica et Cosmochimica Acta*, 60, 4773–4783.

Rubatto, D. (2002). Zircon trace element geochemistry: partitioning with garnet and the link between U–Pb ages and metamorphism. *Chemical Geology*, 184, 123–138.

Rubatto, D. & Hermann, J. (2007). Experimental zircon/melt and zircon/garnet trace element partitioning and implications for the geochronology of crustal rocks. *Chemical Geology*, 241, 38–61.

Rusk, M. (2013). Analysis of Hawaiian Salt Lake Crater Xenoliths. (Unpublished Bachelor Dissertation). University of British Columbia, Okanagan, Kelowna.

Sen, G. (1988). Petrogenesis of spinel Iherzolite and pyroxenite suite xenoliths from the Koolau shield, Oahu, Hawaii: Implications for petrology of the post-eruptive lithosphere beneath Oahu*. *Contributions to Mineralogy and Petrology*, 100, 61–91.

Sen, G. & Jones, R. E. (1990). Cumulate Xenolith in Oahu, Hawaii: Implications for Deep Magma Chambers and Hawaiian Volcanism. *Science*, 249, 1154–1157.

Sen, G., Frey, F. A., Shimizu, N. & Leeman, W. P. (1993). Evolution of the Lithosphere Beneath Oahu, Hawaii - Rare-Earth Element Abundances in Mantle Xenoliths. *Earth and Planetary Science Letters*, 119, 53–69.

Sen, G., Keshav, S. & Bizimis, M. (2005). Hawaiian mantle xenoliths and magmas: Composition and thermal character of the lithosphere. *American Mineralogist*, 90, 871–887.

Sen, I. S., Bizimis, M., & Sen, G. (2010). Geochemistry of sulfides in Hawaiian garnet pyroxenite xenoliths: implications for highly siderophile elements in the oceanic mantle. *Chemical Geology*, 273, 180-192.

Sun, C. & Liang, Y. (2011). Distribution of REE between clinopyroxene and basaltic melt along a mantle adiabat: effects of major element composition, water, and temperature. *Contributions to Mineralogy and Petrology*, 163, 807–823.

Trail, D., Watson, E. B., & Tailby, N. D. (2012). Ce and Eu anomalies in zircon as proxies for the oxidation state of magmas. *Geochimica et Cosmochimica Acta*, 97, 70-87.

Taylor, R. J. M., Harley, S. L., Hinton, R. W., Elphick, S., Clark, C. & Kelly, N. M. (2015). Experimental determination of REE partition coefficients between zircon, garnet and melt: a key to understanding high- Tcrustal processes. *Journal of Metamorphic Geology*, 33, 231–248.

Wiedenbeck, M., Allé, P., Corfu, F., Griffin, W. L., Meier, M., Oberli, F., Quadt, A. V., Roddick, J. C. & Spiegel, W. (1995). Three Natural Zircon Standards For U-Th-Pb, Lu-Hf, Trace Element And REE Analyses. *Geostandards and Geoanalytical Research*, 19, 1–23.

Wirth, R. & Rocholl, A. (2003). Nanocrystalline diamond from the Earth's mantle underneath Hawaii. *Earth and Planetary Science Letters*, 211, 357–369.

Xu, Y. (2002). Evidence for crustal components in the mantle and constraints on crustal recycling mechanisms: pyroxenite xenoliths from Hannuoba, North China. *Chemical Geology*, 182, 301-322.

Yao, L., Sun, C. & Liang, Y. (2012). A parameterized model for REE distribution between low-Ca pyroxene and basaltic melts with applications to REE partitioning in low-Ca pyroxene along a mantle adiabat and during pyroxenite-derived melt and peridotite interaction. *Contributions to Mineralogy and Petrology*, 164, 261–280.

APPENDICES

Appendix A Detailed Sample Processing and Extraction Procedures

Sample preparation and zircon separation were conducted with extreme care in order to prevent any contamination. Seven samples were selected for zircon extraction. They are: SLCX 10 (128.56 g), SLCX 11 (110.09 g), SLCX 12 (20.61 g), SLCX 21 (50.39 g), SLCX 25 (18.55 g), SLCX 26 (22.65 g) and SLCX 47 (138.79 g). The numerical order was preserved during processing as a means of determining the probability of individual separated zircon derived from contamination.

Because there was volcaniclastic nephelinite/nephelinic host basalt attached to the xenolith (Figure 30 a), the first step was to remove the attached material using the selFrag at Queen's University. Before loading each sample, the vessel was carefully cleaned with the following steps: 1) rinsed with tap water, 2) hand-washed with mild detergent using a stiff plastic brush, 3) rinsed with tap water, and 4) the vessel loaded with a Grenville age marble and processed through the selFrag. Samples were loaded with RO water (3 L in total) purchased from Collagen Water. New brushes and plastic containers were used during each cleaning.



Figure 30 SLCX processing photos. a) sample as received. b) sample after 'gentle' 40 pulses. c) sample after sieving. 'B' fraction was then subjected to a 'harder' additional 120 pulses. Photos were taken by Daniel Layton-Mathews, Queen's University.

After each cleaning procedure, samples and 3 L of reverse osmosis water were placed inside the selFrag instrument and subjected to 40 pulses at 130 kV, which 'gently' separated the volcanic material from the xenoliths. A 1.4 mm wet sieve was used to divide the products into A (volcanic material < 1.4 mm in size, Figure 30 b) and B (material > 1.4 mm in size, Figure 30 c) subgroups. The subgroup B, which largely contains xenolith material, was placed back into the selFrag with reverse osmosis water and subjected to 120 pulses at 150 kV for disaggregation

along grain boundaries. With the above procedures, the xenoliths were disaggregated and zircon from along grain boundaries separated.

The products derived from the selFrag at Queen's University were then sieved at the Jack Satterly Geochronology Laboratory, University of Toronto (U of T) to remove coarse mineral grains. A Franz magnetic separator was used to concentrate non-magnetic grains. Before and between samples, the separator was cleaned with water, distilled water and methanol. Magnetic grains were removed from the material with the following steps: 1) free-fall removal of magnetic minerals, 2) two passes through the magnetic separator. Next, the 'non-magnetic' fraction went through methylene iodide heavy liquid for additional separation. Glassware used before and between samples was fastidiously cleaned. Seven zircons were recovered from the xenoliths (four from SLCX 12, third sample processed; and three from SLCX 47, last sample processed).

Because there was the possibility that the recovered zircons were contaminants from previously-processed samples in the instruments, records of samples previously processed in the two laboratories were carefully examined. Prior to the selFrag mineral disaggregation, a large three-week project was conducted by Himalayan structural geologist Dr. Laurent Godin. All of

his samples were Archean granites, roughly 3.2 to 3.0 Ga from the Bundelkhand massif in India.

Our zircons yielded ~ 13 Ma and ~ 80 Ma ages, so it is almost impossible that these zircons were

from his granites. During the separation at University of Toronto, no samples went through the

equipment over the time of our zircon separation, and rocks processed over the year prior to our

project did not have similar ages to our zircons.

To summarize, it is practically impossible that our zircons are contaminants from rocks

processed prior to our project at Queen's University or University of Toronto. The samples went

through the instruments in numerical order, and it is extremely unlikely that after all previous

samples went through the selFrag, contaminating zircons could survive from the multi-cleaning

process and appear when the last sample (SLCX 47) was processed. The zircons cannot be from

the xenolith-host material because the volcaniclastic rocks are < 0.6 Ma old (Clague and Frey,

1982). Therefore, it is clear that the recovered zircons are derived from the Salt Lake Crater

xenoliths.

Appendix B Mineral Composition Data

Table 10 Major Element Concentrations and Calculated Stoichiometry for Clinopyroxene

	SLCX 47 Cpx1	SLCX 47 Cpx2	SLCX 47 Cpx3	SLCX 47 Cpx4	SLCX 12 Cpx1
SiO ₂	50.45	50.24	50.32	50.01	51.40
TiO ₂	1.16	1.15	1.21	1.27	0.99
Al ₂ O ₃	6.50	6.43	6.64	7.02	7.45
Cr ₂ O ₃	0.02	0.04	0.04	0.03	0.39
FeO	6.47	6.51	6.65	6.56	6.04
MnO	0.06	0.05	0.10	0.08	0.09
MgO	13.90	13.95	13.79	13.70	13.77
CaO	19.21	19.17	19.12	18.80	17.71
Na ₂ O	1.90	1.93	1.97	1.96	2.45
K ₂ O	0.02	0.01	0.02	0.01	0.02
NiO	0.04	0.02	0.02	0.04	0.02
Total	99.73	99.52	99.87	99.48	100.33
Number of ions on the basis of 6 O					
Si	1.859	1.857	1.854	1.848	1.870
Ti	0.032	0.032	0.034	0.035	0.027
Al(IV)	0.141	0.143	0.146	0.152	0.130
Al(VI)	0.142	0.137	0.142	0.153	0.189
Cr	0.001	0.001	0.001	0.001	0.011
Fe++	0.200	0.201	0.205	0.203	0.184
Mn	0.002	0.002	0.003	0.003	0.003
Mg	0.764	0.769	0.758	0.755	0.747
Ca	0.759	0.759	0.755	0.744	0.690
Na	0.136	0.138	0.141	0.140	0.173
K	0.001	0.001	0.001	0.001	0.001
Total	4.035	4.040	4.039	4.034	4.025
En	44.35	44.46	44.11	44.35	46.09
Fs	11.59	11.64	11.93	11.92	11.33
Wo	44.06	43.91	43.96	43.74	42.58
Mg#	79	79	79	79	80

* En = Enstatite, Fs = Ferrosilite, Wo = Wollastonite, Mg# = [Mg/(Mg + Fe)]*100%. The total Fe is reported as Fe++.

Table 10 (Continued)

	SLCX 12 Cpx2	SLCX 25 Cpx1	SLCX 25 Cpx2	SLCX 25 Cpx3	SLCX 26 Cpx2
SiO ₂	51.19	51.15	49.98	50.57	49.84
TiO ₂	1.01	0.84	0.90	0.87	1.07
Al ₂ O ₃	7.48	6.88	8.10	7.44	6.27
Cr ₂ O ₃	0.48	0.22	0.23	0.23	0.21
FeO	5.81	6.31	5.96	6.12	5.85
MnO	0.10	0.06	0.05	0.09	0.10
MgO	13.68	14.20	13.54	14.06	13.93
CaO	17.68	18.59	18.87	18.75	19.61
Na ₂ O	2.42	2.04	2.18	2.02	1.76
K ₂ O	0.03	0.01	0.03	0.01	0.04
NiO	0.04	0.03		0.04	0.04
Total	99.92	100.36	99.86	100.20	98.71
Number of ions on the basis of 6 O					
Si	1.869	1.866	1.834	1.849	1.856
Ti	0.028	0.023	0.025	0.024	0.030
Al(IV)	0.131	0.134	0.159	0.151	0.144
Al(VI)	0.191	0.163	0.188	0.170	0.131
Cr	0.014	0.006	0.007	0.007	0.006
Fe++	0.177	0.193	0.183	0.187	0.182
Mn	0.003	0.002	0.002	0.003	0.003
Mg	0.745	0.773	0.741	0.766	0.773
Ca	0.691	0.727	0.742	0.735	0.783
Na	0.172	0.145	0.155	0.143	0.127
K	0.001	0.000	0.001	0.000	0.002
Total	4.022	4.032	4.040	4.035	4.037
En	46.16	45.66	44.47	45.40	44.50
Fs	10.99	11.39	10.98	11.08	10.48
Wo	42.85	42.96	44.55	43.52	45.02
Mg#	81	80	80	80	81

Table 10 (Continued)

	SLCX 45 Cpx1	SLCX 45 Cpx2	SLCX 45 Cpx3	SLCX 21 Cpx1	SLCX 21 Cpx2
SiO ₂	51.35	51.63	51.53	48.58	49.67
TiO ₂	0.59	0.54	0.56	1.44	1.19
Al ₂ O ₃	6.19	6.02	6.11	8.26	7.60
Cr ₂ O ₃	0.34	0.39	0.38	0.03	0.03
FeO	5.32	5.44	5.42	7.82	8.28
MnO	0.08	0.08	0.09	0.08	0.09
MgO	14.37	14.49	14.43	11.77	11.81
CaO	19.37	19.45	19.37	18.33	18.32
Na ₂ O	1.92	1.92	1.92	2.61	2.81
K ₂ O	0.01	0.04	0.01	0.03	0.04
NiO	0.02	0.06	0.06	0.07	0.02
Total	99.58	100.08	99.88	99.02	99.85
Number of ions on the basis of 6 O					
Si	1.884	1.887	1.887	1.818	1.844
Ti	0.016	0.015	0.015	0.041	0.033
Al(IV)	0.116	0.113	0.113	0.182	0.156
Al(VI)	0.152	0.147	0.150	0.183	0.177
Cr	0.010	0.011	0.011	0.001	0.001
Fe++	0.163	0.166	0.166	0.245	0.257
Mn	0.002	0.003	0.003	0.002	0.003
Mg	0.786	0.790	0.788	0.657	0.654
Ca	0.762	0.762	0.760	0.735	0.729
Na	0.137	0.136	0.136	0.190	0.202
K	0.001	0.002	0.001	0.002	0.002
Total	4.029	4.032	4.029	4.054	4.057
En	45.94	45.97	45.97	40.12	39.87
Fs	9.54	9.68	9.68	14.96	15.68
Wo	44.52	44.35	44.35	44.92	44.45
Mg#	83	83	83	73	72

Table 10 (Continued)

	SLCX 21 Cpx3	SLCX 11 Cpx1	SLCX 11 Cpx2	SLCX 11 Cpx3
SiO ₂	49.07	50.11	49.87	49.93
TiO ₂	1.26	1.22	1.23	1.25
Al ₂ O ₃	7.76	6.68	6.72	6.83
Cr ₂ O ₃	0.01	0.04	0.04	0.04
FeO	7.86	6.93	6.77	6.89
MnO	0.09	0.11	0.09	0.12
MgO	12.17	13.52	13.61	13.37
CaO	18.92	18.71	18.77	18.43
Na ₂ O	2.35	2.02	2.01	2.15
K ₂ O	0.02	0.01	0.01	0.10
NiO	0.05	0.04	0.05	0.07
Total	99.56	99.40	99.16	99.18
Number of ions on the basis of 6 O				
Si	1.827	1.856	1.852	1.854
Ti	0.035	0.034	0.034	0.035
Al(IV)	0.173	0.144	0.148	0.146
Al(VI)	0.168	0.148	0.146	0.153
Cr	0.000	0.001	0.001	0.001
Fe++	0.245	0.215	0.210	0.214
Mn	0.003	0.003	0.003	0.004
Mg	0.675	0.746	0.753	0.740
Ca	0.755	0.743	0.747	0.734
Na	0.170	0.145	0.145	0.155
K	0.001	0.000	0.000	0.005
Total	4.052	4.036	4.039	4.040
En	40.32	43.81	44.05	43.86
Fs	14.62	12.61	12.29	12.69
Wo	45.06	43.58	43.66	43.46
Mg#	73	78	78	78

Table 11 Major Element Concentrations and Calculated Stoichiometry for Orthopyroxene

	SLCX 12 Opx1	SLCX 12 Opx2	SLCX 12 Opx3	SLCX 25 Opx1	SLCX 25 Opx2
SiO ₂	53.62	53.19	51.68	53.01	53.12
TiO ₂	0.28	0.28	0.25	0.26	0.27
Al ₂ O ₃	4.60	4.84	4.93	4.35	4.18
Cr ₂ O ₃	0.22	0.20	0.22	0.12	0.11
FeO	11.76	11.76	11.58	13.09	11.64
MnO	0.15	0.15	0.17	0.16	0.15
MgO	28.76	28.40	27.47	28.25	28.83
CaO	0.92	0.97	0.93	0.86	0.86
Na ₂ O	0.23	0.37	0.56	0.20	0.28
K ₂ O	0.01	0.02	0.25	0.02	0.03
NiO	0.05	0.09	0.08	0.06	0.05
Total	100.61	100.27	98.13	100.39	99.53
Number of ions on the basis of 6 O					
Si	1.891	1.885	1.877	1.887	1.895
Ti	0.007	0.007	0.007	0.007	0.007
Al(IV)	0.109	0.115	0.123	0.113	0.105
Al(VI)	0.083	0.087	0.088	0.069	0.070
Cr	0.006	0.006	0.006	0.003	0.003
Fe ⁺⁺	0.347	0.349	0.352	0.390	0.347
Mn	0.004	0.005	0.005	0.005	0.005
Mg	1.512	1.500	1.487	1.499	1.533
Ca	0.035	0.037	0.036	0.033	0.033
Na	0.016	0.026	0.039	0.014	0.020
K	0.000	0.001	0.012	0.001	0.001
Total	4.011	4.017	4.033	4.021	4.019
En	79.84	79.56	79.31	78.00	80.13
Fs	18.32	18.49	18.76	20.28	18.15
Wo	1.84	1.95	1.93	1.72	1.72
Mg#	81	81	81	79	82

* En = Enstatite, Fs = Ferrosilite, Wo = Wollastonite, Mg# = [Mg/(Mg + Fe)]*100%. The total Fe is reported as Fe⁺⁺.

Table 11 (Continued)

	SLCX 25 Opx3	SLCX 26 Opx1	SLCX 26 Opx2	SLCX 11 Opx1
SiO ₂	53.10	51.88	52.20	53.17
TiO ₂	0.25	0.31	0.27	0.32
Al ₂ O ₃	4.04	5.35	5.60	3.96
Cr ₂ O ₃	0.11	0.10	0.07	0.03
FeO	13.11	11.73	11.85	13.08
MnO	0.17	0.14	0.18	0.15
MgO	28.10	28.07	28.04	28.23
CaO	0.88	0.85	0.89	0.88
Na ₂ O	0.19	0.35	0.17	0.15
K ₂ O	0.02	0.05	0.04	0.01
NiO	0.07	0.03	0.07	0.09
Total	100.05	98.86	99.38	100.07
Number of ions on the basis of 6 O				
Si	1.896	1.865	1.867	1.898
Ti	0.007	0.008	0.007	0.009
Al(IV)	0.104	0.135	0.133	0.102
Al(VI)	0.067	0.092	0.102	0.064
Cr	0.003	0.003	0.002	0.001
Fe++	0.392	0.353	0.354	0.390
Mn	0.005	0.004	0.006	0.004
Mg	1.496	1.505	1.495	1.502
Ca	0.034	0.033	0.034	0.034
Na	0.013	0.024	0.012	0.010
K	0.001	0.002	0.002	0.001
Total	4.017	4.025	4.014	4.015
En	77.87	79.62	79.38	77.99
Fs	20.38	18.66	18.82	20.27
Wo	1.75	1.72	1.81	1.74
Mg#	79	81	81	79

Table 12 Major Element Concentrations and Calculated Stoichiometry for Garnet

	SLCX 47 Gt1	SLCX 47 Gt2	SLCX 47 Gt3	SLCX 47 Gt4	SLCX 12 Gt1
SiO ₂	40.73	41.01	40.25	40.95	41.22
TiO ₂	0.38	0.41	0.46	0.30	0.28
Al ₂ O ₃	22.76	23.47	23.10	23.51	23.33
Cr ₂ O ₃	0.03	0.05	0.03	0.04	0.41
FeO	14.43	14.12	13.58	13.96	13.50
MnO	0.32	0.35	0.32	0.31	0.39
MgO	16.46	16.64	16.37	16.88	17.04
CaO	4.84	5.25	5.22	5.23	4.85
Na ₂ O	0.13	0.06	0.11	0.08	0.11
K ₂ O	0.10	0.01	0.03	0.02	0.04
NiO				0.01	0.03
Total	100.20	101.35	99.46	101.30	101.21
Number of ions on the basis of 12 O					
Si	2.974	2.952	2.951	2.948	2.965
Ti	0.021	0.022	0.026	0.016	0.015
Al	1.958	1.991	1.996	1.995	1.977
Cr	0.002	0.003	0.002	0.002	0.023
Fe++	0.881	0.850	0.832	0.841	0.812
Mn	0.020	0.021	0.020	0.019	0.024
Mg	1.791	1.785	1.789	1.812	1.828
Ca	0.379	0.405	0.410	0.404	0.374
Total	8.026	8.029	8.025	8.037	8.019
Alm	28.88	27.96	27.46	27.50	26.94
Prp	58.71	58.72	59.01	59.29	60.64
Grs	12.41	13.32	13.53	13.21	12.41
Mg#	67	68	68	68	69

* Alm = Almandine, Prp = Pyrope, Grs = Grossular, Mg# = [Mg/(Mg + Fe)]*100%. The total Fe is reported as Fe++.

Table 12 (Continued)

	SLCX 12 Gt2	SLCX 12 Gt3	SLCX 25 Gt1	SLCX 25 Gt2	SLCX 25 Gt3
SiO ₂	40.88	40.82	40.97	40.98	40.67
TiO ₂	0.26	0.33	0.23	0.22	0.24
Al ₂ O ₃	23.43	23.24	23.38	23.17	23.19
Cr ₂ O ₃	0.25	0.26	0.29	0.29	0.29
FeO	13.51	13.33	14.81	13.18	14.53
MnO	0.37	0.37	0.43	0.43	0.40
MgO	16.76	16.88	16.41	16.87	16.14
CaO	4.80	4.87	5.11	5.13	5.11
Na ₂ O	0.37	0.30	0.07	0.15	0.11
K ₂ O	0.03	0.17	0.01	0.04	0.05
NiO	0.02	0.04		0.03	0.03
Total	100.70	100.62	101.70	100.50	100.77
Number of ions on the basis of 12 O					
Si	2.962	2.962	2.950	2.969	2.956
Ti	0.014	0.018	0.012	0.012	0.013
Al	2.001	1.987	1.984	1.979	1.987
Cr	0.014	0.015	0.017	0.017	0.017
Fe++	0.818	0.809	0.892	0.799	0.884
Mn	0.023	0.023	0.026	0.027	0.025
Mg	1.810	1.826	1.761	1.822	1.749
Ca	0.373	0.379	0.394	0.398	0.398
Total	8.016	8.019	8.037	8.022	8.029
Alm	27.26	26.84	29.27	26.46	29.15
Prp	60.31	60.59	57.80	60.36	57.72
Grs	12.42	12.57	12.94	13.19	13.13
Mg#	69	69	66	70	66

Table 12 (Continued)

	SLCX 26 Gt1	SLCX 45 Gt1	SLCX 21 Gt1	SLCX 21 Gt2	SLCX 11 Gt1
SiO ₂	40.66	40.58	40.27	40.39	41.05
TiO ₂	0.25	0.49	0.32	0.30	0.33
Al ₂ O ₃	22.98	22.88	22.94	23.00	23.08
Cr ₂ O ₃	0.28	0.09	0.02	0.02	0.06
FeO	13.32	15.48	16.88	16.79	14.70
MnO	0.41	0.30	0.35	0.38	0.36
MgO	16.42	15.73	14.29	14.30	16.21
CaO	5.43	5.12	5.77	5.67	5.14
Na ₂ O	0.19	0.07	0.10	0.08	0.04
K ₂ O	0.04	0.01	0.03	0.02	0.01
NiO	0.02	0.05	0.03	0.04	0.03
Total	99.99	100.80	100.99	100.99	101.01
Number of ions on the basis of 12 O					
Si	2.967	2.959	2.956	2.961	2.972
Ti	0.014	0.027	0.017	0.016	0.018
Al	1.976	1.966	1.984	1.988	1.970
Cr	0.016	0.005	0.001	0.001	0.004
Fe++	0.813	0.944	1.036	1.029	0.890
Mn	0.026	0.018	0.022	0.023	0.022
Mg	1.786	1.710	1.563	1.564	1.750
Ca	0.424	0.400	0.454	0.445	0.399
Total	8.023	8.029	8.034	8.028	8.023
Alm	26.89	30.91	33.93	33.88	29.29
Prp	59.07	55.99	51.21	51.46	57.59
Grs	14.04	13.10	14.86	14.65	13.12
Mg#	69	64	60	60	66

Table 12 (Continued)

	SLCX 11 Gt2	SLCX 11 Gt3
SiO ₂	40.63	40.82
TiO ₂	0.33	0.41
Al ₂ O ₃	23.10	22.97
Cr ₂ O ₃	0.05	0.04
FeO	14.58	14.58
MnO	0.35	0.35
MgO	15.91	15.94
CaO	5.15	5.18
Na ₂ O	0.06	0.05
K ₂ O	0.01	0.01
NiO	0.04	0.02
Total	100.19	100.38
Number of ions on the basis of 12 O		
Si	2.967	2.974
Ti	0.018	0.022
Al	1.987	1.972
Cr	0.003	0.003
Fe++	0.890	0.889
Mn	0.022	0.022
Mg	1.731	1.731
Ca	0.403	0.404
Total	8.020	8.017
Alm	29.44	29.38
Prp	57.25	57.25
Grs	13.21	13.37
Mg#	66	66

Table 13 Major Element Concentrations and Calculated Stoichiometry for Olivine

	SLCX 47 Ol1	SLCX 47 Ol2	SLCX 47 Ol3	SLCX 47 Ol4	SLCX 25 Ol1
SiO ₂	39.05	38.71	38.73	37.94	39.00
TiO ₂	0.04	0.03	0.02	0.03	0.03
Al ₂ O ₃	0.01	0.01	0.01	0.03	0.02
Cr ₂ O ₃	0.01			0.01	0.01
FeO	19.89	19.65	19.73	19.86	20.19
MnO	0.13	0.12	0.16	0.14	0.13
MgO	41.34	40.90	41.16	40.19	40.78
CaO	0.06	0.07	0.08	0.15	0.07
Na ₂ O	0.07	0.05	0.06	0.28	0.03
K ₂ O	0.01	0.03	0.03	0.13	0.01
NiO	0.31	0.27	0.29	0.28	0.27
Total	100.63	99.57	99.98	98.76	100.26
Number of ions on the basis of 4 O					
Si	0.996	0.997	0.995	0.993	0.999
Ti	0.001	0.001	0.000	0.001	0.001
Al	0.000	0.000	0.000	0.001	0.000
Cr	0.000	0.000	0.000	0.000	0.000
Fe++	0.424	0.423	0.424	0.435	0.433
Mn	0.003	0.003	0.004	0.003	0.003
Mg	1.572	1.571	1.576	1.568	1.558
Ni	0.006	0.006	0.006	0.006	0.006
Ca	0.002	0.002	0.002	0.004	0.002
TOTAL	3.005	3.003	3.007	3.010	3.002
Fo	78.75	78.77	78.81	78.30	78.27
Fa	21.25	21.23	21.19	21.70	21.73
Mg#	79	79	79	78	78

* Fo = Forsterite, Fa = Fayalite, Mg# = [Mg/(Mg + Fe)]*100%. The total Fe is reported as Fe++.

Table 13 (Continued)

	SLCX 45 Ol1	SLCX 11 Ol1	SLCX 11 Ol2
SiO ₂	39.32	38.80	38.78
TiO ₂	0.02	0.02	0.01
Al ₂ O ₃	0.01	0.02	0.01
Cr ₂ O ₃	0.02	0.01	
FeO	17.33	20.97	21.07
MnO	0.14	0.18	0.15
MgO	42.96	40.43	40.48
CaO	0.06	0.11	0.07
Na ₂ O	0.02	0.03	0.02
K ₂ O	0.01	0.02	0.02
NiO	0.37	0.29	0.29
Total	99.88	100.58	100.63
Number of ions on the basis of 4 O			
Si	0.998	0.996	0.995
Ti	0.000	0.000	0.000
Al	0.000	0.001	0.000
Cr	0.000	0.000	0.000
Fe++	0.368	0.450	0.452
Mn	0.003	0.004	0.003
Mg	1.625	1.547	1.548
Ni	0.008	0.006	0.006
Ca	0.002	0.003	0.002
TOTAL	3.003	3.006	3.007
Fo	81.55	77.47	77.40
Fa	18.45	22.53	22.60
Mg#	82	77	77

Table 14 Major and Trace Element Concentrations for Clinopyroxene from LA-ICP-MS

	SLCX 11 Cpx1	SLCX 11 Cpx3	SLCX 12 Cpx1	SLCX 12 Cpx2	SLCX 21 Cpx3
<i>wt%</i>					
SiO ₂	50.11	49.93	51.40	51.19	49.07
TiO ₂	1.22	1.25	0.99	1.01	1.26
Al ₂ O ₃	6.68	6.83	7.45	7.48	7.76
Cr ₂ O ₃	0.04	0.04	0.39	0.48	0.01
FeO	6.93	6.89	6.04	5.81	7.86
MnO	0.11	0.12	0.09	0.10	0.09
MgO	13.52	13.37	13.77	13.68	12.17
CaO	18.71	18.43	17.71	17.68	18.92
Na ₂ O	2.02	2.15	2.45	2.42	2.35
K ₂ O	0.01	0.10	0.02	0.03	0.02
NiO	0.04	0.07	0.02	0.04	0.05
Total	99.40	99.18	100.33	99.92	99.56
<i>ppm</i>					
Rb	Bld.	Bld.	0.3	0.039	Bld.
Sr	162.1	165.4	232.3	211.3	163.1
Y	7.49	6.42	6.14	5.24	4.08
Zr	51.2	44.3	39.5	34.5	66.4
Nb	0.399	0.451	1.021	0.93	0.381
Sb	Bld.	Bld.	Bld.	Bld.	Bld.
Cs	Bld.	Bld.	Bld.	Bld.	Bld.
Ba	0.296	0.162	53	0.58	0.192
La	3.82	3.77	4.08	3.89	3.73
Ce	10.97	11.3	11	11.35	13.76
Pr	2.095	2.105	1.842	1.71	2.57
Nd	13.01	12.28	9.08	8.12	14.79
Sm	4.51	4.24	2.72	2.55	4.86
Eu	1.65	1.63	1.094	0.978	1.746
Gd	4.41	3.92	2.49	2.19	4.23
Tb	0.549	0.532	0.377	0.341	0.474
Dy	2.59	2.28	1.9	1.47	1.74
Ho	0.32	0.256	0.235	0.184	0.168
Er	0.517	0.42	0.514	0.481	0.2
Yb	0.165	0.155	0.197	0.174	0.044
Lu	Bld.	0.013	0.0279	0.0216	Bld.
Hf	2.77	2.09	1.44	1.4	3.7

*Bld. = Below detecting limit

Table 14 (Continued)

Ta	0.096	0.08	0.112	0.124	0.048
Pb	1.423	0.414	1.48	0.366	0.214
Th	0.253	0.228	0.053	0.072	0.188
U	0.052	0.0503	0.0177	0.0169	0.0362
P	93	86.3	144.7	135.8	92.8
Sc	36.33	33.85	52.5	49.62	21.28
V	460.5	458.2	417	421.1	436.6
Co	51.35	52.47	39.23	38.22	49.75
Cu	1.692	1.526	4.82	4.65	0.594
Zn	95.5	94.4	53.3	53.8	91.9
As	Bld.	Bld.	Bld.	8.1	Bld.

Table 14 (Continued)

	SLCX 25 Cpx1	SLCX 25 Cpx2	SLCX 25 Cpx3	SLCX 26 Cpx2	SLCX 45 Cpx1
<i>wt%</i>					
SiO ₂	51.15	50.16	50.57	49.84	51.35
TiO ₂	0.84	0.82	0.87	1.07	0.59
Al ₂ O ₃	6.88	7.87	7.44	6.27	6.19
Cr ₂ O ₃	0.22	0.23	0.23	0.21	0.34
FeO	6.31	6.54	6.12	5.85	5.32
MnO	0.06	0.07	0.09	0.10	0.08
MgO	14.20	15.11	14.06	13.93	14.37
CaO	18.59	16.38	18.75	19.61	19.37
Na ₂ O	2.04	1.91	2.02	1.76	1.92
K ₂ O	0.01	0.03	0.01	0.04	0.01
NiO	0.03	0.05	0.04	0.04	0.02
Total	100.36	99.16	100.20	98.71	99.58
<i>ppm</i>					
Rb	Bld.	Bld.	0.44	Bld.	0.098
Sr	158.4	158.3	157.8	116.2	150.4
Y	7.52	10.08	8.44	4.46	7.28
Zr	43.8	43	31	24.9	22.54
Nb	0.605	0.829	0.794	0.928	0.835
Sb	Bld.	Bld.	Bld.	Bld.	Bld.
Cs	Bld.	Bld.	Bld.	Bld.	Bld.
Ba	0.179	0.14	14.1	1.42	0.67
La	4.3	4.58	4.55	3.45	3.1
Ce	12.17	12.83	11.65	9.38	6.78
Pr	2.054	2.133	1.995	1.492	1.099
Nd	10.37	11.11	9.8	8.74	5.9
Sm	3.11	3.33	2.99	2.81	1.99
Eu	1.15	1.166	1.149	1.03	0.743
Gd	2.7	3.16	2.64	2	2.32
Tb	0.465	0.529	0.445	0.357	0.346
Dy	2.2	2.51	2.24	1.59	1.81
Ho	0.291	0.387	0.31	0.185	0.291
Er	0.628	0.89	0.726	0.344	0.7
Yb	0.269	0.437	0.356	0.103	0.48
Lu	0.029	0.042	0.0351	0.0192	0.045
Hf	1.53	1.64	1.27	1.32	0.89

Table 14 (Continued)

Ta	0.175	0.234	0.137	0.073	0.065
Pb	0.421	0.443	0.703	0.33	0.39
Th	0.224	0.288	0.25	0.178	0.19
U	0.0351	0.0337	0.0404	0.0489	0.0471
P	153.8	147.4	136.7	187	192.9
Sc	53.43	62.5	56.16	41.9	50
V	402.1	387	398.9	542	358
Co	35.52	34.02	35.98	41.5	43
Cu	2.2	2.32	2.27	2.74	9.9
Zn	56.6	49.1	48.9	45.1	54.4
As	8.8	Bld.	Bld.	Bld.	3.27

Table 14 (Continued)

	SLCX 45 Cpx3	SLCX 47 Cpx1	SLCX 47 Cpx2	SLCX 47 Cpx3	SLCX 47 Cpx4
<i>wt%</i>					
SiO ₂	51.53	50.45	50.24	50.32	50.01
TiO ₂	0.56	1.16	1.15	1.21	1.27
Al ₂ O ₃	6.11	6.50	6.43	6.64	7.02
Cr ₂ O ₃	0.38	0.02	0.04	0.04	0.03
FeO	5.42	6.47	6.51	6.65	6.56
MnO	0.09	0.06	0.05	0.10	0.08
MgO	14.43	13.90	13.95	13.79	13.70
CaO	19.37	19.21	19.17	19.12	18.80
Na ₂ O	1.92	1.90	1.93	1.97	1.96
K ₂ O	0.01	0.02	0.01	0.02	0.01
NiO	0.06	0.04	0.02	0.02	0.04
Total	99.88	99.73	99.52	99.87	99.48
<i>ppm</i>					
Rb	0.064	0.063	0.039	Bld.	Bld.
Sr	155.6	108.6	103.3	103.5	113.5
Y	4.24	5.79	4.91	5.37	6.34
Zr	19.78	38.3	31.4	35.3	39.5
Nb	0.694	0.406	0.336	0.371	0.521
Sb	0.223	Bld.	Bld.	Bld.	Bld.
Cs	Bld.	Bld.	Bld.	Bld.	Bld.
Ba	0.393	0.4	0.289	0.279	0.243
La	3.12	2.76	2.465	2.7	2.873
Ce	8.01	9.01	8.36	8.69	9.22
Pr	1.186	1.677	1.548	1.611	1.705
Nd	6.06	9.48	8.63	8.97	9.86
Sm	1.85	3.17	2.69	3.11	3.07
Eu	0.708	1.193	1.075	1.218	1.278
Gd	2.07	2.54	2.42	2.6	2.95
Tb	0.233	0.446	0.407	0.416	0.45
Dy	1.16	1.84	1.62	1.74	1.95
Ho	0.162	0.232	0.204	0.205	0.258
Er	0.282	0.431	0.33	0.41	0.452
Yb	0.104	0.16	0.142	0.073	0.17
Lu	0.0077	0.0145	Bld.	0.00019	0.0092
Hf	0.798	1.89	1.6	1.55	1.92

Table 14 (Continued)

Ta	0.078	0.0557	0.0313	0.0401	0.0603
Pb	0.814	0.747	2.11	0.621	0.776
Th	0.192	0.129	0.096	0.119	0.122
U	0.0292	0.0368	0.0219	0.0199	0.0276
P	136.8	170	148	184	145.8
Sc	38.46	38.49	36.98	34.96	36
V	409.2	470	460.7	463.9	462.8
Co	40.83	42.43	43.55	42.99	43
Cu	5.3	3.76	3.22	2.91	3.02
Zn	50.9	61.3	61.4	56.9	57.3
As	Bld.	Bld.	Bld.	Bld.	Bld.

Table 15 Major and Trace Element Concentrations for Garnet from LA-ICP-MS

	SLCX 11 Gt1	SLCX 11 Gt3	SLCX 12 Gt1	SLCX 12 Gt2	SLCX 12 Gt3
<i>wt%</i>					
SiO ₂	40.63	40.82	41.22	40.88	40.82
TiO ₂	0.33	0.41	0.28	0.26	0.33
Al ₂ O ₃	23.10	22.97	23.33	23.43	23.24
Cr ₂ O ₃	0.05	0.04	0.41	0.25	0.26
FeO	14.58	14.58	13.50	13.51	13.33
MnO	0.35	0.35	0.39	0.37	0.37
MgO	15.91	15.94	17.04	16.76	16.88
CaO	5.15	5.18	4.85	4.80	4.87
Na ₂ O	0.06	0.05	0.11	0.37	0.30
K ₂ O	0.01	0.01	0.04	0.03	0.17
NiO	0.04	0.02	0.03	0.02	0.04
Total	100.19	100.38	101.21	100.70	100.62
<i>ppm</i>					
Rb	Bld.	Bld.	Bld.		Bld.
Sr	0.611	1.39	0.914	0.77	1.425
Y	39.25	48.24	20.94	52.3	27.63
Zr	46.4	45	17.1	33.6	20.9
Nb	0.0182	0.036	0.036	Bld.	0.04
Sb	Bld.	Bld.	Bld.	Bld.	Bld.
Cs	Bld.	Bld.	Bld.	Bld.	Bld.
Ba	0.35	0.92	0.7	Bld.	0.89
La	Bld.	Bld.	0.0017	Bld.	Bld.
Ce	0.12	0.1	0.096	0.38	0.081
Pr	0.037	0.063	0.041	0.102	0.047
Nd	0.86	0.78	0.413	4.7	0.63
Sm	1.2	1.37	0.79	3.4	0.9
Eu	0.967	0.982	0.525	2.33	0.63
Gd	3.6	3.85	1.63	4.9	1.91
Tb	0.944	0.998	0.485	1.23	0.561
Dy	7.75	8.38	3.86	11.9	4.35
Ho	1.518	1.84	0.751	1.96	1.02
Er	4.16	5.21	2.22	7.1	3.03
Yb	2.98	4.71	2.01	7.7	3.15
Lu	0.318	0.534	0.245	0.95	0.442
Hf	0.91	0.79	0.162	0.39	0.185

Table 15 (Continued)

Ta	Bld.	Bld.	Bld.	Bld.	Bld.
Pb	0.896	1.002	0.355	Bld.	0.24
Th	Bld.	Bld.	Bld.	Bld.	Bld.
U	Bld.	Bld.	Bld.	0.0038	Bld.
P	117.3	126.1	263	402	282
Sc	75.7	72.7	84.3	186.5	83.8
V	164.8	157.6	115.4	121.7	109.6
Co	85.6	89.5	64	85.2	63.4
Cu	0.33	1	0.316	0.18	0.314
Zn	102.6	119.5	71.1	122	59.6
As	Bld.	Bld.	Bld.	Bld.	Bld.

Table 15 (Continued)

	SLCX 21 Gt1	SLCX 25 Gt1	SLCX 25 Gt2	SLCX 26 Gt1	SLCX 47 Gt1
<i>wt%</i>					
SiO ₂	40.27	40.97	40.98	40.66	40.73
TiO ₂	0.32	0.23	0.22	0.25	0.38
Al ₂ O ₃	22.94	23.38	23.17	22.98	22.76
Cr ₂ O ₃	0.02	0.29	0.29	0.28	0.03
FeO	16.88	14.81	13.18	13.32	14.43
MnO	0.35	0.43	0.43	0.41	0.32
MgO	14.29	16.41	16.87	16.42	16.46
CaO	5.77	5.11	5.13	5.43	4.84
Na ₂ O	0.10	0.07	0.15	0.19	0.13
K ₂ O	0.03	0.01	0.04	0.04	0.10
NiO	0.03		0.03	0.02	
Total	100.99	101.70	100.50	99.99	100.20
<i>ppm</i>					
Rb	Bld.	0.045	0.041	Bld.	Bld.
Sr	0.743	0.637	0.691	0.396	0.48
Y	23.97	51.52	42.39	25.53	29.65
Zr	37.7	35.3	42.6	17.33	31.6
Nb	0.0048	0.051	0.083	0.049	0.046
Sb	Bld.	Bld.	Bld.	Bld.	Bld.
Cs	Bld.	Bld.	Bld.	Bld.	Bld.
Ba	0.292	0.35	0.262	0.242	0.197
La	0.0076	0.0042	Bld.	Bld.	Bld.
Ce	0.162	0.18	0.15	0.079	0.09
Pr	0.075	0.079	0.086	0.0375	0.0414
Nd	0.73	0.84	0.55	0.476	0.642
Sm	1.46	0.99	0.89	0.82	1.08
Eu	0.966	0.783	0.717	0.493	0.617
Gd	3.68	2.71	2.36	1.6	2.06
Tb	0.804	0.839	0.793	0.565	0.682
Dy	5.8	7.87	6.48	4.55	5.24
Ho	0.967	1.849	1.501	0.989	1.13
Er	2.1	5.91	4.6	2.54	3.04
Yb	0.92	6.19	4.9	2.07	2.33
Lu	0.058	0.844	0.633	0.238	0.254
Hf	0.493	0.282	0.46	0.311	0.495

Table 15 (Continued)

Ta	0.0049	Bld.	Bld.	Bld.	Bld.
Pb	0.487	0.209	0.236	0.366	0.718
Th	Bld.	Bld.	Bld.	Bld.	Bld.
U	Bld.	Bld.	Bld.	Bld.	Bld.
P	140.3	236.8	244	261	205
Sc	31.39	119.4	117.1	68.1	54.84
V	129.8	118.7	124.2	155.1	159.3
Co	88	62.36	60.04	64.98	69.4
Cu	Bld.	0.249	0.71	0.386	0.543
Zn	113.4	74.5	64.2	49.7	63.5
As	5.41	26	Bld.	Bld.	Bld.

Table 15 (Continued)

	SLCX 47 Gt2	SLCX 47 Gt3	SLCX 47 Gt4
<i>wt%</i>			
SiO ₂	41.01	40.25	40.95
TiO ₂	0.41	0.46	0.30
Al ₂ O ₃	23.47	23.10	23.51
Cr ₂ O ₃	0.05	0.03	0.04
FeO	14.12	13.58	13.96
MnO	0.35	0.32	0.31
MgO	16.64	16.37	16.88
CaO	5.25	5.22	5.23
Na ₂ O	0.06	0.11	0.08
K ₂ O	0.01	0.03	0.02
NiO			0.01
Total	101.35	99.46	101.30
<i>ppm</i>			
Rb	0.052	0.066	Bld.
Sr	0.581	0.629	0.707
Y	36.47	37.52	39.36
Zr	43.9	29.8	30.2
Nb	0.042	0.022	0.0259
Sb	Bld.	Bld.	Bld.
Cs	Bld.	Bld.	Bld.
Ba	0.317	0.417	0.403
La	Bld.	Bld.	Bld.
Ce	0.068	0.081	0.075
Pr	0.0414	0.0326	0.0351
Nd	0.54	0.58	0.445
Sm	0.97	0.91	0.94
Eu	0.662	0.605	0.646
Gd	2.54	2.1	2.29
Tb	0.828	0.724	0.753
Dy	6.19	6.19	6.63
Ho	1.386	1.381	1.499
Er	3.87	4.14	4.3
Yb	2.87	3.68	3.65
Lu	0.322	0.406	0.44
Hf	0.706	0.594	0.565

Table 15 (Continued)

Ta	Bld.	Bld.	Bld.
Pb	0.746	0.886	1.314
Th	Bld.	Bld.	Bld.
U	Bld.	Bld.	Bld.
P	197	341	199
Sc	75.4	73.9	79.1
V	174.8	159.3	166
Co	70.64	66.49	70.39
Cu	3.27	3.58	3.4
Zn	65.6	63.2	69.8
As	Bld.	Bld.	105

Table 16 Ages (Ma) of 4 Zircons with Correlated Drilling Depth

Depth (μm)	Zircon1			Zircon2			Zircon3			Zircon4		
	Age	U ppm	U/Th	Age	U ppm	U/Th	Age	U ppm	U/Th	Age	U ppm	U/Th
0	14.14	1374.87	6.25	12.27	585.60	3.89	17.38	979.82	6.65	0.00	1513.49	
0.05	12.26	1449.09	7.00	13.13	511.61	3.99	14.39	1045.02	6.57	0.00	3159.25	
0.1	12.10	1263.55	7.19	13.94	497.81	4.58	11.87	1052.17	6.28	11.67	3569.70	0.52
0.15	14.13	1091.43	6.70	15.56	484.99	3.94	14.12	883.81	6.04	9.90	3819.83	0.64
0.2	12.80	1199.41	6.27	16.30	460.58	3.83	15.47	848.76	6.28	13.05	3345.78	0.58
0.25	13.67	1036.98	5.47	13.84	499.24	4.12	12.66	875.53	6.76	12.89	3447.75	0.59
0.3	13.61	964.39	5.89	15.55	497.36	3.69	11.46	875.62	6.67	12.35	3324.70	0.48
0.35	13.30	932.63	5.42	14.71	488.43	3.92	11.93	847.81	6.67	10.86	3444.83	0.52
0.4	14.08	914.37	5.70	15.54	483.21	3.51	11.34	732.38	5.74	12.46	3176.11	0.61
0.45	12.81	911.95	5.62	14.19	493.67	3.84	13.08	625.58	5.11	12.05	3016.20	0.73
0.5	13.79	868.23	4.90	14.39	487.88	3.37	14.54	592.24	5.94	12.48	2944.37	1.10
0.55	14.84	822.76	5.02	12.50	510.99	3.28	14.45	607.67	5.56	17.21	2451.59	1.33
0.6	13.14	904.13	4.75	14.61	466.98	3.55	13.76	639.07	6.03	13.07	2969.56	1.61
0.65	15.67	853.10	5.10	13.92	437.98	3.33	11.31	671.17	6.64	12.12	2700.41	1.46
0.7	11.50	869.12	4.94	14.61	393.66	3.15	11.18	609.25	6.09	13.46	2053.68	1.47
0.75	14.50	750.48	4.41	16.13	427.28	3.53	12.38	587.85	5.98	15.47	1849.03	1.60
0.8	13.54	799.21	4.94	14.07	421.75	3.44	13.53	565.78	6.54	15.58	1827.00	1.51
0.85	13.10	811.38	4.12	15.83	406.32	3.05	14.13	509.78	6.56	14.23	2010.14	1.47
0.9	13.74	777.24	4.11	15.11	435.63	3.34	12.66	540.46	6.77	15.50	1983.87	1.50
0.95	12.45	727.85	4.34	15.46	439.97	3.12	10.57	492.57	5.73	12.96	1788.60	1.49
1	11.28	636.31	4.26	14.83	472.31	3.14	11.83	488.39	6.46	16.96	1510.06	1.31
1.05	14.95	515.93	3.93	13.44	512.74	3.19	11.94	516.32	6.02	14.54	1510.02	1.36
1.1	12.73	506.74	4.41	13.64	462.76	2.95	11.06	475.09	5.68	12.70	1556.25	1.46
1.15	16.44	490.19	4.22	14.76	453.00	2.96	9.53	431.52	5.59	14.41	1449.45	1.38
1.2	13.91	542.52	4.55	14.50	453.27	3.24	14.43	414.22	5.85	13.82	1348.74	1.30

*Ages are measured isotopic $^{206}\text{Pb}/^{238}\text{U}$ dates corrected for common lead, see detailed instruction in Chapter III. Data are as reported by the instrument.

Table 16 (Continued)

Depth (μm)	Zircon1			Zircon2			Zircon3			Zircon4		
	Age	U ppm	U/Th	Age	U ppm	U/Th	Age	U ppm	U/Th	Age	U ppm	U/Th
1.25	13.06	528.86	4.93	16.81	430.55	2.90	11.53	435.17	5.62	14.83	1315.24	1.02
1.3	12.40	503.33	4.55	14.20	471.84	2.89	13.44	437.72	5.57	12.68	1363.54	1.16
1.35	13.11	412.26	4.31	13.28	461.96	2.79	12.61	490.24	5.22	12.74	1210.11	1.14
1.4	12.20	409.43	4.02	14.93	428.29	2.83	12.16	478.95	6.01	16.90	1112.34	1.02
1.45	13.69	372.61	4.13	13.77	437.95	2.56	12.02	469.84	5.34	11.80	1208.41	0.84
1.5	13.42	379.21	5.44	13.46	415.42	2.67	13.77	453.11	5.48	12.56	1141.86	0.60
1.55	12.98	365.43	4.53	15.79	377.14	2.65	11.04	451.49	4.83	13.00	1053.62	0.86
1.6	14.33	353.85	4.84	13.64	410.44	2.52	11.61	426.15	4.33	15.89	959.61	0.81
1.65	13.57	352.93	5.06	13.81	394.63	2.66	14.31	415.89	5.38	17.31	924.44	0.84
1.7	13.67	334.91	5.16	13.75	391.94	2.50	11.32	463.56	5.22	15.67	946.22	0.78
1.75	13.73	348.55	6.03	13.91	346.26	2.58	13.48	453.94	5.22	14.63	905.17	0.53
1.8	16.41	352.00	4.65	15.86	350.24	2.74	10.71	507.48	5.02	16.61	865.50	0.62
1.85	13.19	354.67	3.79	16.45	384.66	2.35	11.43	526.80	5.30	14.07	899.87	0.54
1.9	13.33	313.15	6.46	12.37	418.34	2.88	12.12	548.00	4.32	13.12	910.68	0.51
1.95	14.57	304.73	3.82	15.44	373.01	2.46	13.83	567.95	5.82	18.70	909.19	0.48
2	13.55	306.34	5.19	13.44	349.57	2.54	11.40	610.25	5.82	9.87	1059.87	0.48
2.05	14.68	277.71	4.25	15.68	315.73	2.30	12.06	598.78	5.24	14.88	922.58	0.36
2.1	12.63	322.46	3.76	14.79	326.46	2.52	12.33	607.58	5.02	12.94	921.99	0.30
2.15	14.93	321.03	4.18	15.47	332.58	2.42	13.98	659.62	4.95	11.79	924.38	0.40
2.2	16.18	329.31	3.86	13.45	353.05	2.51	11.97	733.99	4.95	12.11	998.10	0.32
2.25	13.38	337.82	3.83	15.54	338.74	2.46	14.64	722.81	4.71	13.23	1016.17	0.27
2.3	14.88	318.47	3.98	14.05	357.64	2.22	12.39	765.02	4.96	10.65	1156.77	0.26
2.35	12.63	319.33	4.11	15.16	361.19	2.26	15.36	801.64	4.96	12.12	1204.96	0.23
2.4	13.69	303.29	3.44	14.61	372.91	2.42	11.14	889.80	4.72	11.15	1099.00	0.24
2.45	15.11	281.58	3.61	14.22	360.27	2.26	12.01	782.25	4.75	12.54	1159.89	0.26

Table 16 (Continued)

Depth (μm)	Zircon1			Zircon2			Zircon3			Zircon4		
	Age	U ppm	U/Th	Age	U ppm	U/Th	Age	U ppm	U/Th	Age	U ppm	U/Th
2.5	15.68	294.79	3.83	11.55	329.53	2.29	12.51	795.72	5.99	13.06	1068.57	0.24
2.55	12.69	312.23	3.93	16.65	338.74	2.06	12.54	808.17	6.01	13.06	1089.21	0.28
2.6	12.24	290.59	2.85	14.83	347.81	2.19	15.21	818.93	5.28	6.67	1197.09	0.25
2.65	13.26	266.31	3.50	15.05	342.78	2.17	11.92	874.37	6.00	8.77	1307.90	0.20
2.7	13.92	282.92	3.30	13.73	342.88	2.09	13.13	821.66	6.24	9.60	1302.06	0.21
2.75	14.53	293.74	3.21	14.14	341.21	2.36	14.60	854.48	5.22	10.96	1267.23	0.22
2.8	16.43	282.28	3.34	13.69	358.62	2.22	13.89	933.51	5.75	7.75	1211.69	0.19
2.85	14.00	286.20	3.07	13.98	361.92	2.03	13.13	979.11	5.73	10.03	1074.60	0.21
2.9	12.16	300.39	2.47	15.71	352.23	2.02	12.37	1001.86	5.79	8.96	1113.07	0.15
2.95	13.34	275.08	2.55	13.09	363.29	2.01	13.81	989.39	6.01	10.26	842.64	0.33
3	16.35	293.07	2.80	13.12	342.09	1.96	15.92	982.21	6.22	15.76	783.77	0.46
3.05	11.86	333.50	2.28	12.65	329.09	2.13	11.64	1041.72	6.17	12.31	804.81	0.54
3.1	15.70	287.11	2.32	13.65	298.02	1.89	15.10	933.00	6.51	9.95	782.38	0.47
3.15	14.65	286.01	2.27	13.45	292.04	2.05	13.50	980.38	6.24	12.19	738.84	0.34
3.2	13.45	297.17	2.12	14.38	291.35	2.12	14.64	1008.22	6.69	13.36	781.28	0.41
3.25	12.66	295.59	2.02	13.73	295.83	1.99	13.09	1066.92	6.30	8.95	712.56	0.40
3.3	14.28	303.52	1.63	14.09	266.43	1.98	13.67	1039.05	7.49	12.46	631.11	0.46
3.35	11.55	297.27	1.53	15.48	240.84	1.91	15.69	1000.22	7.69	13.05	633.58	0.59
3.4	11.57	307.19	1.76	19.20	237.33	1.96	11.91	1038.24	8.64	11.35	611.91	0.66
3.45	12.08	315.89	1.58	14.98	274.40	1.85	12.92	1005.48	7.93	8.95	559.62	0.69
3.5	15.51	322.59	1.70	13.88	281.88	1.98	12.91	1000.33	7.80	12.82	512.43	0.78
3.55	13.04	333.44	1.52	14.86	260.14	2.07	13.53	1003.53	9.34	15.61	545.91	0.92
3.6	12.40	347.28	1.47	17.29	265.34	1.78	14.02	1034.18	9.02	14.21	547.59	1.01
3.65	12.09	329.05	1.44	18.00	278.09	2.13	13.96	1042.88	7.91	12.71	530.36	0.89
3.7	12.57	317.40	1.35	14.99	341.24	1.93	12.03	1065.99	8.52	14.20	495.11	1.00

Table 16 (Continued)

Depth (μm)	Zircon1			Zircon2			Zircon3			Zircon4		
	Age	U ppm	U/Th	Age	U ppm	U/Th	Age	U ppm	U/Th	Age	U ppm	U/Th
3.75	13.47	323.71	1.39	15.23	361.72	1.96	13.71	1030.17	7.85	16.68	454.87	1.08
3.8	14.27	327.62	1.38	13.81	372.39	1.89	10.34	1052.19	8.84	13.45	440.42	1.04
3.85	13.44	327.40	1.26	14.88	345.44	1.91	13.76	957.55	7.76	13.37	446.54	1.05
3.9	13.29	315.59	1.24	14.32	362.77	1.96	12.08	977.83	9.60	13.47	411.13	1.06
3.95	11.88	318.39	1.37	15.24	380.55	1.94	14.01	943.23	7.80	13.00	417.51	1.08
4	13.85	339.08	1.27	12.45	411.52	1.99	13.10	1029.66	9.51	14.86	444.62	1.10
4.05	13.41	338.75	1.38	12.81	389.89	1.94	14.23	1008.34	8.06	17.94	444.45	1.07
4.1	13.19	337.73	1.42	14.70	370.12	1.84	11.76	1105.48	9.00	15.89	471.34	0.99
4.15	14.32	333.20	1.48	16.38	401.14	1.89	14.91	1048.19	8.24	15.53	451.57	0.92
4.2	12.26	313.00	1.58	13.80	427.34	1.88	15.08	1181.92	9.25	12.90	444.83	1.02
4.25	14.62	295.63	1.60	12.55	429.35	1.68	9.92	1289.82	8.07	14.93	452.86	0.93
4.3	14.03	339.55	1.57	15.07	397.17	1.72	13.14	1104.87	8.74	11.65	437.11	0.84
4.35	15.34	331.05	1.54	14.88	422.89	1.79	12.79	1109.37	7.42	11.54	432.58	0.84
4.4	12.28	349.07	1.70	13.46	443.32	1.80	13.65	1102.59	9.81	10.95	411.25	0.68
4.45	12.65	323.21	1.54	12.61	433.79	1.57	11.54	1166.65	8.58	12.24	378.35	0.77
4.5	11.10	315.77	1.69	13.83	409.08	1.62	12.27	1067.98	9.78	12.81	388.95	0.79
4.55	15.23	305.24	1.56	14.95	417.35	1.69	12.52	1038.21	7.70	12.44	379.06	0.71
4.6	12.89	327.19	1.56	13.55	465.75	1.62	13.24	1049.63	7.66	13.56	378.54	0.69
4.65	12.60	335.23	1.65	15.89	463.90	1.66	14.51	1130.79	7.58	12.24	385.13	0.74
4.7	15.42	305.46	1.59	13.42	501.15	1.66	12.09	1211.75	7.65	13.03	349.34	0.74
4.75	14.07	334.49	1.44	12.96	452.69	1.57	12.07	1182.29	7.54	14.47	353.27	0.61
4.8	13.43	344.27	1.45	15.19	426.96	1.65	11.12	1118.95	8.02	13.57	384.24	0.65
4.85	13.29	341.05	1.35	12.32	454.24	1.67	13.03	1053.91	8.77	10.60	379.10	0.74
4.9	12.42	342.81	1.36	12.50	433.81	1.60	12.31	1094.71	8.33	13.62	340.01	0.72
4.95	13.72	361.21	1.41	11.42	394.41	1.68	15.01	1105.08	7.72	13.64	338.46	0.60

Table 16 (Continued)

Depth (µm)	Zircon1			Zircon2			Zircon3			Zircon4		
	Age	U ppm	U/Th	Age	U ppm	U/Th	Age	U ppm	U/Th	Age	U ppm	U/Th
5	12.08	350.88	1.41	13.33	355.92	1.63	11.85	1220.00	8.15	13.22	351.32	0.59
5.05	11.43	332.49	1.47	12.61	347.01	1.74	12.51	1191.20	8.03	12.94	358.82	0.61
5.1	12.63	313.77	1.48	15.79	341.64	1.69	14.91	1202.92	8.30	13.82	343.59	0.59
5.15	13.43	304.11	1.58	16.61	364.28	1.65	11.54	1306.70	8.06	11.87	350.04	0.57
5.2	13.07	309.74	1.79	14.15	399.32	1.67	12.76	1251.95	7.41	12.89	339.25	0.61
5.25	14.70	345.64	1.63	12.11	386.05	1.67	13.43	1205.31	7.31	14.02	330.80	0.64
5.3	13.27	364.37	1.56	13.43	377.12	1.71	13.01	1192.72	6.54	18.58	316.51	0.74
5.35	13.64	362.51	1.51	16.54	345.22	1.67	12.47	1216.36	6.99	11.54	329.67	0.74
5.4	12.93	342.30	1.52	12.80	365.40	1.70	10.30	1216.68	7.01	12.69	313.77	0.81
5.45	13.81	325.23	1.48	14.34	356.64	1.61	14.12	1110.86	7.28	13.86	296.09	0.87
5.5	13.01	350.10	1.61	15.56	349.30	1.79	11.59	1171.99	7.78	11.05	288.90	0.95
5.55	12.12	328.35	1.53	13.82	371.70	1.69	12.33	1075.68	7.51	14.69	294.24	1.00
5.6	13.35	303.11	1.51	15.32	377.50	1.66	15.93	1124.48	6.79	11.37	281.54	1.00
5.65	15.25	294.98	1.61	14.36	412.38	1.63	13.89	1263.28	6.98	13.91	259.25	1.06
5.7	13.82	295.21	1.47	13.13	417.98	1.59	10.70	1322.90	7.20	14.35	276.83	1.11
5.75	13.56	303.71	1.56	15.50	393.99	1.64	12.51	1232.36	7.43	15.13	283.99	1.19
5.8	13.20	320.29	1.62	14.29	412.53	1.67	13.26	1258.52	7.89	12.13	270.84	1.16
5.85	12.83	328.41	1.61	14.36	417.29	1.57	13.24	1282.47	7.05	13.80	251.93	1.17
5.9	14.42	319.68	1.58	15.06	377.96	1.58	14.19	1313.37	7.74	14.10	273.03	1.21
5.95	12.36	291.58	1.46	13.88	407.32	1.54	12.22	1396.93	6.99	12.65	258.10	1.03
6	13.89	301.28	1.52	12.12	388.61	1.64	12.68	1339.81	7.82	15.59	251.96	1.08
6.05	13.88	303.21	1.34	13.43	373.48	1.55	12.88	1302.72	6.90	12.38	252.59	1.03
6.1	12.33	321.60	1.31	15.46	359.62	1.57	10.98	1308.89	7.29	12.17	238.01	1.00
6.15	12.59	376.18	1.37	14.48	393.44	1.55	11.38	1215.33	6.59	15.21	214.38	1.10
6.2	11.15	351.26	1.33	14.65	396.62	1.64	11.41	1132.83	6.97	12.20	203.26	1.14

Table 16 (Continued)

Depth (μm)	Zircon1			Zircon2			Zircon3			Zircon4		
	Age	U ppm	U/Th	Age	U ppm	U/Th	Age	U ppm	U/Th	Age	U ppm	U/Th
6.25	14.44	343.10	1.34	12.54	411.47	1.54	15.44	1071.54	6.37	14.78	211.53	1.21
6.3	13.04	348.86	1.29	13.21	402.21	1.58	10.96	1186.82	6.73	13.28	222.41	1.31
6.35	11.90	330.71	1.36	14.65	381.16	1.49	12.56	1061.42	6.24	13.55	224.67	1.43
6.4	12.85	296.19	1.42	13.59	386.00	1.51	14.83	998.70	5.94	14.40	205.78	1.54
6.45	14.27	292.80	1.45	15.24	367.07	1.53	14.33	1004.16	5.57	14.27	207.98	1.62
6.5	12.25	296.10	1.49	11.64	395.77	1.57	13.35	920.30	5.23	13.33	206.01	1.55
6.55	13.37	296.67	1.58	13.94	345.38	1.56	17.29	831.15	5.60	14.66	199.95	1.45
6.6	12.38	287.48	1.59	14.72	315.69	1.55	16.75	841.07	4.71	15.42	190.50	1.57
6.65	13.59	293.49	1.66	15.35	319.00	1.52	18.69	815.36	4.86	14.49	206.04	1.36
6.7	14.10	283.54	1.55	14.21	313.48	1.63	17.06	832.57	4.48	13.04	199.32	1.52
6.75	15.28	266.15	1.64	13.43	316.29	1.46	17.79	882.81	5.01	16.10	195.86	1.34
6.8	12.62	265.91	1.62	15.27	302.48	1.49	15.75	879.63	4.26	12.79	200.67	1.76
6.85	14.05	268.57	1.57	17.38	312.03	1.54	17.54	776.44	3.99	14.15	178.66	1.61
6.9	11.96	266.97	1.67	15.09	338.92	1.58	18.63	740.65	4.14	14.58	176.80	1.51
6.95	14.72	264.87	1.65	13.70	314.67	1.54	18.75	687.44	4.21	15.09	177.25	1.38
7	14.77	269.23	1.74	15.38	286.59	1.55	24.34	633.99	3.73	11.09	178.70	1.62
7.05	14.16	271.86	1.63	13.14	304.36	1.62	23.43	693.01	3.99	16.64	161.15	1.50
7.1	13.36	270.16	1.62	14.67	292.31	1.50	21.60	758.31	3.59	13.49	167.34	1.63
7.15	12.58	264.87	1.66	15.52	268.39	1.58	20.42	794.29	3.72	15.38	171.83	1.83
7.2	12.41	288.53	1.76	16.79	279.88	1.50	20.92	776.77	3.79	14.23	166.96	1.71
7.25	12.77	264.58	1.66	14.06	290.46	1.51	21.13	724.92	3.54	17.13	160.28	1.80
7.3	15.95	260.20	1.66	17.85	293.56	1.50	21.88	720.18	3.48	13.42	173.35	1.72
7.35	11.32	263.60	1.70	14.49	314.15	1.59	20.20	717.36	3.90	12.08	184.48	1.61
7.4	14.04	252.36	1.67	13.67	298.34	1.54	26.15	701.83	3.60	15.14	183.51	1.73
7.45	13.62	271.46	1.57	14.34	291.12	1.49	20.95	767.40	3.61	14.58	177.09	1.54

Table 16 (Continued)

Depth (µm)	Zircon1			Zircon2			Zircon3			Zircon4		
	Age	U ppm	U/Th	Age	U ppm	U/Th	Age	U ppm	U/Th	Age	U ppm	U/Th
7.5	13.09	272.72	1.49	13.59	297.12	1.48	24.10	741.22	3.89	13.52	175.62	1.83
7.55	13.82	267.24	1.74	14.72	289.21	1.49	21.82	780.79	3.72	13.27	172.53	1.58
7.6	11.58	257.55	1.52	15.70	290.14	1.53	23.36	840.56	3.70	15.29	159.97	1.85
7.65	15.02	252.42	1.53	15.34	316.45	1.67	18.58	935.14	3.83	14.53	154.81	1.86
7.7	12.29	269.76	1.57	12.83	310.33	1.55	19.05	902.36	3.84	13.27	154.17	1.89
7.75	15.31	260.04	1.60	13.82	296.43	1.46	18.18	907.82	3.78	16.31	163.61	1.69
7.8	11.88	273.54	1.63	15.34	301.17	1.66	22.33	906.74	3.87	13.64	145.63	2.03
7.85	14.96	257.29	1.61	13.54	302.13	1.53	21.13	1050.55	3.73	14.99	135.91	1.90
7.9	14.45	268.35	1.56	14.80	290.11	1.53	18.14	1158.59	3.61	16.02	140.27	1.96
7.95	11.59	290.60	1.50	14.59	290.40	1.54	17.08	1126.30	3.68	14.20	138.45	1.65
8	12.24	293.30	1.53	15.18	283.57	1.52	17.58	1132.44	3.36	20.11	137.98	1.63
8.05	12.14	290.87	1.46	15.36	285.26	1.55	16.25	1161.48	3.42	16.31	137.36	2.04
8.1	14.63	261.02	1.58	14.71	269.25	1.46	16.80	1156.99	3.44	18.99	144.28	1.66
8.15	13.45	265.69	1.47	16.85	254.82	1.50	18.99	1129.81	3.22	16.22	157.05	1.87
8.2	12.74	273.12	1.44	15.30	275.53	1.61	21.46	1168.56	3.26	17.21	166.68	1.76
8.25	13.26	270.48	1.40	15.92	287.67	1.55	19.81	1247.57	3.11	15.32	166.53	1.61
8.3	13.22	292.19	1.49	15.58	296.42	1.56	18.99	1273.41	3.07	18.83	170.61	1.16
8.35	12.91	289.50	1.35	14.10	291.27	1.46	21.34	1292.97	2.96	17.94	165.74	1.41
8.4	12.09	286.13	1.40	15.74	284.51	1.61	20.09	1319.04	2.79	15.86	172.93	1.49
8.45	12.89	268.20	1.43	14.25	286.17	1.64	20.63	1310.50	2.78	18.88	146.24	1.39
8.5	13.62	266.44	1.40	11.70	270.38	1.50	24.24	1169.22	2.68	16.87	160.34	1.35
8.55	13.97	262.72	1.47	14.74	263.40	1.46	24.80	1138.25	2.60	15.11	132.32	1.45
8.6	12.72	272.60	1.44	15.68	254.02	1.49	26.83	1118.10	2.65	21.85	135.03	1.20
8.65	14.86	250.40	1.44	14.12	259.19	1.42	24.11	1114.78	2.49	22.12	144.86	0.96
8.7	11.96	249.15	1.43	15.43	263.45	1.44	25.55	1027.92	2.44	12.01	158.44	1.11

Table 16 (Continued)

Depth (μm)	Zircon1			Zircon2			Zircon3			Zircon4		
	Age	U ppm	U/Th	Age	U ppm	U/Th	Age	U ppm	U/Th	Age	U ppm	U/Th
8.75	13.57	243.14	1.47	14.80	261.85	1.50	27.72	950.66	2.31	26.45	148.61	1.06
8.8	13.58	235.29	1.47	17.25	260.35	1.56	32.19	934.84	2.23	18.12	158.52	1.04
8.85	12.09	230.23	1.33	14.91	283.74	1.51	30.34	981.09	2.22	14.55	149.79	1.07
8.9	14.50	215.22	1.43	13.52	270.83	1.59	34.09	946.13	2.14	19.68	145.70	1.05
8.95	12.84	228.89	1.47	14.12	253.27	1.65	29.34	1004.86	2.04	15.57	144.81	1.11
9	12.56	231.89	1.49	14.35	275.04	1.45	34.48	916.73	2.00	19.90	136.93	1.23
9.05	14.03	228.12	1.43	14.21	294.32	1.61	37.29	877.69	1.94	13.40	146.95	1.30
9.1	15.65	228.86	1.45	13.43	276.73	1.52	38.51	806.94	1.82	17.84	155.46	1.25
9.15	14.79	232.76	1.53	15.37	268.63	1.47	36.00	753.93	1.83	16.84	153.49	1.59
9.2	13.45	253.10	1.29	15.00	285.53	1.48	45.59	647.97	1.77	16.62	149.21	1.46
9.25	13.44	247.24	1.45	15.40	282.24	1.49	40.73	683.83	1.87	15.04	159.84	1.69
9.3	11.86	247.77	1.39	12.99	271.07	1.50	47.93	580.63	1.70	11.03	145.69	1.24
9.35	13.44	235.56	1.51	15.55	264.68	1.51	62.43	515.53	1.62	15.02	137.47	1.63
9.4	11.67	233.58	1.49	13.16	261.63	1.48	55.39	544.82	1.68	14.57	142.24	1.42
9.45	13.91	215.04	1.38	14.44	234.86	1.63	62.97	511.95	1.56	14.60	146.87	1.43
9.5	14.61	206.59	1.61	15.34	238.14	1.64	57.47	532.95	1.52	11.59	159.68	1.53
9.55	14.94	209.82	1.47	15.15	237.22	1.61	63.22	497.18	1.57	13.69	146.75	1.45
9.6	11.87	219.01	1.45	16.19	252.82	1.55	66.33	491.79	1.50	13.78	150.67	1.65
9.65	12.44	210.46	1.56	13.73	266.62	1.55	66.20	494.12	1.45	11.72	151.95	1.25
9.7	12.93	198.17	1.40	15.97	256.66	1.63	61.85	522.26	1.47	16.38	145.81	1.29
9.75	13.59	188.80	1.63	12.63	291.80	1.55	65.36	497.48	1.38	15.74	161.04	1.50
9.8	13.39	193.20	1.39	13.92	264.94	1.61	72.79	480.55	1.32	10.97	149.18	1.43
9.85	13.87	197.95	1.58	13.48	233.62	1.79	62.84	479.81	1.32	13.87	163.75	1.37
9.9	14.67	201.59	1.48	17.46	223.03	1.56	69.00	446.01	1.35	18.70	158.59	1.50
9.95	14.18	197.94	1.45	15.13	245.74	1.70	72.74	418.25	1.28	16.26	166.54	1.66

Table 16 (Continued)

Depth (μm)	Zircon1			Zircon2			Zircon3			Zircon4		
	Age	U ppm	U/Th									
10	12.00	205.35	1.62	13.24	243.79	1.78	79.43	408.71	1.29	14.98	164.70	1.60
10.05	13.66	199.59	1.36	12.20	240.92	1.73	77.36	408.32	1.23	10.28	173.30	1.44
10.1	13.18	184.49	1.68	50.37	238.01	1.76	79.66	418.63	1.26	17.87	162.81	1.86
10.15	15.76	184.75	1.51	14.12	230.39	1.74	75.37	431.69	1.27	15.37	192.27	1.77
10.2	15.46	179.72	1.65	14.56	233.86	1.57	81.72	431.44	1.30	14.57	194.87	1.67
10.25	16.89	183.87	1.55	16.67	224.43	1.86	72.65	467.58	1.30	11.81	190.63	1.84
10.3	14.33	190.01	1.60	14.28	246.95	1.64	72.56	462.34	1.29	15.02	183.35	2.11
10.35	16.90	183.04	1.58	14.13	219.00	1.98	74.71	445.55	1.24	14.04	210.33	2.12
10.4	17.62	192.69	1.82	13.39	210.53	1.58	85.61	428.86	1.33	14.97	210.13	2.26
10.45	20.15	198.64	1.70	14.59	188.17	1.53	81.61	463.40	1.20	12.66	221.67	2.03
10.5	17.34	213.54	1.83	16.82	190.61	1.67	78.57	466.42	1.26	15.70	235.93	2.31
10.55	20.42	215.42	1.72	15.30	198.09	1.67	81.50	439.07	1.14	14.69	251.98	2.28
10.6	20.38	204.03	1.82	16.58	194.60	1.75	82.26	427.70	1.21	15.97	259.74	2.58
10.65	20.67	193.03	1.83	13.65	218.20	1.84	80.03	428.00	1.19	18.42	256.01	2.67
10.7	25.16	187.04	2.39	15.00	210.21	1.73	90.00	406.34	1.22	15.44	281.01	2.54
10.75	25.22	195.30	2.02	14.24	201.69	1.68	84.90	436.96	1.23	19.21	258.14	2.54
10.8	27.21	200.86	1.91	15.58	198.16	1.70	82.60	452.23	1.22	18.90	237.59	2.69
10.85	29.55	216.75	2.33	15.31	200.28	1.93	81.24	455.50	1.20	19.73	247.66	2.59
10.9	28.47	219.27	2.22	14.22	190.66	1.71	83.11	452.50	1.18	13.57	248.56	2.36
10.95	30.86	201.81	2.26	14.98	176.54	1.85	72.87	446.24	1.19	20.77	224.58	2.42
11	35.97	192.39	2.04	17.82	185.64	1.76	90.46	383.31	1.13	17.41	240.48	2.06
11.05	44.89	202.67	2.04	14.79	213.24	1.92	84.31	385.24	1.09	21.65	232.71	2.81
11.1	35.32	230.48	2.12	14.45	228.95	1.90	96.05	394.27	1.18	15.69	229.70	2.29
11.15	40.73	223.67	2.06	16.35	214.98	1.90	76.40	438.59	1.17	15.41	214.78	2.44
11.2	38.41	219.74	2.01	14.36	239.47	1.72	82.84	422.79	1.16	16.90	217.85	2.52

Table 16 (Continued)

Depth (μm)	Zircon1			Zircon2			Zircon3			Zircon4		
	Age	U ppm	U/Th									
11.25	50.30	205.10	1.67	13.21	237.58	1.83	88.24	428.85	1.20	12.04	236.43	2.48
11.3	45.43	216.20	1.99	12.92	232.81	1.78	86.38	452.84	1.16	12.86	242.18	2.52
11.35	51.17	214.11	1.82	15.13	213.91	1.71	80.15	469.44	1.22	15.75	237.02	2.53
11.4	51.70	219.83	1.73	15.94	202.00	1.58	74.72	474.54	1.21	14.69	243.91	2.52
11.45	50.74	215.69	1.82	15.38	219.95	1.72	84.78	446.22	1.17	15.99	260.11	3.11
11.5	58.34	210.41	1.57	13.93	233.35	1.77	82.16	470.57	1.19	15.04	270.10	2.63
11.55	56.65	219.65	1.59	14.86	256.85	1.81	79.25	486.15	1.23	14.17	263.74	2.06
11.6	57.71	236.76	1.47				79.80	514.25	1.28	16.67	240.44	2.15
11.65	62.55	216.09	1.54				72.46	550.63	1.37	23.87	254.64	1.94
11.7	66.53	213.33	1.54				67.47	560.01	1.32	19.31	302.06	1.65
11.75	71.29	225.40	1.53				75.04	516.83	1.31	16.17	315.17	1.48
11.8	69.12	247.36	1.38				67.89	516.28	1.25	15.65	279.82	1.09
11.85	72.40	241.33	1.31				83.54	484.18	1.25	16.02	266.53	1.19
11.9	79.62	250.95	1.33				79.75	514.62	1.23	14.49	270.69	1.15
11.95	76.40	286.33	1.22				71.03	565.87	1.22	21.52	269.33	1.39
12	73.44	292.66	1.27				74.71	550.28	1.28	21.07	275.62	1.09
12.05	82.24	292.93	1.17				69.16	556.98	1.21	19.16	271.53	1.10
12.1	74.48	309.70	1.19				75.90	521.60	1.22	22.39	264.79	0.84
12.15	75.04	315.81	1.16							22.06	270.05	1.21
12.2										20.44	345.17	0.92
12.25	76.87									19.21	370.39	1.27

Table 17 Mean Age of Four Zircons

	Zircon1	Zircon2	Zircon3 rim	Zircon3 core	Zircon4
Mean (Ma)	13.4	14.5	12.9	80.8	14.2
2SE abs.	0.2	0.2	0.2	2.0	0.3
2SD abs.	2.1	2.6	2.6	10.1	4.7
2SD %	15.7	17.7	19.9	12.4	33.2
2SE %	1.1	1.2	1.8	2.5	2.2
Depth range (μm)	0-10	0-11.5	0-6.25	10-11.25	0-12.25

Table 18 LA-ICP-MS Depth Profiling Trace Element Concentrations for Zircon1 (SLCX 47)

Depth (μm)	Ti	Y	Nb	La	Ce	Nd	Sm	Eu	Gd	Tb	Dy	Ho	Er	Tm	Yb	Lu	Hf	
0.00																		
0.28	30.49	2854.47	2.11	Bdl.	0.77	3.74	4.78	Bdl.	36.97	13.62	258.61	102.19	537.19	112.37	1193.77	193.28	12080.32	
0.55	0.01	3675.81	2.46	Bdl.	0.90	Bdl.	5.59	Bdl.	67.32	17.93	349.87	124.99	562.54	128.60	1234.62	192.70	16582.12	
0.83	0.01	2476.66	Bdl.	Bdl.	Bdl.	3.64	Bdl.	Bdl.	35.89	9.91	111.60	69.06	320.09	77.24	898.55	129.36	12668.95	
1.11	0.01	2527.25	5.46	Bdl.	4.98	Bdl.	Bdl.	Bdl.	26.66	6.63	238.75	80.24	562.32	90.16	892.56	164.04	15618.49	
1.38	0.01	1612.12	2.19	Bdl.	0.80	Bdl.	14.96	1.30	21.44	5.33	89.99	49.97	289.89	65.91	557.41	104.90	11748.83	
1.66	0.01	1069.55	Bdl.	Bdl.	Bdl.	3.19	Bdl.	Bdl.	27.79	1.44	170.18	35.25	163.22	56.62	409.74	71.19	9660.35	
1.93	0.01	1332.23	2.53	Bdl.	Bdl.	Bdl.	Bdl.	Bdl.	19.78	12.29	131.50	35.28	254.91	85.16	695.98	106.16	14779.37	
2.21	56.42	1143.51	Bdl.	Bdl.	0.70	Bdl.	Bdl.	Bdl.	52.54	6.22	99.79	40.84	236.38	48.47	392.57	73.09	10932.00	
2.49	0.01	1123.14	1.72	Bdl.	1.89	3.11	23.54	2.05	6.74	15.36	66.05	50.57	135.08	24.88	457.82	72.29	10490.43	
2.76	0.01	1391.36	Bdl.	Bdl.	Bdl.	7.64	Bdl.	Bdl.	16.55	24.00	63.70	35.67	227.34	57.27	516.99	99.60	13373.83	
3.04	0.01	1482.93	Bdl.	Bdl.	1.82	Bdl.	Bdl.	Bdl.	19.47	14.12	136.26	51.05	222.81	67.38	584.56	102.67	13141.46	
3.32	0.01	1295.29	1.87	Bdl.	2.75	Bdl.	Bdl.	Bdl.	1.12	58.81	13.71	123.50	39.91	340.69	63.33	401.59	66.60	10046.67
3.59	0.01	1285.03	Bdl.	Bdl.	3.37	Bdl.	4.19	Bdl.	28.82	10.45	90.78	55.26	197.81	63.18	345.87	87.77	11112.00	
3.87	69.54	1756.36	Bdl.	Bdl.	4.28	4.25	5.33	1.39	18.30	9.48	179.32	56.44	224.96	66.16	532.31	111.39	11130.98	
4.14	0.01	1789.46	Bdl.	Bdl.	3.71	4.62	17.32	1.50	14.87	32.86	145.74	68.53	391.08	71.70	683.59	120.64	11522.73	
4.42	61.83	1630.94	Bdl.	Bdl.	1.52	15.13	18.88	2.46	24.31	11.75	113.47	66.58	291.81	68.59	534.29	113.22	11064.11	
4.70	0.01	2012.88	4.53	Bdl.	1.67	8.34	20.77	2.70	35.67	14.78	199.79	63.24	361.80	67.25	683.89	108.40	11399.24	
4.97	0.01	2004.00	10.71	Bdl.	3.16	Bdl.	4.91	Bdl.	33.75	19.23	100.44	64.52	327.82	83.12	560.97	87.28	11495.94	
5.25	0.01	1861.66	2.08	Bdl.	2.30	3.84	19.09	Bdl.	45.05	6.79	154.87	79.40	304.14	59.26	593.43	91.41	9923.32	
5.53	0.01	1966.05	Bdl.	Bdl.	1.65	16.58	10.28	1.34	61.74	12.79	172.93	62.43	241.75	67.89	622.85	98.37	10961.23	
5.80	0.01	2026.38	2.27	Bdl.	1.68	12.68	Bdl.	2.72	35.91	22.32	125.75	56.83	276.80	76.03	612.33	108.92	9608.37	
6.08	0.01	1726.89	Bdl.	Bdl.	3.02	11.44	4.71	Bdl.	8.08	16.74	215.16	79.72	276.88	63.49	444.79	96.70	9584.90	
6.35	35.57	1960.13	6.99	Bdl.	1.72	4.35	10.73	Bdl.	9.20	15.25	199.82	59.89	325.63	52.44	594.21	104.00	11032.28	
6.63	0.01	2114.45	7.96	Bdl.	4.91	Bdl.	24.46	Bdl.	41.97	26.08	227.84	56.55	341.24	61.41	677.22	111.64	13027.82	

*All concentrations in ppm. Bdl. = below detecting limit. Data are as reported by the instrument.

Table 18 (Continued)

Depth (μm)	Ti	Y	Nb	La	Ce	Nd	Sm	Eu	Gd	Tb	Dy	Ho	Er	Tm	Yb	Lu	Hf
6.91	0.01	2073.79	17.34	Bdl.	5.35	10.84	26.66	1.73	34.30	33.15	240.27	87.06	371.76	58.11	737.68	123.46	12908.30
7.18	0.01	2099.83	2.58	Bdl.	2.87	4.86	17.90	1.55	66.51	10.60	265.21	64.57	501.86	50.44	696.58	107.08	11773.82
7.46	0.01	1856.98	Bdl.	Bdl.	1.66	4.23	Bdl.	2.69	53.33	12.89	149.44	98.93	319.27	64.35	445.67	103.14	10120.42
7.74	0.01	1924.67	Bdl.	Bdl.	3.76	Bdl.	23.47	Bdl.	50.32	33.35	169.20	93.28	298.28	63.56	684.55	129.86	10761.96
8.01	0.01	1777.74	Bdl.	Bdl.	2.51	4.26	5.21	Bdl.	67.00	27.75	269.14	87.72	417.48	60.56	570.18	105.02	10319.41
8.29	0.01	1948.13	4.43	Bdl.	0.82	4.20	15.38	Bdl.	87.91	18.21	283.35	68.37	315.56	75.86	555.65	94.68	10652.33
8.56	0.01	1955.49	2.45	Bdl.	1.82	4.66	11.36	Bdl.	43.81	20.16	150.09	61.26	310.59	51.01	562.94	100.05	8860.77
8.84	0.01	2333.38	6.66	Bdl.	3.71	6.35	Bdl.	Bdl.	46.31	24.66	268.85	70.95	361.65	101.95	756.76	131.56	13270.99
9.12	0.01	2100.74	Bdl.	Bdl.	2.88	4.93	Bdl.	Bdl.	41.02	23.36	122.17	53.07	344.49	77.45	531.40	93.57	10977.73
9.39	0.01	1728.94	Bdl.	Bdl.	4.35	Bdl.	10.85	Bdl.	41.84	17.33	123.80	54.96	232.87	45.86	409.65	65.11	9379.11
9.67	0.01	1530.26	5.22	Bdl.	1.94	Bdl.	Bdl.	3.13	46.67	21.48	123.55	82.32	360.01	62.35	518.47	96.21	9312.24
9.95	41.81	1374.22	Bdl.	Bdl.	3.95	Bdl.	Bdl.	3.18	42.21	10.93	155.32	52.57	264.18	48.81	489.72	89.27	9198.68
10.22	0.01	2381.81	3.65	Bdl.	Bdl.	7.03	8.48	Bdl.	21.79	36.10	244.38	75.00	404.92	89.59	570.24	96.85	14371.42
10.50	0.01	1315.16	Bdl.	Bdl.	1.80	Bdl.	16.81	Bdl.	9.60	5.96	94.19	37.14	191.04	48.84	410.86	78.00	9631.90
10.77	0.01	1588.38	2.96	Bdl.	1.10	Bdl.	6.89	3.56	41.32	9.78	82.76	45.66	295.35	36.41	470.10	103.56	9872.63
11.05	0.01	1220.28	4.71	Bdl.	3.51	Bdl.	Bdl.	1.42	18.79	15.56	52.68	32.85	299.05	34.77	301.38	91.52	7941.58
11.33	0.01	1452.35	5.53	Bdl.	4.12	Bdl.	Bdl.	Bdl.	55.12	18.26	85.01	66.92	306.98	44.21	399.36	100.18	10142.98
11.60	0.01	1680.98	9.46	Bdl.	7.06	6.14	7.35	1.90	88.08	10.42	176.43	69.39	228.77	64.05	500.49	104.08	9939.79
11.88	0.01	1379.12	4.95	Bdl.	7.40	4.84	Bdl.	Bdl.	39.55	14.33	159.46	47.23	196.59	48.81	346.24	80.15	6536.77
12.16	0.01	2090.86	9.20	Bdl.	18.33	Bdl.	Bdl.	Bdl.	12.25	10.14	25.76	26.99	55.64	9.45	79.92	13.89	1421.04
12.43	0.01	1148.23	Bdl.	Bdl.	17.37	Bdl.	Bdl.	Bdl.	Bdl.	Bdl.	Bdl.	Bdl.	Bdl.	Bdl.	30.08	105.61	

Table 19 LA-ICP-MS Depth Profiling Trace Element Concentrations for Zircon2 (SLCX 47)

Depth (μm)	Ti	Y	Nb	La	Ce	Nd	Sm	Eu	Gd	Tb	Dy	Ho	Er	Tm	Yb	Lu	Hf
0.00																	
0.28	6979.80	2878.90	11.95	Bdl.	Bdl.	Bdl.	10.65	Bdl.	43.55	19.70	181.01	76.87	490.59	102.46	710.28	113.99	11786.43
0.55	256.85	1885.38	2.08	Bdl.	1.71	Bdl.	Bdl.	Bdl.	18.18	29.91	182.45	95.72	301.49	85.28	929.56	110.97	15184.24
0.83	443.83	2656.97	Bdl.	Bdl.	Bdl.	Bdl.	25.50	Bdl.	31.27	19.29	246.54	109.79	384.01	87.83	898.11	130.29	13520.00
1.11	137.62	2269.19	Bdl.	Bdl.	0.91	Bdl.	5.90	Bdl.	43.44	21.83	110.70	49.22	350.50	96.69	820.69	120.65	12714.33
1.38	0.03	1607.57	6.65	Bdl.	0.69	Bdl.	Bdl.	Bdl.	36.51	16.51	130.86	45.95	242.08	51.09	604.13	102.01	10080.45
1.66	147.54	2583.92	Bdl.	Bdl.	0.96	Bdl.	Bdl.	Bdl.	51.24	14.75	227.74	76.72	382.84	58.66	659.47	134.12	17163.28
1.93	109.91	1369.15	Bdl.	Bdl.	2.14	Bdl.	4.65	Bdl.	15.19	6.25	206.97	53.03	171.86	47.11	493.30	77.08	9864.85
2.21	0.03	1293.06	Bdl.	Bdl.	4.02	Bdl.	17.45	Bdl.	42.76	4.40	178.84	35.20	281.19	55.53	483.29	68.12	9828.81
2.49	0.04	1378.27	3.48	Bdl.	2.88	8.25	4.70	Bdl.	19.19	9.47	143.06	91.55	234.13	32.95	321.96	56.42	9731.68
2.76	0.05	1971.80	6.30	Bdl.	3.48	19.95	5.67	Bdl.	23.17	17.14	106.30	67.93	321.66	67.79	559.23	76.30	11755.08
3.04	219.80	1448.10	Bdl.	Bdl.	0.70	8.03	4.56	Bdl.	37.23	18.37	128.12	49.53	270.16	45.00	539.24	78.82	8668.72
3.32	110.90	1581.90	Bdl.	Bdl.	0.70	Bdl.	Bdl.	Bdl.	18.69	16.91	101.88	61.26	251.65	42.81	447.05	73.66	8538.52
3.59	0.04	1425.52	1.88	Bdl.	2.34	8.98	15.26	2.26	53.98	10.24	101.25	42.54	292.57	39.63	377.19	51.28	9757.02
3.87	0.05	1296.36	Bdl.	Bdl.	Bdl.	Bdl.	5.80	1.29	23.67	21.41	196.90	43.67	204.07	55.72	522.56	76.56	11461.10
4.14	267.07	1754.23	Bdl.	Bdl.	0.83	Bdl.	Bdl.	Bdl.	35.47	10.94	228.96	72.76	265.71	86.05	571.11	121.26	9449.41
4.42	0.05	2243.85	3.87	Bdl.	2.41	9.32	10.50	2.33	25.71	17.62	233.62	49.84	419.03	102.27	680.26	127.29	10735.19
4.70	0.05	2774.72	2.11	Bdl.	Bdl.	10.22	Bdl.	Bdl.	84.48	21.22	181.79	101.20	458.85	85.12	755.86	133.88	10085.52
4.97	0.06	2961.12	Bdl.	Bdl.	Bdl.	Bdl.	39.13	Bdl.	58.54	28.44	366.47	102.05	520.22	93.13	1053.05	190.92	11893.19
5.25	0.05	2601.51	Bdl.	Bdl.	4.16	9.67	Bdl.	Bdl.	53.14	36.41	152.48	63.72	353.71	80.32	652.13	85.94	8890.39
5.53	0.06	2437.47	4.75	Bdl.	2.98	11.56	6.48	Bdl.	52.83	26.06	303.22	97.80	444.19	77.34	693.02	104.09	12249.66
5.80	0.05	2053.38	6.02	Bdl.	0.84	Bdl.	32.91	Bdl.	58.17	29.43	211.88	87.48	319.73	51.26	695.15	107.90	8642.43
6.08	0.06	2595.08	7.27	Bdl.	1.02	11.86	13.25	Bdl.	124.30	15.55	387.75	87.16	516.74	91.16	945.39	155.74	11283.21
6.35	449.01	2627.89	4.27	Bdl.	0.90	10.49	Bdl.	Bdl.	47.71	17.65	130.07	76.99	375.92	75.92	658.91	123.45	8994.53
6.63	0.07	3679.00	14.27	Bdl.	3.59	28.08	7.82	Bdl.	31.88	26.21	247.05	120.48	596.14	135.97	1020.16	149.99	12732.96

*All concentrations in ppm. Bdl. = below detecting limit. Data are as reported by the instrument.

Table 19 (Continued)

Depth (μm)	Ti	Y	Nb	La	Ce	Nd	Sm	Eu	Gd	Tb	Dy	Ho	Er	Tm	Yb	Lu	Hf
6.91	0.06	2491.43	Bdl.	Bdl.	0.95	Bdl.	18.55	Bdl.	50.42	8.29	173.66	67.59	317.77	75.43	562.99	124.54	9927.40
7.18	0.06	2203.44	Bdl.	Bdl.	Bdl.	Bdl.	29.93	Bdl.	43.92	14.04	224.15	62.10	363.95	63.69	606.81	96.15	9014.17
7.46	0.07	2350.94	8.06	Bdl.	5.65	13.32	22.15	Bdl.	60.19	9.90	345.57	49.71	372.96	90.05	644.50	134.51	12980.26
7.74	0.06	1903.82	Bdl.	Bdl.	2.99	11.78	19.56	1.44	106.27	17.47	213.55	76.84	273.40	101.49	611.83	137.49	9925.62
8.01	0.07	2100.10	Bdl.	Bdl.	2.29	Bdl.	22.45	Bdl.	54.90	22.56	192.63	96.67	326.65	102.92	737.58	93.26	11836.95
8.29	0.05	1782.00	5.64	Bdl.	1.59	18.77	20.72	Bdl.	67.53	8.67	169.66	36.37	239.30	48.37	500.70	94.32	8048.79
8.56	0.08	2439.04	Bdl.	Bdl.	1.24	Bdl.	Bdl.	Bdl.	39.57	21.68	246.17	88.71	353.11	86.09	592.51	104.72	11684.16
8.84	0.07	1954.71	Bdl.	Bdl.	2.16	Bdl.	14.11	Bdl.	57.49	30.72	173.34	59.52	295.73	82.37	456.96	77.76	9151.46
9.12	0.06	1853.89	9.40	Bdl.	0.99	11.82	12.99	Bdl.	84.67	6.52	121.57	62.13	405.50	84.25	475.53	84.02	9126.13
9.39	0.07	2160.95	2.60	Bdl.	1.10	Bdl.	7.21	Bdl.	29.36	21.72	379.47	83.19	351.34	61.71	521.01	110.52	10238.78
9.67	0.06	1844.71	Bdl.	Bdl.	1.93	23.01	12.60	Bdl.	25.66	21.09	147.39	35.48	269.32	45.76	484.94	86.02	8861.46
9.95	0.07	1604.90	Bdl.	Bdl.	4.10	12.24	Bdl.	Bdl.	49.08	22.41	164.45	41.50	223.18	45.15	578.16	97.81	10821.66
10.22	365.10	2011.49	Bdl.	Bdl.	3.05	12.15	Bdl.	Bdl.	5.40	11.11	225.09	56.11	306.24	67.12	485.86	74.69	10163.38
10.50	0.07	1783.66	4.81	Bdl.	1.02	24.51	13.37	Bdl.	27.21	17.89	234.48	45.23	274.08	55.46	539.47	80.01	11564.77
10.77	327.68	1289.42	Bdl.	Bdl.	0.90	Bdl.	Bdl.	Bdl.	23.99	19.72	144.72	44.89	176.19	36.68	337.40	73.37	8780.99
11.05	0.08	1399.58	2.54	Bdl.	Bdl.	Bdl.	Bdl.	Bdl.	34.53	11.83	214.94	65.85	235.47	53.16	471.11	77.85	10667.15
11.33	0.08	1914.97	Bdl.	Bdl.	2.39	14.40	7.82	Bdl.	38.18	28.76	118.82	94.92	393.82	54.72	469.55	89.81	11480.21
11.60	0.08	1828.98	Bdl.	Bdl.	1.11	Bdl.	14.47	Bdl.	23.55	14.52	169.14	44.96	308.75	69.38	590.63	69.25	10272.69

Table 20 LA-ICP-MS Depth Profiling Trace Element Concentrations for Zircon3 (SLCX 12)

Depth (μm)	Ti	Y	Nb	La	Ce	Nd	Sm	Eu	Gd	Tb	Dy	Ho	Er	Tm	Yb	Lu	Hf
0.00																	
0.28	3.32	1773.53	3.82	Bdl.	1.02	Bdl.	6.95	Bdl.	24.23	12.08	150.32	49.08	260.09	53.15	483.48	91.80	8226.62
0.55	4.42	2423.98	9.59	Bdl.	Bdl.	Bdl.	Bdl.	Bdl.	22.49	14.68	218.13	83.93	364.50	120.32	872.92	142.38	12765.25
0.83	5.53	1155.41	2.12	Bdl.	1.12	Bdl.	3.84	Bdl.	8.94	6.08	65.66	53.05	185.68	63.55	527.80	87.91	6900.22
1.11	6.63	1618.64	3.16	Bdl.	Bdl.	Bdl.	Bdl.	Bdl.	4.43	12.64	149.61	75.08	275.90	50.73	693.54	136.11	11284.69
1.38	7.73	1677.43	6.23	Bdl.	Bdl.	Bdl.	Bdl.	Bdl.	21.76	8.88	115.13	59.05	307.44	49.88	776.34	87.01	10118.97
1.66	8.84	2089.23	Bdl.	Bdl.	2.25	Bdl.	7.69	2.95	29.78	34.03	227.66	78.31	365.16	92.94	969.37	100.82	16899.11
1.93	9.95	1718.08	Bdl.	Bdl.	3.09	Bdl.	Bdl.	Bdl.	28.62	11.68	78.14	64.16	318.63	74.20	808.34	120.83	11010.04
2.21	11.05	1773.19	9.38	Bdl.	2.45	Bdl.	Bdl.	Bdl.	21.66	14.14	178.28	90.01	270.02	92.39	908.50	201.40	14686.65
2.49	12.16	1961.49	2.92	Bdl.	3.81	50.02	Bdl.	Bdl.	16.16	4.95	172.27	63.40	285.49	83.61	774.44	131.93	10670.98
2.76	13.26	1715.97	3.01	Bdl.	7.82	Bdl.	10.71	Bdl.	20.72	21.98	207.12	72.05	309.98	61.99	874.07	155.76	10573.15
3.04	14.37	1718.81	7.13	Bdl.	4.93	Bdl.	8.44	Bdl.	26.13	4.00	139.29	47.11	183.30	67.59	767.92	135.93	10108.72
3.32	15.47	1534.42	20.08	Bdl.	12.61	Bdl.	Bdl.	Bdl.	7.87	1.60	98.30	53.37	216.58	53.83	602.05	134.59	9650.62
3.59	16.58	1335.03	17.36	Bdl.	4.48	Bdl.	Bdl.	Bdl.	9.50	3.87	118.69	50.34	296.01	55.91	612.35	159.61	11405.27
3.87	17.68	1599.78	8.05	Bdl.	18.64	Bdl.	7.10	Bdl.	16.47	17.92	153.42	37.26	285.28	55.92	999.46	140.60	15159.34
4.14	18.79	1630.79	11.09	Bdl.	20.87	Bdl.	6.50	Bdl.	5.03	10.26	199.70	81.05	256.07	73.63	909.35	142.79	13585.84
4.42	19.89	3761.86	7.40	Bdl.	17.06	Bdl.	Bdl.	Bdl.	5.02	2.05	73.87	59.64	276.62	76.73	690.17	141.10	11176.23
4.70	21.00	1206.78	12.24	Bdl.	18.76	Bdl.	Bdl.	Bdl.	12.43	11.83	54.83	63.24	232.46	34.27	559.23	127.93	10994.25
4.97	22.10	1715.40	18.90	Bdl.	15.40	Bdl.	6.60	Bdl.	25.51	8.33	127.58	73.57	270.42	76.31	947.15	233.29	16732.40
5.25	23.21	1671.98	Bdl.	Bdl.	9.29	Bdl.	5.79	4.42	17.92	10.96	98.82	66.48	256.00	84.09	772.02	193.78	10828.02
5.53	24.31	1166.04	30.31	Bdl.	25.60	Bdl.	Bdl.	Bdl.	18.09	16.61	119.78	53.71	258.55	90.68	839.68	166.40	10353.74
5.80	25.42	1337.60	11.96	Bdl.	15.88	12.40	Bdl.	1.98	16.03	11.44	147.39	62.88	245.73	73.96	758.41	151.19	11315.31
6.08	26.52	1625.23	39.87	Bdl.	27.41	14.98	Bdl.	Bdl.	48.44	7.90	142.52	47.24	412.77	53.93	1103.44	169.30	12130.00
6.35	27.63	1560.93	7.75	Bdl.	19.48	Bdl.	Bdl.	2.55	36.14	16.85	121.54	56.92	203.90	95.27	1126.45	215.68	12845.26
6.63	28.73	1390.56	15.75	Bdl.	25.29	Bdl.	10.84	Bdl.	8.38	8.54	67.80	42.63	248.17	83.96	929.12	245.09	12017.20

*All concentrations in ppm. Bdl. = below detecting limit. Data are as reported by the instrument.

Table 20 (Continued)

Depth (μm)	Ti	Y	Nb	La	Ce	Nd	Sm	Eu	Gd	Tb	Dy	Ho	Er	Tm	Yb	Lu	Hf
6.91	29.84	1826.64	8.24	Bdl.	37.11	Bdl.	Bdl.	Bdl.	5.46	6.69	184.92	71.81	227.14	102.55	1165.66	309.61	14230.35
7.18	30.94	1445.50	29.20	Bdl.	31.59	Bdl.	11.11	Bdl.	17.17	5.25	107.40	45.50	245.41	81.94	1174.69	214.09	10440.07
7.46	32.05	1542.56	15.09	Bdl.	43.22	Bdl.	Bdl.	Bdl.	14.94	12.19	146.57	73.89	258.79	112.47	1242.48	254.59	12542.60
7.74	33.15	1768.61	12.80	Bdl.	36.56	Bdl.	10.91	Bdl.	21.06	12.03	161.19	67.85	359.03	87.09	1081.45	259.83	11059.11
8.01	34.26	2303.67	15.46	Bdl.	57.45	15.69	Bdl.	1.25	20.30	8.28	156.85	53.77	374.50	100.07	1137.60	256.46	10293.21
8.29	35.36	2065.12	44.49	Bdl.	56.81	15.02	Bdl.	Bdl.	34.00	17.83	193.01	86.46	398.81	84.95	1065.30	218.41	9867.13
8.56	36.47	2073.10	32.70	Bdl.	54.03	Bdl.	5.54	2.10	55.56	19.17	150.99	41.66	262.11	59.80	813.83	136.57	8706.78
8.84	37.57	1994.13	3.71	Bdl.	68.39	44.83	6.26	Bdl.	43.50	11.83	135.17	65.54	291.37	63.01	815.39	167.98	10742.98
9.12	38.68	2526.52	14.11	Bdl.	86.53	37.81	7.92	Bdl.	18.34	7.48	171.03	36.28	355.93	64.16	788.41	121.48	12301.78
9.39	39.78	1879.41	12.18	Bdl.	66.57	Bdl.	13.64	5.18	31.59	23.62	93.02	66.93	284.61	73.67	577.37	96.46	9904.91
9.67	40.89	1831.58	8.52	Bdl.	88.38	Bdl.	7.14	Bdl.	88.17	15.73	235.27	86.38	355.14	64.82	630.76	94.14	9911.63
9.95	41.99	1798.41	12.59	Bdl.	65.46	Bdl.	Bdl.	Bdl.	48.78	17.68	175.58	50.52	197.21	65.49	489.82	124.63	9041.75
10.22	43.10	1694.38	4.41	Bdl.	90.04	17.56	29.45	Bdl.	85.21	23.17	359.68	84.22	295.26	77.66	527.00	111.23	10617.19
10.50	44.20	1740.19	11.10	Bdl.	72.70	29.40	12.33	1.17	19.03	15.52	98.06	50.37	217.56	54.44	521.50	91.69	8435.67
10.77	45.31	2108.28	Bdl.	Bdl.	104.68	54.13	15.14	4.31	75.91	9.52	206.38	64.30	406.72	79.82	640.18	121.68	10708.49
11.05	46.41	1591.27	8.93	Bdl.	74.39	Bdl.	Bdl.	Bdl.	51.42	4.66	143.04	58.07	243.53	67.20	605.73	115.54	9593.30
11.33	47.52	1640.41	Bdl.	Bdl.	70.27	15.76	13.23	1.25	40.81	33.28	165.30	75.61	307.61	47.02	467.07	68.27	9165.10
11.60	48.62	2304.36	Bdl.	Bdl.	109.07	Bdl.	17.04	1.61	52.54	18.75	241.85	86.21	211.67	81.41	775.41	124.73	11287.67
11.88	49.73	2536.55	25.86	Bdl.	53.30	Bdl.	17.04	Bdl.	39.42	21.43	241.91	66.75	273.19	66.81	672.65	104.34	8607.78
12.16	50.83	1606.57	4.63	Bdl.	56.49	Bdl.	Bdl.	1.44	29.35	2.39	77.82	19.88	152.57	26.12	141.41	31.09	2390.13
12.43	51.94	1819.95	Bdl.	Bdl.	61.33	Bdl.	Bdl.	Bdl.	Bdl.	16.56	Bdl.	Bdl.	Bdl.	48.93	Bdl.	311.15	

Table 21 LA-ICP-MS Depth Profiling Trace Element Concentrations for Zircon4 (SLCX 12)

Depth (μm)	Ti	Y	Nb	La	Ce	Nd	Sm	Eu	Gd	Tb	Dy	Ho	Er	Tm	Yb	Lu	Hf
0.00																	
0.28	0.23	3874.69	Bdl.	Bdl.	22.14	13.50	19.16	3.18	46.75	9.47	479.34	113.51	558.65	112.01	1188.81	274.55	14429.24
0.55	100.16	2927.82	Bdl.	Bdl.	23.12	26.11	12.35	1.02	63.28	25.62	313.53	114.73	423.68	102.73	1053.09	186.90	10900.49
0.83	0.25	2775.50	4.55	Bdl.	11.44	116.28	27.50	Bdl.	40.25	20.37	220.03	99.94	549.31	83.44	1042.46	200.04	10588.19
1.11	0.27	2862.03	2.52	Bdl.	33.84	48.38	15.26	5.05	22.33	6.78	185.19	114.98	534.62	131.98	987.62	179.61	13264.26
1.38	0.22	1828.62	2.02	Bdl.	23.82	51.89	12.28	6.10	17.96	18.18	338.59	61.10	277.41	63.41	784.29	134.52	10605.16
1.66	0.20	1627.82	7.55	Bdl.	26.21	193.77	22.92	6.64	20.96	8.48	170.67	75.53	375.44	81.06	595.90	181.03	9550.67
1.93	0.24	1894.11	Bdl.	Bdl.	79.18	158.15	61.22	6.75	99.50	8.06	270.14	56.72	404.64	73.30	1008.09	174.05	13695.22
2.21	52.56	1943.05	6.29	Bdl.	49.49	229.14	31.89	11.60	60.63	13.22	189.94	60.03	360.08	58.69	683.86	144.01	11886.04
2.49	67.32	2439.29	5.35	Bdl.	66.58	223.81	73.31	6.73	35.74	14.47	215.63	56.95	306.53	111.50	846.60	138.83	11077.31
2.76	0.22	1815.82	8.23	Bdl.	22.62	53.10	18.84	1.04	64.29	3.72	117.77	57.42	288.32	66.23	544.76	120.03	11358.38
3.04	0.22	1585.81	6.15	Bdl.	11.27	52.92	Bdl.	2.07	22.88	1.85	110.46	45.44	188.39	39.31	573.55	96.53	10090.41
3.32	234.34	1713.56	Bdl.	Bdl.	14.60	Bdl.	14.06	1.16	10.27	14.56	85.26	68.00	174.45	64.62	574.80	111.56	10273.26
3.59	67.05	1655.33	Bdl.	Bdl.	8.89	16.95	Bdl.	1.32	29.31	18.99	106.15	88.39	295.60	70.14	655.93	136.50	12264.60
3.87	0.29	2006.59	Bdl.	Bdl.	11.46	52.47	16.55	Bdl.	24.19	22.04	200.77	57.82	286.24	59.36	622.47	87.51	12827.19
4.14	0.30	1587.85	5.52	Bdl.	5.87	17.91	8.48	Bdl.	30.96	20.05	186.88	63.75	235.70	72.16	609.53	87.62	11478.04
4.42	0.31	1785.13	Bdl.	Bdl.	12.11	36.97	8.75	2.89	12.78	2.59	154.28	63.43	295.79	39.19	636.08	114.50	11278.26
4.70	75.22	1750.63	5.78	Bdl.	9.85	56.41	Bdl.	Bdl.	64.99	26.31	235.41	54.96	320.88	99.64	552.42	93.96	13244.94
4.97	0.34	1806.80	Bdl.	Bdl.	2.68	20.44	Bdl.	Bdl.	42.38	8.58	245.18	77.90	355.94	77.95	616.08	104.29	11833.05
5.25	0.36	1843.27	Bdl.	Bdl.	4.17	42.49	10.05	3.31	36.70	26.74	132.96	64.77	354.81	78.76	656.68	156.79	12290.95
5.53	0.35	1616.77	Bdl.	Bdl.	6.80	41.56	Bdl.	Bdl.	64.61	8.72	162.55	47.51	295.28	48.41	489.64	96.93	10397.49
5.80	0.35	1677.72	Bdl.	Bdl.	11.03	Bdl.	Bdl.	Bdl.	50.95	5.89	164.81	40.14	246.97	93.70	585.93	121.10	12753.13
6.08	89.94	1566.03	Bdl.	Bdl.	2.90	Bdl.	20.97	Bdl.	38.27	3.10	115.55	64.72	251.81	60.98	513.39	62.45	11629.03
6.35	0.31	1389.52	2.85	Bdl.	3.67	37.40	8.85	Bdl.	32.29	13.07	165.73	42.73	258.89	69.25	411.43	68.88	7858.10
6.63	0.35	1464.73	Bdl.	Bdl.	1.36	20.79	Bdl.	3.24	64.62	23.25	151.76	47.51	214.03	41.80	457.44	117.10	10328.88

*All concentrations in ppm. Bdl. = below detecting limit. Data are as reported by the instrument.

Table 21 (Continued)

Depth (μm)	Ti	Y	Nb	La	Ce	Nd	Sm	Eu	Gd	Tb	Dy	Ho	Er	Tm	Yb	Lu	Hf
6.91	0.35	1415.65	Bdl.	Bdl.	Bdl.	21.07	Bdl.	Bdl.	58.20	8.83	186.74	32.09	284.15	64.63	496.00	82.12	9345.79
7.18	0.29	1132.27	2.60	Bdl.	3.36	34.23	8.10	1.33	11.82	9.57	80.29	52.13	182.16	48.87	415.99	55.56	7701.48
7.46	0.36	1300.76	Bdl.	Bdl.	2.84	65.20	20.57	Bdl.	30.01	6.07	101.95	33.09	215.83	62.03	528.11	75.22	9329.52
7.74	162.39	1164.12	2.98	Bdl.	2.57	19.66	9.30	1.53	47.48	30.20	153.64	22.44	306.65	45.70	477.47	87.12	9698.73
8.01	0.39	1751.48	10.72	Bdl.	7.71	47.19	Bdl.	Bdl.	89.56	13.18	110.66	41.90	267.66	62.32	409.33	81.59	11163.58
8.29	88.97	1315.51	Bdl.	Bdl.	1.40	Bdl.	20.26	Bdl.	36.94	32.89	156.19	67.88	189.71	54.28	478.67	74.01	10448.95
8.56	0.40	1402.03	Bdl.	Bdl.	4.66	Bdl.	11.24	1.85	49.19	9.95	123.82	69.31	294.72	65.25	430.43	115.48	10896.78
8.84	0.41	1913.64	Bdl.	Bdl.	Bdl.	Bdl.	69.43	Bdl.	33.74	13.65	114.67	31.00	285.89	82.62	433.42	142.54	10081.30
9.12	83.25	1098.50	Bdl.	Bdl.	5.19	Bdl.	18.79	Bdl.	27.39	5.54	82.75	47.82	161.73	56.59	367.11	59.98	8608.88
9.39	0.35	1646.97	Bdl.	Bdl.	2.73	20.90	Bdl.	Bdl.	43.23	14.58	141.48	42.37	288.51	48.50	442.54	92.38	10886.65
9.67	0.37	1630.57	Bdl.	Bdl.	5.76	66.16	Bdl.	Bdl.	30.41	24.61	126.33	92.21	382.47	97.70	424.48	123.60	10611.56
9.95	0.34	1599.14	Bdl.	Bdl.	2.65	Bdl.	Bdl.	Bdl.	13.99	11.32	137.40	51.42	301.64	40.67	679.66	96.21	12457.56
10.22	0.32	1334.24	Bdl.	Bdl.	9.95	Bdl.	9.01	Bdl.	19.69	2.66	138.82	28.95	181.89	66.25	498.31	73.82	9299.71
10.50	0.34	1209.65	6.09	Bdl.	5.31	Bdl.	Bdl.	Bdl.	21.01	5.67	137.56	54.05	194.07	57.84	414.41	129.07	10653.82
10.77	0.39	1643.46	Bdl.	Bdl.	Bdl.	70.42	Bdl.	Bdl.	56.59	13.08	183.24	50.51	315.29	71.71	604.74	136.34	11411.92
11.05	0.35	1663.91	6.36	Bdl.	Bdl.	Bdl.	30.15	Bdl.	29.27	11.84	187.99	80.69	240.30	55.95	457.49	70.82	9543.19
11.33	0.36	1729.81	Bdl.	Bdl.	2.85	174.97	Bdl.	Bdl.	37.65	18.28	159.31	71.96	270.43	52.96	563.20	138.67	10780.49
11.60	0.33	1416.24	2.82	Bdl.	1.23	Bdl.	8.92	Bdl.	45.48	5.26	108.02	52.54	200.00	41.72	522.23	60.82	9079.55
11.88	0.35	1719.37	5.72	Bdl.	3.76	38.39	Bdl.	Bdl.	52.85	10.69	129.80	70.41	203.31	56.55	501.41	96.86	8235.31
12.16	0.36	1604.78	20.82	Bdl.	Bdl.	Bdl.	Bdl.	Bdl.	9.62	3.89	Bdl.	14.14	9.87	11.76	64.42	9.00	659.55